Master Thesis
Civil Engineering

Understanding Structures and Earthquakes in Groningen

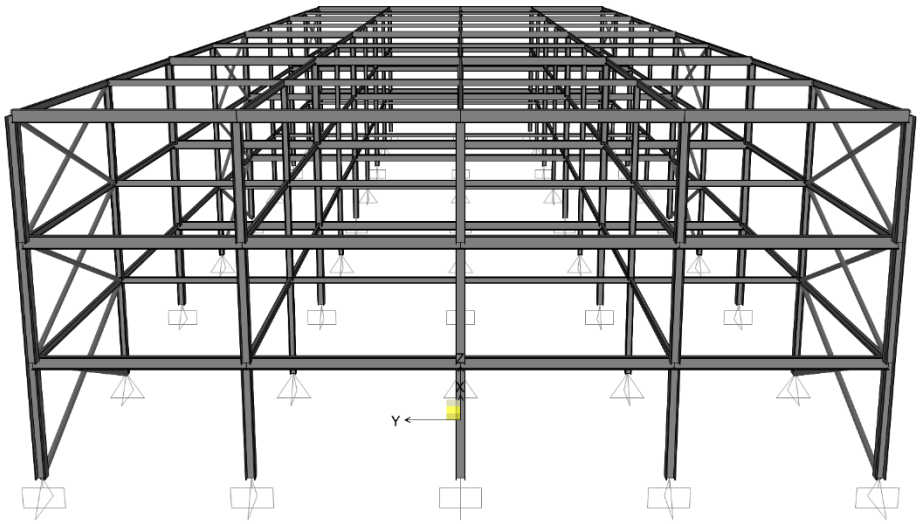

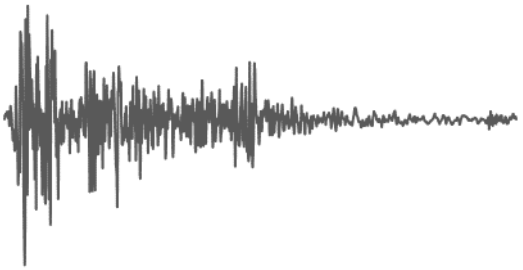

TU Delft

Gemeente Rotterdam

Rajat Kapoor

Understanding Structures and Earthquakes in Groningen

By

Rajat Kapoor

in partial fulfilment of the requirements for the degree of

Master of Science

in Civil Engineering

at the Delft University of Technology,

29th August 2018

Supervisor:	Dr. Ir. C.B.M Blom	TU Delft
Thesis committee:	Prof. Dr. M. Veljkovic	TU Delft
	Dr. Ir. C.B.M Blom	TU Delft Gemeente Rotterdam
	Dr. P. Može	University of Ljubljana
	Ir. L.J.M Houben	TU Delft

Acknowledgements

The present thesis is a part of Master of Science course at the faculty of Civil Engineering and Geosciences at Delft University of Technology, the Netherlands. I would like to thank all the concerned faculty members who helped me grow as a professional by providing valuable knowledge during the course of two-year program.

Special thanks to Dr. ir. C.B.M Blom, Gemeente Rotterdam who provided me with this opportunity to work as a graduate intern at the company to fulfil the purpose of this master thesis. I am indebted for his support, guidance and motivation throughout this journey. Prof. dr. Milan Veljkovic, chair of steel and composite structures at TU Delft for being the chairman of my graduation committee and providing valuable feedback during the intermediate progress meetings. I am extremely overwhelmed with the support of Dr. Primož Može, University of Ljubljana for sharing his knowledge and experience during his stay at TU Delft and for providing his valuable time and feedback during weekly meetings. Special thanks to L.J.M Houben for being a part of this thesis committee and support all this time being the coordinator for MSc program at TU Delft.

This thesis is dedicated to my family, who gave me this opportunity to pursue MSc Civil Engineering and have always been a source of motivation throughout these two years. It would not have been possible without their support.

Last and not the least, the friends I made here, who made this journey beautiful, who stood-by during all the good and tough times. Thank you, guys, for making it a memorable one.

Rajat Kapoor

Abstract

Rapid extraction of gas in the north-eastern Groningen province of the Netherlands has led to an increase in the occurrence of induced earthquakes in the region due to subsidence of gas bearing sandstone layers. This process manifests itself in the form of ground motions at the surface. Netherlands, historically being an inactive tectonic zone, has not paid much attention to detail structures withstand lateral seismic forces in the past. This has led to an alarming situation amongst the residents and government authorities since damage has been reported in the form of claims for compensation. The predominant presence of old masonry houses has further aggravated the situation because of quasi-brittle material characteristics weak in tension. A large-scale research campaign was launched after the historical seismic event at Huizinge in 2012 with an aim to assess and safeguard building structures in the region although much of the research has been focussed on behaviour of masonry houses. NPR 9998 which serves as a national guideline in the Netherlands for seismic assessment and retrofitting was published and is continuously being updated with the latest developments. However, it is equally important to address other typology of structures in terms of material and geometry. With this objective, it was decided to start with a fundamental study on the seismic analysis methods with specific regards to steel structures.

The present thesis provides a comprehensive review of the lateral behaviour of affected structure initially and the fundamental differences in the induced earthquakes when compared with deep tectonic earthquakes. This is followed by state-of-the-art of linear and nonlinear seismic analysis methods which forms the basis of guidelines & codes presented in the NPR 9998 and EN 1998 context. Further, an understanding on the generation of seismic action in response spectrum format from recorded ground motions which is the most widely adopted one across seismic design codes worldwide. The case study adopted for this study is a steel office building preliminary designed for non-seismic actions. Global seismic demands are determined using linear-static and linear-dynamic analysis methods with verification of specific criteria to be satisfied for safety of steel structures. Modelling parameters and methodologies are discussed in detail with regards to using simplified numerical models for analysis based on recommendations from Eurocodes and Internaltional codes. A variation model to assess the likely performance level using nonlinear static pushover analysis for a specific intensity of ground motion in terms of peak ground acceleration was made. Conclusions in the form of applicability of analysis methods are made towards the end with affected structures primarily vibrating in the fundamental mode, the present study can serve as a reference guide for a practicing engineer carrying out seismic analysis. Discussions about the background of design principles is made alongside the analysis for a clear understanding.

This thesis is expected to fill the knowledge gap for a design engineer carrying out seismic assessment of structures in the Groningen region of the Netherlands by providing a fundamental understanding of seismic demands imposed on a structure and assessment of capacity deficiency by carrying out non-linear pushover analysis. Recommendations based on NPR, Eurocodes and international codes have been made to simplify numerical modelling of the structure. Similar analysis can be undertaken for other types of structures prone to be affected by induced earthquakes by adopting corresponding material nonlinear models and considering level of interaction with the ground in terms of soil-structure interaction where the same may lead to modification of structural response.

Contents

List of figures

List of Tables

1. Introduction

Rapid Extraction of Gas in the North-Eastern part of the Netherlands has gained a considerable attention in the recent years owing to generation of induced Earthquakes in the process. Netherlands, naturally being an inactive seismic zone, is experiencing tremors and the major area of concern being structures viz. masonry houses, industrial structures, bridges etc. which were built in the past without having been designed for seismic activity. This requires verification of structural capacity of a large number of buildings, bridges in the region to ensure long term safety of people.

Figure 1.1 Typical crack in the URM wall

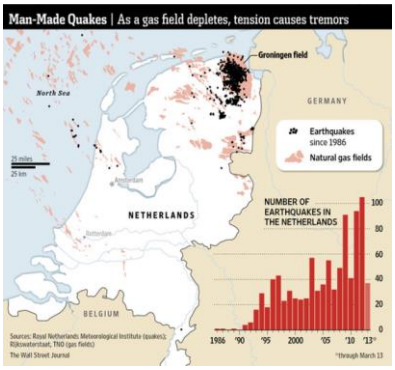

Figure 1.2 Number of induced Earthquakes with time

1.1 Background

The Groningen gas field discovered in the 1960's is one of the biggest and most profitable gas fields in the world. The Dutch petroleum company "Nederlandse Aardolie Maatschappij" (NAM) – a consortium then jointly owned by giants Shell and Exxon Mobil started oil extraction in the year 1963. The gas-initially-in-place (GIIP) of the field is estimated at 2880 billion cubic meters and the cumulative recovery from the field as on 01-01-2017 is 75 percent of the GIIP [1].

There has been no history of seismic activity in the region before oil companies started exploiting natural gas. Rapid gas extraction over the years led to a severe and unpredictable situation leaving about two-thirds of the reservoir empty. The induced earthquakes occur as a result of pressure changes in the gas reservoir beneath the earth surface, leading to reservoir compaction. This compaction manifests itself as surface subsidence causing earthquakes. As a consequence, more than 1000 earthquakes ranging from 0.1 to 3.6 on the Richter scale have been recorded since early 1990's. At the first glance, magnitude of these ground motions does not seem to be as terrifying as compared to historical tectonic earthquakes around the world, it is the shallow geology, prevailing soil conditions and the characteristics of typical UnReinforced Masonry construction (henceforth called URM) in the Groningen region which aggravated the situation and has been a reason for unrest amongst the residents. The magnitude of damage is far more than suggested by the Richter scale intensity.

Initial damages reported by the citizens were denied by NAM and the government claiming that there is no causal link between gas extraction and the earthquakes. The growing evidence of damage, a large-scale research program and the increasing frequency of earthquakes as a function of cumulative gas extraction [figure 1.3] made them accept this connection having received more than 50,000 damage reports from citizens seeking compensation for the structural damage as well as loss of property value in Groningen city.

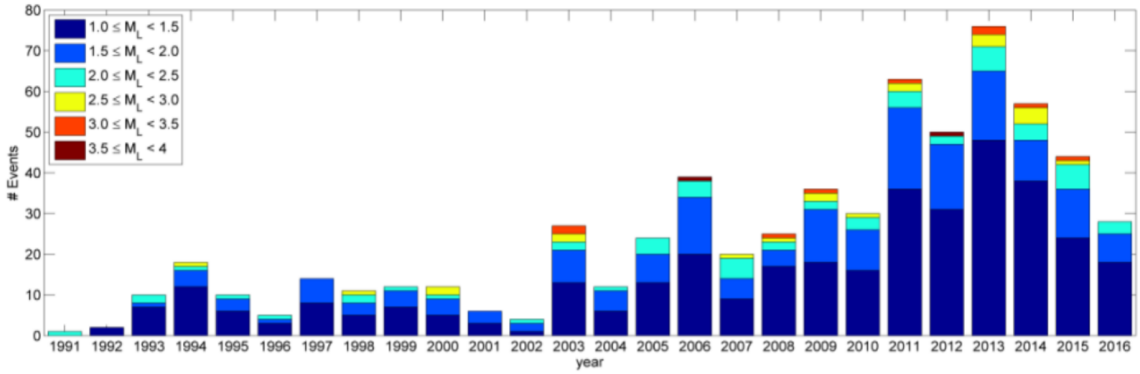

Figure 1.3 Number of events occuring with the contour of the Groningen gas field as a function of time and magnitude (M_L) up to 15.11.2016 [2]

The continuous increase in the seismic activity became a critical concern with time and a number of research programs aimed to understand the cause of these earthquakes were initiated. The point of argument was that if there is a dependency between production and seismicity, then the production should be optimized in such a way that the risk posed by induced earthquakes would be minimal. A decision was made in January 2014 to cut down the production rate, specifically in the centre of the gas field which had the highest rate of seismicity, largest magnitude event and the highest compaction values. It is observed in figure 1.3 above that for the year 2014, there is a decrease in the number of events as compared to the previous ones conforming to the argument that a reduction in production could possibly lead to a reduced rate of compaction [3].

EN1998, Design of structures for earthquake resistance, lay guidelines for design and detailing of structures subjected to earthquakes. The return period of earthquakes is based on recorded set of data in the past and probabilistic analysis i.e. the probability of occurrence of an earthquake of a certain magnitude in a region in certain number of years. The elastic response spectrum and design response spectrum have been derived based on an ensemble of ground motions considering the effect of ground conditions, soil factor as well as the importance factor of the structures.

However, historically due to Netherlands being an inactive seismic zone, there was an absence of National Annex to Eurocode 8 providing specifications for the design, detailing or retrofitting of structures due to the effects of earthquakes. The problem of induced seismicity as stated above and increasing situation of panic amongst the residents of Groningen due to tremors led to research at a large scale by the concerned authorities and institutions to cope up with an alarming situation. ‘Nederlandse Praktijkrichtlijn (NPR) 9998’ for the design of earthquake resistant new structures and evaluation of existing structures was published by ‘Nederlands Normalisatie Instituut (NEN)’ committee of experts on 18 December 2015. The NPR has included safety levels and values for both new & existing constructions and it has been made mandatory to comply with this safety standard in the Netherlands.

NPR9998 offers engineers and contractors a technical support for design and assessment of buildings and a rough calculation according to the specifications of this document indicated whether a building is strong enough to withstand the burden of an earthquake of certain magnitude. The scope of NPR is limited to north-east part of the Netherlands so far, which has been affected by induced earthquakes. A latest version of this document published by NEN, NPR 9998: 2017 supersedes NPR 9998:2015 and is based on the latest state of the art research being carried out during this period by the competent authorities.

1.2 Research Objectives

The published guidelines in the NPR 9998 are based on an extensive research by the involved authorities, stake holders and research institutions. It recommends provisions from the available literature, national and international trials, and other knowledge sources [4]. This master thesis aims at understanding the basis of provisions in NPR 9998: 2017 and the interpretation of those provisions to a specific case of structures in Groningen. A detailed study about the applicability of seismic analysis methods for a case study structure in Groningen and feasibility of those methods will be ascertained. The effect magnitude of ground motions on the damage assessment would be evaluated since the recorded maximum peak ground acceleration (PGA) in the Groningen region is much lower than the expected PGA which can occur (based on Probabilistic Seismic Hazard Analysis, PSHA) and lead to consequences which are still unknown.

To support the above objectives of this study, the following key questions are considered essential to be answered towards the end of this research thesis:

- How can we assess the existing structures in Groningen area of the Netherlands based on available literature and seismic guidelines?
- What is the most appropriate seismic analysis method for assessment given the type of structures and seismic activity in the Groningen?
- How can we assess steel structures, for e.g. an existing steel office building structure designed for non-seismic loading based on the availability of seismic records in the region?

In addition to the above key questions, to address these issues, several related points that will arise as the thesis progress will be addressed subsequently.

As an outcome of this thesis supported by the above key questions, it will serve as a knowledge guide for a practicing engineer to fulfill the knowledge gap in understanding seismic concepts based on the available literature and interpretation of guidelines. A comprehensive understanding of the development of seismic input in the form of design response spectrum from recorded accelerograms on-site is foreseen as a significant knowledge and pre-requisite for an engineer responsible for seismic assessment to understand the action effects on a structure. Till date, the research in Groningen region of the Netherlands has primarily been focused on the response of URM houses of different typologies. However, it has been decided to extend this to assess the performance of steel structures. To address this, seismic assessment of an office building structure realized in steel has been agreed upon to assess the demands imposed on the structure by the ground motions. An analysis on a global level is made which principally forms the basis of seismic assessment for different typology of structures for example, bridges, quay-walls that forms a significant part of harbour structures, sheet piles etc., the difference lies the material behaviour and constitutive relations.

1.3 Research Methodology

In a quest to fulfil the above-mentioned research objectives, this master thesis report has been organized in different chapters in the following format. Chapter 1 gives an insight in to the situation at hand and provides a stepping stone towards the research area. The background information about the problem has been discussed briefly followed by clearly laying out research objectives and outcomes as a result of this master thesis.

In the next chapter, a comprehensive background information about the topics relevant for this thesis would be gathered from the available literature, codal guidelines and journals and will be presented explicitly in context to the situation in Groningen region. The contents which are seen important for this research includes discussion about the fundamental differences between the induced earthquakes and the tectonic earthquakes, analysis and assessment guidelines from design codes, a detailed overview of the characteristics of affected structures in the region, seismic action effects, state-of-the-art of seismic analysis recommended in codes and literature for linear and nonlinear analysis, and discussion about the seismic assessment of a steel structure.

Chapter 3 focuses on analysis of seismic input for the design of a structure based on the data recorded by the accelerometers. A detailed study on the development of design spectrum is considered indispensable to be included as a part of this thesis to enable a practicing engineer to understand the basics of seismic action effects recommended in the guidelines. A brief discussion about the non-linear site response amplification will be addressed based on which site-specific response spectra is provided by the NPR 9998.

The next part of this report, chapter 4 will assess the case study decided for this thesis. Seismic assessment of a regular steel office building will be performed to address equal importance to safeguard infrastructure in the region as well. The structure will be suitably analyzed based on guidelines subjected to a design seismic loading recommended for the region. A finite element model will be generated and analyzed subjected to the same ground motion. Nonlinear behaviour of components has been addressed based on European and FEMA guidelines to model material nonlinearity. The last part would be comparison of results from the above analysis procedures.

Chapter 5 will discuss the obtained results from chapter 4 in the form of a comparison and suitability of analysis methods to a specific situation to assess strength and damage limit states.

The report wraps up with chapter 6 which presents the conclusions and recommendations for further areas of research based on this thesis respectively.

Detailed calculations made in chapter 4 have been included in relevant appendices attached towards the end of the report and have been recalled suitably.

2. Fundamentals of Seismic Structural Behaviour and Analysis

The scope of this chapter is to provide a comprehensive review of the information relevant for this thesis. The section begins with a brief background information on the origin of induced earthquakes in Groningen field. Subsequently, fundamental differences between the characteristics of induced earthquakes are compared with naturally occurring tectonic earthquakes in terms of duration, peak ground accelerations and frequency content of the input seismic signal. This section will be followed by a detailed overview of the behavior of unreinforced masonry structures which forms a major portion of characteristic structures in the Netherlands. The predominant failure modes of URM structures when subjected to lateral seismic loads will be elaborated. This is considered important to understand the structural capacity to resist seismic demands imposed by the earthquakes. Figure 2.1. shows typical Dutch masonry typologies.

Figure 2.1 a) Terraced b) Semi-detached c) Detached d) Labourers cottage [5]

After a description about the commonly found typologies of URM constructions in the region, relevant provisions for the analysis of such structures from the design codes EN1998 and guideline NPR9998 will be elaborated. A brief understanding of the performance levels mentioned in the design codes corresponding to a reference return period of earthquakes is considered important to specify the design seismic action. Analysis methods used in Structural Engineering will be discussed to capture the impact of seismic action on the structure viz. lateral force, response spectrum, static pushover method and non-linear time history analysis.

Following the basic concepts, the performance of steel Moment Resisting Frames (MRF) and Concentrically Braced Frames (CBF) will be discussed which would serve as a guide to chapter 4 of the thesis.

2.1 Origin of Induced Earthquakes in Groningen

An earthquake results in ground shaking caused by a sudden release in enormous amount of energy in the Earth's crust. This energy may originate from different sources, such as dislocations of crust, volcanic eruptions, or even by artificial explosions or the collapse of underground cavities, such as mines [6]. Earthquake occurrence can be explained by theory of 'plate tectonics' in the following way: The surface beneath the Earth is composed of plates, or large and stable slabs, which forms the crust, lithosphere and the upper mantle. These slabs, or tectonic plates, are in a state of continuous sliding one over the other and there is a relative movement between different plates. Large forces take place at the edges of these tectonic plates and results in build up of stress. These highly stressed plate boundaries results in straining of the rocks and seismic energy is released in the form of an earthquake when these plates are no longer able to bear the strains. These normally occur at a depth of several tens of kilometers and sometimes at even several hundred kilometers. This theory provides a simple and most general explanation for naturally occurring tectonic earthquakes contributing almost 95% of worldwide seismic energy release [6] but mostly confined to locations where these plate boundaries occur.

As mentioned above, seismic energy can also be released in the form of earthquakes triggered by human activity, henceforth called induced earthquakes. This human activity is pertained to gas extraction in the Groningen region of the Netherlands. The structure containing Groningen gas reservoir is an NNW-SSE trending high formed by natural faulting during the late Jurassic to early Cretaceous [7]. The reservoir is covered by Late Permian Zechstein carbonate, anhydrite and halite evaporated which provide an excellent seal. The Groningen gas field covers an area of approximately 900 km^2 and is located below a relatively densely populated area with some 250000 houses including several urban centers. The average thickness of the gas-bearing sandstone is 100m (approx.). Nearly 1800 larger and smaller faults have been mapped in the region based on the available 3D seismic cube tracking [8].

The gas is extracted from sandstone layer at a depth of nearly 3 km from the earth's surface. Cumulative extraction of gas causes a reduction in reservoir pressure and subsequent differential compaction in the layers. This compaction of layers manifests itself as surface subsidence and leads to faulting thereby, resulting in induced earthquakes. Detailed study behind the topography and geology of the Groningen field is beyond the scope of this thesis. The reader is referred to a vast amount of research available from geology point of view.

While the subsidence in Groningen field was accelerating due to an increased rate of gas production, induced seismicity started to occur with the first production induced earthquake with a local magnitude (M_L of 2.4 at Middlestum in 1991. Even though this magnitude of the event was, seismologically speaking, not high, intensities as high as VI were observed because of shallow depth of the event and soft surface soil layers in the area [10] causing damage to the masonry houses.

1986	First induced earthquake observed in North-Netherlands (Assen M= 2.8)
Early '90	Multidisciplinary Study (1993) concluded: "Gezien de resultaten van het onderzoek naar de relatie tussen gaswinning en aardbevingen komt de commissie tot de slotsom dat onder bepaalde omstandigheden aardbevingen het gevolg zijn van gaswinning." "Given the results of the research into the relationship between gas production and earthquakes, the committee concludes that under certain circumstances earthquakes are caused by gas production."
1995	Seismic network operational
1995	KNMI estimates a maximum magnitude for Groningen: M_{max}= 3.3
1995	Agreement between NAM, Groningen and Drenthe on damage claim handling
1997	Roswinkel earthquake with M= 3.4
1998	KNMI adjusts estimate of maximum magnitude: M_{max}= 3.8-4.0
2001	Establishment of Tcbb (Technische commissie bodembeweging)
2001	Alkmaar earthquakes with M= 3.5 and M= 3.2
2003	Technisch Platform Aardbevingen (TPA) established
2004	KNMI adjusts estimate of maximum magnitude: M_{max}= 3.9
2004	First Probabilistic Seismic Hazard Analysis by TNO and KNMI
2006	Westeremden earthquake with M= 3.4
2009	Calibration study by TNO (Damage analysis)
2011	Deltares assesses the Building Damage in Loppersum and confirms M_{max}= 3.9
2012	Huizinge earthquake with M= 3.6
2012	Launch of Study and Data Acquisition Plan Induced Seismicity Groningen
2013-16	Launch of several compensation schemes for local residents
2015	NAM transfers handling of damage claims and strengthening of houses to newly founded Centrum Veilig Wonen
2015	Dutch Safety Board issues report and recommendations

Figure 2.2 Timeline of events before and after the earthquake of 16th August 2012 in Huizinge [9]

2.2 Fundamental Differences: Induced vs Tectonic Earthquakes

Following a brief introduction from previous section about the origin differences in induced and tectonic earthquakes, this section focuses on the characteristic differences between the two types. Broadly speaking, the two differ in terms of magnitude, and frequency content of the seismic signal. An important difference is the depth of hypocenter (figure 2.3) and duration of the signal. This duration of seismic signal influences the potential damage to structures on the surface. The location below the earth's surface where the earthquake originated is called the hypocenter, and the location directly above it on the surface is the epicenter [11].

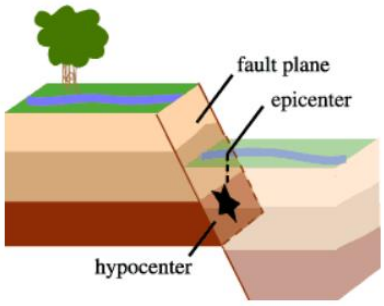

Figure 2.3 Definition of hypocentre and epicentre of an earthquake [11]

Recent studies by conducted by [12] either concludes or assume that the Ground Motion Prediction Equations (GMPE's) derived from tectonic and human-induced earthquakes are comparable for similar magnitudes and hypocenter distances after specifically calibrating them for shallow and small seismic events. However, the difference in the structural response to tectonic and induced earthquakes has not been widely assessed in the past. This is an important aspect since the structural response depends on various other parameters as well, in addition to PGA and response spectra, and has direct/indirect implications on the seismic design, damage claims and government local guidelines.

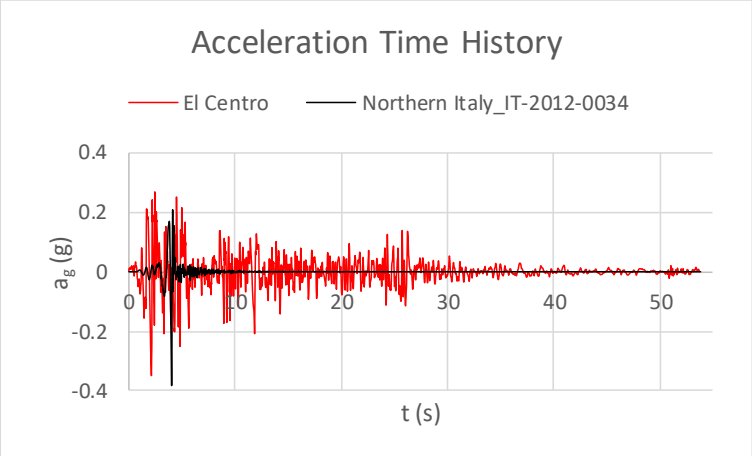

Figure 2.4 Accelerogram for a scaled shallow depth earthquake compared with El Centro ground motion

Figure 2.4 shows typical differences between the magnitude of ground acceleration and duration of seismic signal of the horizontal component of a) short duration scaled signal of a shallow event from Italy (event ID IT-2012-0034, ESM Database) and b) historical EL Centro ground motion. The ground motion duration is an important seismological charateristic for the assessment of seismic demand. Structural members and systems subjected to repeated cycles of strong motions become increasingly vulnerable to damage. For ductile structures responding beyond their elastic limits, the magnitude of permanent deformations depends on how the ground shaking is sustained [6].

The frequency content of input ground motions is equally important in influencing the dynamic response of structural systems. When the frequency content of a predominant earthquake ground motion closely matches the natural period of a structural system, the dynamic response is significantly enhanced and thus may cause severe damage [13]. Hence, it makes absolute sense to evaluate the frequency bands of ground motions. A fast fourier transform is applied to a seismic recording, that decomposes it into the frequencies it is consisted of. Figure 2.5 and 2.6 shows frequency domain representation of the above discussed two types of earthquakes [adopted from TU Delft tool from lectures on Structural response to Earthquakes, CIE5260].

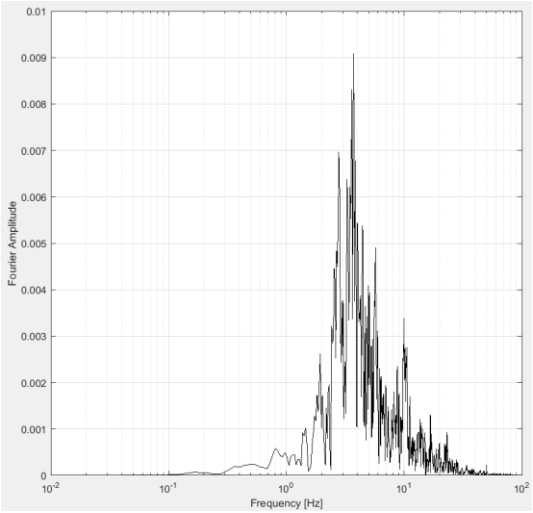

Figure 2.5 Fourier transform of a shallow Induced Earthquake (Huizinge, 2012)

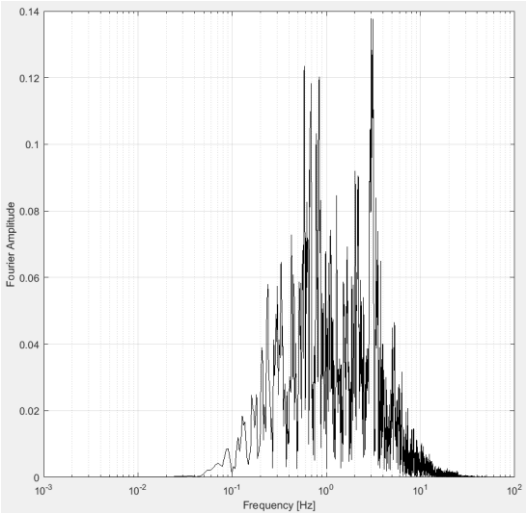

Figure 2.6 Fourier transform of a deep Tectonic Earthquake (Iniskin, Alaska, 2016)

These two specific events show typical differences in the fourier amplitude and the concentration of peaks in the band of frequencies. In the case of a shallow event, the maximum amplitude is concentrated in a narrow range of frequencies whereas for a tectonic event, it is well distributed in a wider range. It has implications on the analysis in a way that there is relatively narrow range of structures that respond in the frequency with a peak fourier amplitude that are severely affected as a consequence. A higher energy is transmitted to the structure responding in the same frequency in a short duration of time. On the contrary, there is wide range of affected structural frequencies in the event of a deep tectonic earthquake.

Another important parameter which influences the seismic behaviour of structural systems is the duration and number of cycles of the ground motion especially for low-cycle fatigue damage [6] for e.g. the fracture and buckling of steel components in a moment-resisting frame and braced frame which depends on the number of inelastic load reversals. It is, therefore, important to account for the effects of duration and number of cycles of ground motion in the structure more importantly in cases where a structure is expected to respond inelastically. A number of definitions of duration of an earthquake have been proposed by researchers (Housner, 1965, Trifunac and Brady, 1975, Novikova and Trifunac, 1994). The most commonly adopted definition is the term Significant duration which is defined as the time intervals over which a portion of the total energy integral is accumulated. It is generally calculated between the 5% and 95% of the arias intensity of the ground motion record i.e.

$$\mathrm{AI} = \frac{\pi}{2g}\int_0^{t_r} a^2\,(t)\,dt \qquad (2.1)$$

Where a(t) is the acceleration record and t_r is the total duration of the accelerogram. Figure 2.7 shows the difference in the significant duration of the above discussed two types of ground motions. As a critical point, for equal accelerations, greater duration is more damaging, whereas for equal energy release, shorter duration presents a greater seismic hazard since the amount of energy transmitted to a structure takes place in a short duration of time due to high number of load reversal cycles.

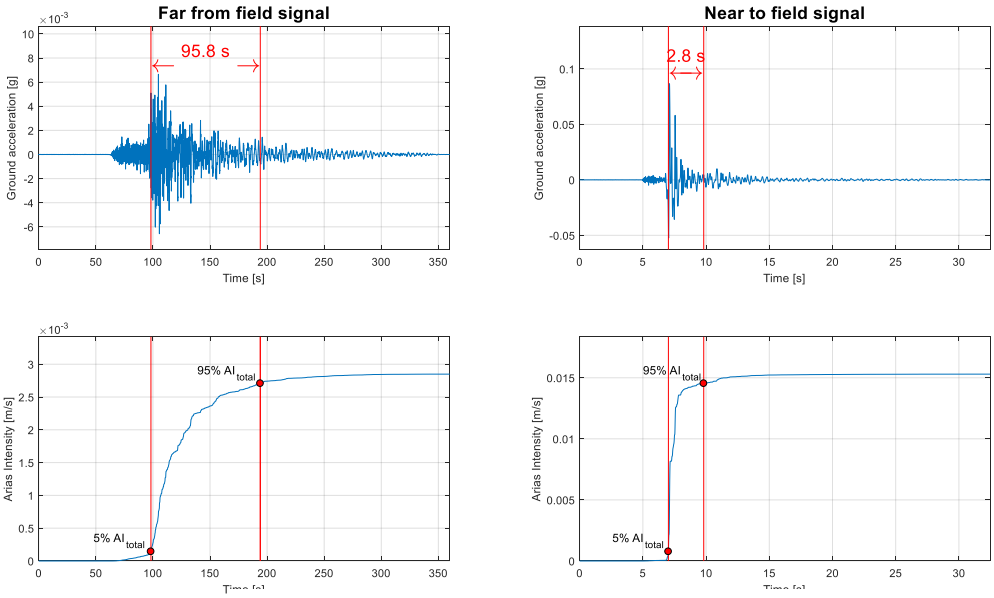

a b

Figure 2.7 Significant duration of a) tectonic earthquake b) shallow induced earthquake

2.3 Typical Characteristics of Affected Structures

Before moving further towards the analysis methodologies, it is imperative to understand the stock of building and infrastructure available in the Groningen region of the Netherlands which is affected by induced earthquakes and led to large-scale research projects across the country. Primarily, unreinforced masonry type construction is prevalent in the area. A large number of residential buildings, further categorized as terraced houses, semi-detached, detached, cottages, mansions and villas, can be found in the Groningen region. Typical representation of these types can be observed in figure 2.1. The predominant presence of terraced houses, which are two-storied units built in series, see figure 2.8, forming a building block, with floor diaphragm usually realized in concrete or wood, are found to be the most vulnerable to earthquakes as these were not designed following seismic regulations.

Figure 2.8 A typical Dutch masonry terraced house

The abundance of masonry construction stems from the following facts: easy availability of constituent material (bricks or stones, mortar), easy erection and overall economy in construction. The finished product acts as a single unit when bricks (or stones) are laid in a

specific arrangement (or bond) and bound together by means of a binding material, mortar. This arrangement of bricks bounded by mortar makes masonry a composite material and the mechanical properties are dependent on the type of bricks and mortar specifications. It is suitable to carry compressive loads; however, the shear and tensile strength is relatively low [14].

2.3.1 Seismic Behavior of URM Buildings

As a part of seismic assessment and retrofitting of existing URM buildings, it is important to understand the potential seismic deficiencies and failure hierarchy of these buildings and their components [15]. The most commonly found seismic deficiencies in the kind of structures include inadequately restrained elements at a height, unrestrained parapets, chimneys, gable end walls and façade elements. In the event of an earthquake, these are usually the first ones to fail and pose a serious risk to community extending well outside the building premises.

Following the hierarchy, the next most critical elements are face-loaded walls, their connection to diaphragms and return walls. Though their failure may not lead to a structure's catastrophic collapse, they may pose a severe threat to life safety.

The failure modes of URM buildings can be broadly classified as:

- Local failures – toppling of parapets, walls (not carrying joists) subjected to face load, falling materials from damaged in-plane walls.

- Global failures – include failure modes leading to total collapse of a structure due to loss of load path and deficient structural configuration.

The primary cause of commonly observed damage patterns is the low tensile strength of bricks and mortar. Both shear and flexural stresses develop as a result of low tensile strength of these materials. Typical failure typologies observed in URM buildings are shown in figure 2.9. Lateral forces parallel to the plane of the wall i.e. in-plane forces cause tensile stresses and diagonal cracking whereas forces perpendicular to the plane of the wall i.e. out-of-plane forces cause flexural stresses, rocking of the wall in case of flexible diaphragms and exhibit cracking.

The in-plane seismic demand on walls of a URM building decreases up the height as well as the capacity also decreases due to decrease in the vertical (stabilizing load). In contrast, out-of-plane demands are greatest at the upper level of walls due to higher accelerations, however, the out-of-plane capacity is lowest due to a lack of vertical load on them. It is for this reason that toppling of gable walls starts from the top unless there is a rigid connection of these walls with the diaphragm. Figure 2.10 shows the out-of-plane behaviour of a masonry wall as a function of its height.

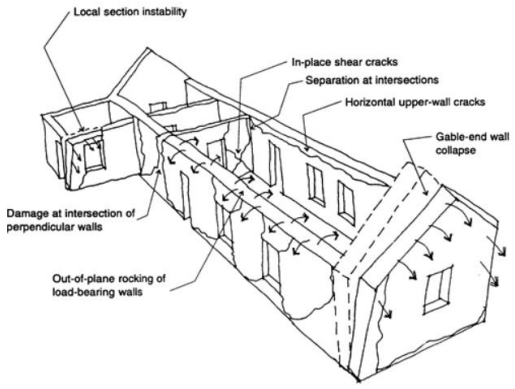

Figure 2.9 Typical failure modes of a URM building [16]

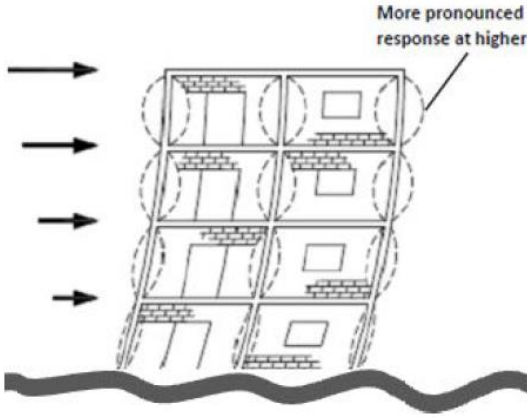

Figure 2.10 Out-of-plane behaviour of masonry wall as a function of its height [17]

Walls subjected to face-loads

One of the major causes of failure of masonry buildings is the out-of-plane loaded wall collapse under face load, particularly when timber floor and roof are supported on these walls. The seismic performance of URM face-loaded walls depends on the type of diaphragm and connections between wall-diaphragm and wall-wall. Figure 2.11 elaborates the seismic response of out-of-plane loaded walls related to type of diaphragm (flexible or rigid) and wall-diaphragm connections.

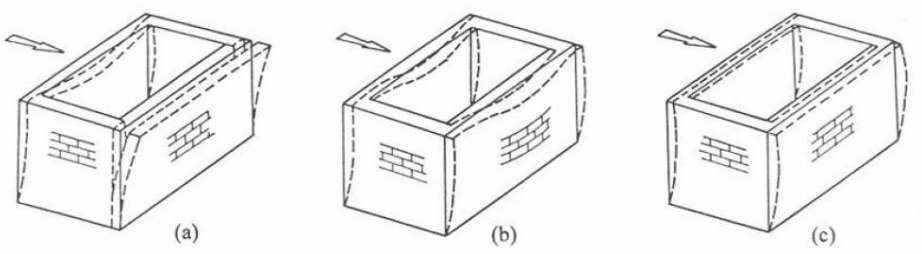

Figure 2.11 Effect of diaphragm type on face-loaded walls a) poor wall-wall connection and no diaphragm, b) good wall-wall connection and flexible diaphragm, c) good wall-wall connection and rigid diaphragm [15]

Figure 2.12 shows typical failures of URM buildings related to collapse of face-loaded walls. In the left figure, one can observe the out-of-plane instability of wall subjected to face loads due to lack of positive ties between face-loaded wall and rest of the building. The figure on the right shows a typical collapse mechanism of a gable end wall with a difference in response when it is adequately attached to the roof or ceiling which can survive lateral seismic loading.

Cavity wall which is yet another common feature observed in URM typologies of structures in Groningen region can be particularly vulnerable to face-loading. There have been several cases of severe structural damage and collapse of this kind of construction in other parts of the world as well. Particularly, the outer-leaf of a cavity wall has a potential to topple during a seismic event and depends on the slenderness ratio, poor or degraded ties, tie flexibility, pull-out failure of ties due to weak mortar bed, or absence of ties at all.

Figure 2.12 Typical failure patterns of an out-of-plane loaded wall subjected to face loads. [18]

Walls subjected to in-plane loads

In-plane loaded walls are typically the shear walls loaded in a direction parallel to wall length due to seismic effects. In-plane URM walls are less prone to damage as compared to out-of-plane loaded walls due to stocky elements (walls, piers and spandrels). This is because the spectral displacements are insignificant compared to member dimensions along the length. The predominant modes of failure include sliding, rocking of walls or individual piers, diagonal tension cracking, toe crushing or a combination of these. Figure 2.13 shows typical in-plane failure modes of a URM wall section.

In-plane masonry walls can be either penetrated or unpenetrated. A wall which is penetrated consists of piers between the openings and spandrel below and above the openings. Rocking mode of URM piers results in crushing of pier end zones and delamination of bricks if the mortar is weak. Figure 2.13 right shows one such situation [19]. Sliding shear of a particular mortar course can occur over a limited length in walls with moderate to low axial forces.

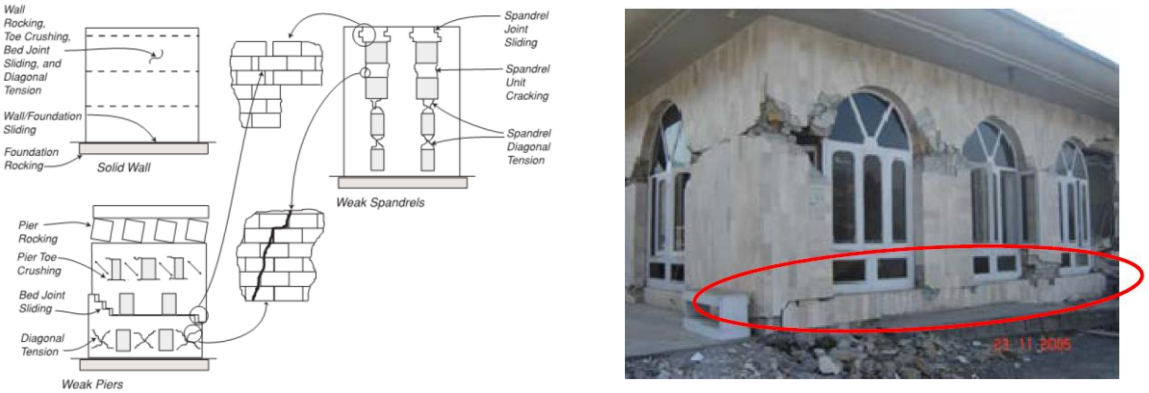

Figure 2.13 Typical failure modes of an in-plane loaded URM wall [20]

Another typical type of damage, observed in long and squat piers and on the bottom storey of buildings, is diagonal tension cracking, also known as X-shaped cracking (figure 2.14) when tensile stresses in piers exceed the tensile strength of masonry which is inherently low. In the case of penetrated walls, where spandrels are weak as compared to piers, spandrels may damage catastrophically turning squat piers into slender piers (figure 2.15) resulting in reduction of wall capacity with increased deflections. The increase in deflection elongates the fundamental period of vibration of the structure and reduce seismic demands, which in a way seems a mitigating effect, even though the effect of failure of spandrels and overall life safety needs to be considered. It is essential to determine the displacement demands imposed by the earthquake and compare it with the capacity of the structure.

Figure 2.14 X-shaped cracking in slender URM piers [21]

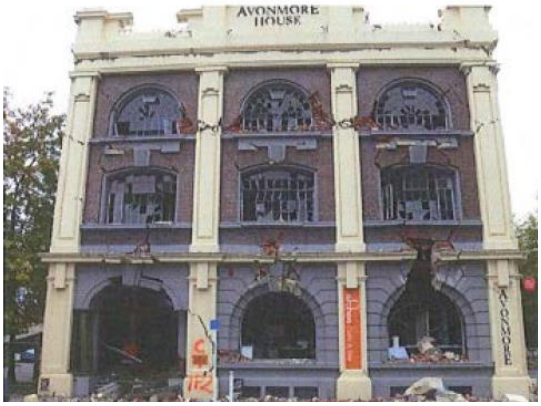

Figure 2.15 Failure of spandrels resulting in slender piers [21]

Diaphragms

Most commonly used material for diaphragms in URM buildings is timber which is flexible and may result in large diaphragm displacements during a seismic action. This will impose large displacement demand on the supporting face-loaded walls and could lead to failure as shown in figure 2.16.

Figure 2.16 Out-of-plane wall failure due to excessive roof diaphragm displacement [22]

Connections

The following types of typical damage to wall-diaphragm connections have been observed in the past earthquakes [23]:

- punching shear failure of masonry
- yield or rupture of connector rod
- rupture at joint between connector rod and joist plate
- splitting of joist or stringer

- splitting or fracture of anchor plate
- yield or rupture of threaded unit

The opening-up of connections between the face-loaded and return walls after a few cycles of seismic loading occurs as a result of stiffness incompatibility between flexible face-loaded walls and stiff in-plane loaded return walls. This results in loss of flange effect and softening at the junction leading to change in the dynamic characteristics of walls and piers. While it results in considerable damage to the wall fabric, it does not necessarily lead to catastrophic damage.

Another critical component is the wall-floor or wall-roof connections. Figure 2.17 shows typical components of such a connection and failure modes are outlined in the beginning of this section. Punching shear failure of the wall (as shown in figure 2.18) is characterised by failure of mortar bed and head joints around the perimeter of the anchor plate. For such a type of connection in the case of a cavity wall, it is possible that the failure extent on the interior wall surface covers a broader area.

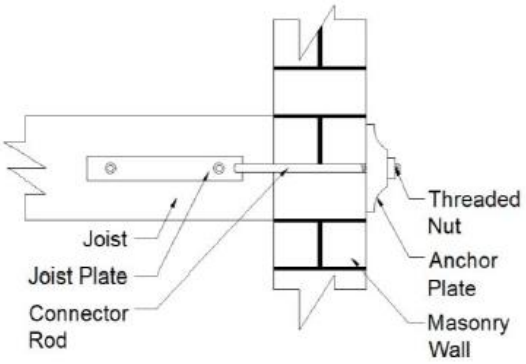

Figure 2.17 Components of wall-floor assembly [23]

Figure 2.18 Punching shear failure of wall at anchor plate [23]

2.3.2 Summary of Failure Mechanisms

The previous section discussed the behavior of URM buildings subjected to lateral seismic loading and the same can be termed as quasi-brittle at the material level where micro cracks grow in to a network of cracks before collapse occurs. This section summarizes the primary types of failure mechanisms associated with URM walls. As a part of the main load-bearing system, masonry walls are expected to sustain lateral loading without collapse and transmit the loads to the foundation system through stiff in-plane walls which acts as a fundamental load path for transmission of loads to the foundation. At the same time, the connection between adjacent walls, the boundary conditions and the cyclic seismic forces cause the perpendicular walls to act as out-of-plane loaded as well. The mechanisms that lead to failure of the face-loaded wall is called *I mode collapse mechanisms* and it should be prevented to activate the in-plane resistance of walls. The in-plane resistance of walls is much higher than face-loaded walls, and the associated failure mechanisms are so called *II mode collapse mechanisms*.

The most common failure modes of URM structures can be summed up as:

- In-plane failures

- Out-of-plane failures
- Combination of in-plane and out-of-plane failures
- Lack of anchorage
- Poorly designed connections
- Failures related to diaphragm

The out-of-plane failures, or mode I mechanisms, can be classified as bending (one-way or two-way) and corner mechanisms which, in addition to the way in which load is applied, also depends on the boundary conditions along its edges. The in-plane failures, also mode II mechanisms, generally recognized includes rocking of wall-elements, sliding along bed joints, toe crushing and diagonal tension. Mode I mechanism related to out-of-plane failure of a URM wall, even though a local phenomenon, may lead to global collapse if the wall supports joist beams or the roof of a building. The key performance indicator of such a type of wall depends on its connection with other structural elements. As highlighted in the previous section, seismic demands are more pronounced at upper levels of a building structure, whereas the flexural capacity is lower due to a lack of vertical stabilizing load on top. Nevertheless, several studies [24] includes evidences which show that masonry walls acting out-of-place performed better in comparison to their expected seismic resistance. This suggests that investigations on material resistance model (or strength approach) should not be the limiting approach for assessment of face-loaded walls. Rather, this issue needs to be addressed as a stability problem, where geometrical non-linearities allow advantage to be taken of the wall's displacement reserve capacity.

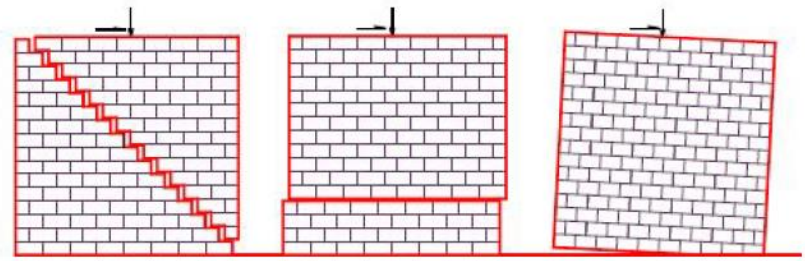

Figure 2.19 In-plane failure mechanisms (Mode II) – Shear, Sliding and Flexure failures [25]

2.4 Force and Displacement based Seismic Design

From structural engineering point of view, the primary objective of performing seismic calculations is to either design a new building which will sustain a design seismic action, or to assess the structural capacity of an existing building to achieve specific performance level when it is subjected to design seismic loads. Traditional approach for design as well as assessment of a structure has been based on the comparison of design action with the respective member resistance i.e. $E_d < R_d$ which forms the basis of many international codes and guidelines. The strength of structural members, calculated based on stiffness considering the initial geometric properties of the elements, is checked with the resulting design forces. Therefore, the stiffness considered is independent of the strength. In real situation, this is not the case. Detailed analysis, and experimental evidence shows that this assumption is invalid, in a sense that stiffness is essentially proportional to strength for a given section [26]. In order to differentiate the force-based and displacement-based design, it is essential to examine the two methods in detail and appreciate the importance of analysis on the basis of displacement.

Even though the current force-based design methodology is considerably improved when compared with the past, there are still fundamental problems associated with the procedure particularly when it is applied to masonry and reinforced concrete structures. Figure 2.20 briefly reviews the force-based design procedure which is currently adopted in modern seismic design codes. The description below is a simplified representation of current force-based design.

The first step includes estimation of structural geometry, including the member sizes. Based on the preliminary member sizes, member elastic stiffness is estimated which can be either for uncracked section or reduced section stiffness to reflect the softening caused by cracking and depends on assumptions made by a specific seismic design code. The computed (or estimated) member stiffness is then used to calculate the fundamental period(s) of vibration, either equivalent SDOF or multi-modal dynamic analysis approach which in its fundamental form is given by the expression:

$$T = 2\,\pi\,.\sqrt{\frac{m_e}{K}} \tag{2.2}$$

where m_e: effective seismic mass (conveniently taken as total mass);

In seismic codes, for e.g. NPR9998, EN1998-1, the fundamental period is given in terms of height dependency, which is independent of member stiffness, geometry or mass distribution. However, this is just a simplified assumption to estimate fundamental time period. In practice, it is always recommended to perform modal analysis, as will be shown in chapter 4, which can yield significant differences thereby affecting seismic demands.

$$T_1 = C_t.H^{\frac{3}{4}} \tag{2.3}$$

where:
C_t: depending on the structural system, is 0.085 for moment resistant space steel frames, 0.075 for moment resistant space concrete frames and 0.050 for all other structures;

Once the fundamental period(s) of the structure is determined, seismic base shear force, F_b, for each direction in which the building is analysed, is determined using the following expression (EN1998-1):

$$F_b = S_d(T_1).m_e\,.\lambda \tag{2.4}$$

where:
$S_d(T_1)$: ordinate of acceleration design spectrum (discussed in section 3.2);
T_1: fundamental period of vibration for lateral motion in the direction considered;
m_e: total mass (or effective seismic mass), above the foundation or top of a rigid basement;

λ: correction factor, which is equal to: $\lambda = 0.85$, if $T_1 \leq 2T_c$ and the building has more than two storeys or $\lambda = 1.0$ otherwise.

The effect of elastic force reduction on account of ductility is explicitly taken into account by using a q-factor approach in Eurocodes corresponding assessed ductility capacity of the structural system. In general, the design base shear force can be found as:

$$F_{b,d} = \frac{F_b}{R_\mu} \tag{2.5}$$

The seismic design base shear, thus computed, is distributed to different storeys in a structure by approximating fundamental mode shapes by horizontal displacements increasing linearly along the height as outlined in section 2.4.1.

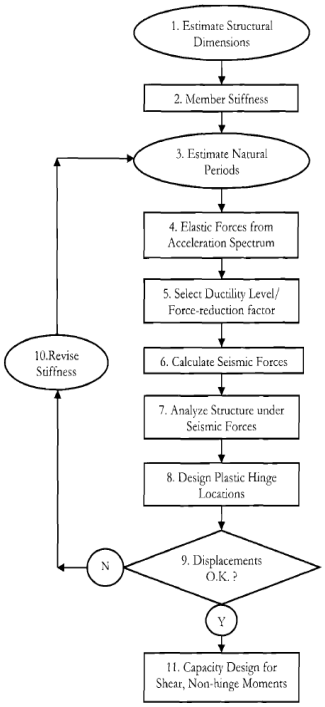

Figure 2.20 Simplified force-based analysis [26]

The vector of lateral seismic forces is then used to analyse the structure and required moment capacities at potential locations of inelastic action (plastic hinge formation) is determined. Structural design of members at plastic hinge locations is carried out, and corresponding rotations/displacements are estimated. The computed displacements are then compared with code-specified guidelines and accordingly checked if redesign is required. Once the displacements are satisfactory, a capacity-based design is the last step to evaluate the actions and compare them with the member strength.

To list a few problems associated with force-based seismic design methods, firstly, selection of appropriate member stiffness. The member sizes are assumed first to determine the seismic forces acting on the structure which are then distributed among these members based on the assumed element stiffness. If member sizes are modified at a later stage, these calculated member forces will no longer be valid, and recalculation is required, which is rarely carried out in practice and makes the process an iterative one.

Regardless of what assumption is made in the beginning for initial member stiffness, it is assumed independent of the strength, refer figure 2.21a for a moment-curvature relationship.

$$El = \frac{M_N}{\varphi_\gamma} \tag{2.7}$$

where M_N is the moment capacity and φ_γ is the yield curvature considering equivalent bi-linear representation of above moment-curvature relationship. The assumption, as highlighted above, of constant initial member stiffness implies that the yield curvature is essentially proportional to flexural strength. Detailed analysis, and experimental evidence show that this assumption is invalid, and the stiffness is essentially proportional to strength and yield curvature is essentially independent of strength, for a given section (refer 2.21b) [26].

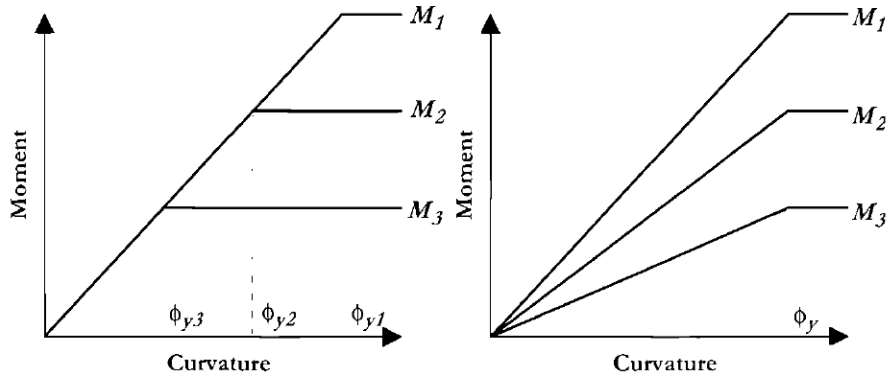

Figure 2.21 (a) Force-based: Constant Stiffness (b) Displacement-based: Constant yield curvature [26]

Hence, the stiffness which is considered as the main parameter in force-based approach, is not a function of member strength, which is the end-product of calculations. In force-based design approach, a force-reduction factor (or q-factor) is employed to account for the inelastic response of system subjected to seismic forces, leading to a decrease in the structural stiffness proportional to increase in deformations. However, this approach of reducing the elastic forces in proportion to the force-reduction factors has been shown to be an inappropriate one, as this approach is based on the assumption that the inelastic response of a system subjected to seismic loading is equivalent to the elastic response of the same system under the influence of reduced forces, which may not be true in case of dissipative structures like masonry.

Secondly, significant variations in the calculated time-periods can result following different considerations of member stiffness. The approximate height dependent relationship (eq. 2.6) can differ significantly when compared to the actual time-period calculated using modal analysis. Although, it might be a conservative approach to adopt a lower time period in seismic design (acceleration on the plateau), strength is seldom an issue than the displacement capacity. A lower time period would mean a lower displacement demands and hence, non-conservative.

Next, the force-reduction factors and ductility demand cocept on which simplied behaviour factor approach is based on, has a varied range of existence. For example, with a wide choice of appropriate definition of yield and ultimate displacements in the literature, there exists a considerable variation in the assessed ductility capacity of the structures leading to wide bracket of force-reduction factors for a given framing arrangement. It becomes essential to evaluate these factors using non-linear methods for a given geometry to substantiate the adopted one.

In lieu of these few mentioned shortcomings, the importance of displacement-based methods in seismic assessment of structures has come out to be better appreciated amongst the research community.

2.5 Seismic Analysis (Linear & Non-Linear)

Following the study in the previous sections related to seismic behaviour of structures in the elastic and inelastic regime, this section provides a brief state of the art analysis methods employed in design & assessment of structures to seismic actions. The current Performance-based seismic design (PBD) is an extension of the classical Limit State Design (LSD) where in the latter philosophy, design action E_d is compared to the design strength R_d, in PBD the seismic demand (D) which is imposed by an earthquake is compared to structural capacity (C) which are interrelated quantities. The demands which an earthquake imposes on the structure is, nevertheless, highly uncertain in terms of seismic hazard, site response, structural material, response idealization models etc., and for the same reason, an estimation of the seismic behaviour is made rather than deterministic approach. An optimization is made in terms of structural capacity based on the consequences of seismic action corresponding to a reference return-period of an earthquake.

The following figure 2.22 shows a summary of analysis methods adopted & recommended by literature as well seismic design & assessment codes which will be dealt further in detail in this section.

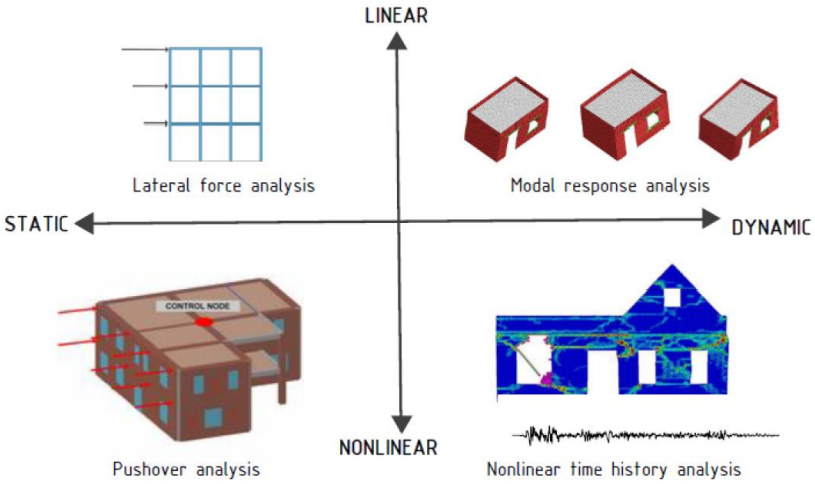

Figure 2.22 Linear & Non-Linear Seismic Analysis methods

The methods can be summarized as below in increasing order of complexity:

1. Lateral Force Analysis – Linear Static
2. Modal Response Spectrum Analysis – Linear Dynamic
3. Pushover Analysis – Non-Linear Static
4. Non-Linear Time History Analysis – Non-Linear Dynamic

Even though modal response spectrum analysis is termed as linear dynamic, principally the structure is analysed with static loads, the term dynamic originates from the method it uses to compute structural time period and mode shapes as well as solving the equation of SDoF system at each time instant to obtain response spectrum from seismic accelerogram. The following sections deals with the explanation and application of these methods to seismic analysis of structures. Before moving to particular sections, it is important to recapitulate basics related to dynamics of structures which forms the basis to seismic analysis. Figure 2.23 shows a single degree of freedom system model with a mass-spring-dashpot having parameters m, k and c respectively subjected to a ground acceleration $\ddot{u}_g$.

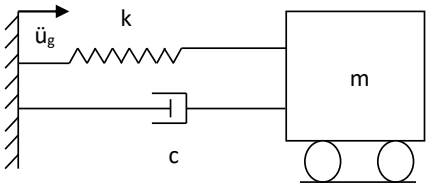

Figure 2.23 Single Degree of Freedom system idealization

The equation of motion of such a system in terms of relative displacements to the ground can be written in the following two identical forms:

$$m\ddot{u} + c\dot{u} + ku = -m\ddot{u}_g \tag{2.8}$$

$$\ddot{u} + 2\xi\omega_n\dot{u} + \omega_n^2 u = -\ddot{u}_g \tag{2.9}$$

where:
u is the displacement of mass m relative to the ground;
$\ddot{u}_g$ is the ground acceleration;
ω_n is the fundamental natural frequency of vibration given by, $\sqrt{(k/m)}$;
ξ is the damping ratio, expressed as a percentage of critical damping.

The structural response to ground acceleration can be computed using numerical methods, such as Newmark numerical integration, at each time instant during the recorded accelerogram. Once the response history to a specific seismic signal is computed, response quantities, for example displacements, base shear, bending moments can be computed to be combined with other action effects as per EN1990-1.

The relative displacement response of a system, initially at rest i.e. u(0) = $\dot{u}$(0) = 0, subjected to a known ground acceleration $\ddot{u}_g$ can be calculated using Duhamel's integral by:

$$u(t) = -\frac{1}{\omega_D}\int_0^t \ddot{u}_g(\tau)\exp(-\xi\omega_n(t-\tau))\sin(\omega_D(t-\tau))d\tau \tag{2.10}$$

where
$\omega_D = \sqrt{(1-\xi^2)}$ is the damped natural frequency of the system

Analysing the above equation, the response of this linear SDoF system, putting aside $\ddot{u}_g$, is governed by two parameters:

- the natural period of vibration, $T = 2\pi / \omega_n$
- damping ratio, ξ

The above discussion naturally implies that the response of all SDoF systems, with same T & ξ, subjected to a particular component of ground motion would be same. This forms the basis for response spectrum approach employed in earthquake engineering. A response spectrum is a plot of the peak value of a response quantity as a function of natural period T and the damping ratio ξ of a linear oscillator [13]. Further, depending on the response quantity chosen, it refers to Displacement response spectrum, Velocity response spectrum and Acceleration response spectrum. This concept has been dealt in more detail in chapter 3 of this report. For now, seismic analysis methods will be elaborated in a way they are employed for design and assessment of structures subjected to seismic loading.

2.5.1 Lateral Force Analysis

The simplified procedure, also known as linear static approach, has been developed for systems with multiple degrees of freedom corresponding to multiple storeys, where beams are considered rigid axially as well as in flexure and the shear building assumption is adequate to capture the seismic force demands on the building structure. The method consists of idealizing such a structure in a generalized SDoF system having generalized system properties (mass, stiffness & force) in the following form:

$$\ddot{u} + 2\xi\omega_n\dot{u} + \omega_n^2 u = -\Gamma\ddot{u}_g \tag{2.11}$$

where:
$\omega_n^2 = \sqrt{(\tilde{k} / \tilde{m})}$ is the natural vibration frequency of the system;
$\tilde{m} = \sum m_i \cdot \psi_i^2$; ψ refers to coordinate of an appropriate shape function chosen to reflect the deflected shape.

$$\tilde{k} = \sum k_i \cdot (\psi_i - \psi_{i-1})^2 \tag{2.12}$$

$$\Gamma = L / \tilde{m} \tag{2.13}$$

$$L = \sum m_i \cdot \psi_i \tag{2.14}$$

The generalized response u(t) subjected to a specified ground motion (or design spectrum) can be determined. The floor displacements relative to the ground can be found as follows:

$$u_{i,max} = \psi_i \cdot u_{max} = \psi_i \cdot \Gamma \cdot D \tag{2.15}$$

where D is the spectral ordinate from displacement response spectrum corresponding to natural frequency of generalized SDoF system. The above equation can be re-written, with S_{ae} as elastic spectral acceleration, as:

$$u_{i,max} = \psi_i \cdot \Gamma \cdot (S_{ae} / \omega_n^2) \tag{2.16}$$

The equivalent static forces, F_i associated with floor displacements and corresponding total base shear, F_b can be evaluated as:

$$F_i = k_i \cdot u_{i,max} = \psi_i \cdot m_i \cdot \Gamma \cdot S_{ae} \tag{2.17}$$

$$F_b = \sum F_i = \tilde{L} \cdot \Gamma \cdot S_{ae} \tag{2.18}$$

From the above two expressions, the applied static force at each floor level j, can be expressed in terms of total base shear.

$$F_i = \Gamma \cdot S_{ae} \cdot \psi_i \cdot m_i = (F_b / \tilde{L}) \cdot \psi_i \cdot m_i \tag{2.19}$$

$$F_i = F_b \cdot \frac{\psi_i \cdot m_i}{\sum \psi_i \cdot m_i} \tag{2.20}$$

The above equation for static forces acting at the floor level i, in terms of base shear (F_b) forms the basis of Lateral Force Method of analysis given in design codes. The application of this method has been elaborated in chapter 4.3 of this report. For a detailed derivation of generalized parameters and equation of motion adopted in this method, the reader is referred to classical earthquake engineering textbook. Another point worth mentioning here is that the same method can be adopted for continuous systems (with distributed mass and elasticity)

which is equivalent to approximating a system having an infinite degree of freedom by a generalized SDoF system. Example of such a system includes a chimney or a wind turbine support structure.

2.5.2 Modal Response Spectrum Analysis

Also known as the linear dynamic analysis, this is the most widely adopted method in the design of earthquake resistant MDoF systems for a number of reasons, i.e. easy implementation in FEA programs, its simplicity, straightforwardness and ability to provide an insight into the dynamic behaviour of the structure. A modal analysis is carried out as a first step by solving the eigenvalue problem to obtain eigenfrequencies and eigenmodes of the corresponding undamped system. The solution is computed in the modal coordinates and the problem coupled with response spectrum for each mode is solved in the modal domain. Finally, the response is computed in the real coordinate system and combined using statistical methods to give the maximum probable forces and moments acting on the structure. In earthquake engineering, it is usually the maximum response quantities that are of interest for the design structure rather than the complete time history response since it is highly unlikely that the same response for that particular earthquake will be found for another one because each seismic event is unique. So, it makes sense to find an envelope of responses rather than the response at each and every instant of time. The procedure is brief explained below step by step.

The generic equation of motion for a uniaxial ground acceleration is:

$$\boldsymbol{M\ddot{x}} + \boldsymbol{C\dot{x}} + \boldsymbol{Kx} = -\boldsymbol{Mr}\ddot{u}_g \tag{2.21}$$

where **M**, **C** and **K** refers to the system mass matrix, damping matrix and stiffness matrix respectively, **r** is the influence vector, $\ddot{u}_g$ is the ground acceleration and **x** is the vector of displacements. This equation can be solved in multiple ways, however, we will restrict this section to modal analysis based on the modes of undamped system in the time domain. It is pertinent to highlight the fact that this method is exact for undamped systems and is approximate for damped systems using Rayleigh damping, nevertheless, it provides a considerable insight into the linear dynamic response of the system.

Step 1: Derivation of characteristic equation. The formulation of eigenvalue problem provides the characteristic equation, which governs the free vibrations of an undamped system.

$$\boldsymbol{M\ddot{x}} + \boldsymbol{Kx} = \boldsymbol{0} \tag{2.22}$$

The general solution to the above equation can be searched for in the following form:

$$\boldsymbol{x}(t) = \sum \widetilde{\boldsymbol{X_i}} \cdot exp(s_i t)\,;\; i = 1\ to\ 2N \tag{2.23}$$

Substituting in the above characteristic equation, one gets:

$$({s_i}^2\,\boldsymbol{M} + \boldsymbol{K}) \cdot \boldsymbol{X_i} = 0\ or\ (-{\omega_i}^2\,\boldsymbol{M} + \boldsymbol{K}) \cdot \boldsymbol{X_i} = 0 \tag{2.24}$$

For a non-trivial solution of the above equation, it is required that:

$$\det({s_i}^2\,\boldsymbol{M} + \boldsymbol{K}) = 0\ or \det(-{\omega_i}^2\,\boldsymbol{M} + \boldsymbol{K}) = 0 \tag{2.25}$$

The positive roots of the above equation yield the eigenfrequencies and corresponding eigenvectors can be found. It is assumed that the solution to the forced vibrations can be expressed in the following form (subscript 'i' here is the mode number):

$$\boldsymbol{x}(t) = \sum \Phi_i \cdot u_i(t)\,;\; i = 1\; to\; N \tag{2.26}$$

where
x(t) is the response vector in real coordinate system
Φ_i is the eigenvector
$u_i(t)$ is the response displacement for each mode i, which a system is composed of. It is not to be confused with u_i in previous section where 'i' stood for degree of freedom and u_i was the response displacement at degree of freedom i.

The equation of motion for undamped system subjected to seismic excitation is:

$$\boldsymbol{M\ddot{x} + Kx = -Mr\ddot{u}_g} \tag{2.27}$$

Substituting eq. 2.26 in the equation of motion 2.27 yields:

$$\boldsymbol{M\Phi\ddot{u} + K\Phi u = -Mr\ddot{u}_g} \tag{2.28}$$

Pre-multiplying the above equation by Φ^T yields:

$$\boldsymbol{\Phi^T M\Phi\ddot{u} + \Phi^T K\Phi u = -\Phi^T Mr\ddot{u}_g} \tag{2.29}$$

Using the orthogonality property of modes and the fact that modal mass and stiffness matrices are diagonal, the derived equation of motion can be written as:

$$\boldsymbol{M\ddot{u} + \Omega^2 Mu = -\Phi^T Mr\ddot{u}_g} \tag{2.30}$$

The above equation of motion can be written in a scalar form for each modal coordinate u_i:

$$m_{ii}^*\ddot{u}_i + m_{ii}^*\omega_i{}^2 u_i = -L_i\ddot{u}_g \tag{2.31}$$

or in an equivalent way as:

$$\ddot{u}_i + \omega_i{}^2 u_i = -\Gamma_i\ddot{u}_g \tag{2.32}$$

where
$\omega_i{}^2 = k_{ii}{}^* / m_{ii}{}^* = \Phi_i{}^T \boldsymbol{K}\Phi_i / \Phi_i{}^T \boldsymbol{M}\Phi_i$

$\Gamma_i = L_i / m_{ii}{}^* = \Phi_i{}^T \boldsymbol{Mr} / \Phi_i{}^T \boldsymbol{M}\Phi_i$

The term Γ_i is called the modal participation factor, which is the most widely adopted in earthquake engineering practice. The response to the equation in modal coordinate with zero initial conditions can be found with the application of Duhamel's integral as outlined before:

$$u_i = \frac{1}{\omega_i}\int_0^t \Gamma_i\,\ddot{u}_g(t)\sin\big(\omega_i(t-\tau)\big)\,d\tau \tag{2.33}$$

Once the response in terms of modal displacements are obtained using above method, the response in real coordinate system, as defined earlier, can be written as:

$$x(t) = \sum \phi_i . u_i(t); i = 1 \; to \; N \tag{2.34}$$

Each vibration mode activates a certain portion of total mass of the system which is defined as modal mass. Naturally, the sum of mass corresponding to each mode of vibration of the system is equal to total mass. Thus,

$$m_i \; = \; \Gamma_i \; \cdot \; \mathrm{L}_i \; = \; {\mathrm{L}_i}^2 \; / \; {m_{ii}}^* \; = \; ({\Phi_i}^T \boldsymbol{Mr})^2 \; / \; {\Phi_i}^T \boldsymbol{M} \Phi_i \tag{2.35}$$

and,

$$m_{total} \; = \sum m_i \; ; i = 1 \; to \; N \tag{2.36}$$

The truncation of the number of modes to be considered in determining the response of system in the real coordinates depends on the mass participation criteria. Eurocode 8 recommends the truncation of modal contribution based on the following criteria:

$$\sum m_i \; \geq \; 0.90 \, m_{total}$$

Analysis using Response Spectrum Method

The theory outlined above forms a basis for calculation of linear dynamic response using response spectrum analysis in a step-by-step manner as described below (adopted from Lecture Notes CIE5260, Apostolos Tsouvalas, 2017 [39]):

1) Derive the design response spectrum. This spectrum gathers all peak responses of a SDoF oscillator of a certain period T_i and certain damping "ξ_i". The spectra differ in different applied directions of seismic excitation.

2) Solve the eigenvalue problem of the MDoF system to obtain the eigenfrequencies ω_i and normalized eigenmodes Φ_i. This step follows transformation of the actual equations of motion to the modal domain.

3) For each modal DoF, the peak response quantity is obtained. This can refer to displacements, forces or moments.

4) Once the individual responses are obtained, statistically combine the individual response to find the probable peak response. If multiple directions are involved, statistically combine individual responses along each direction.

The equation of a MDoF system reads:

$$\boldsymbol{M\ddot{x}} \; + \; \boldsymbol{C\dot{x}} + \boldsymbol{Kx} \; = \; -\boldsymbol{Mr}\ddot{u}_g \tag{2.37}$$

which when transferred to modal coordinates u_i, results in decoupled set of N equations:

$$\ddot{u}_i \; + \; 2\xi_i \omega_i \dot{u}_i \; + \; {\omega_i}^2 \; = \; -\Gamma_i \ddot{u}_g \; ; \; i \; = \; 1 \; to \; N \tag{2.38}$$

The seismic input is provided in terms of a response spectrum, which gives the maximum response of an SDoF system with time period (T_i) and damping ratio (ξ_i), the maximum displacement for each modal coordinate u_i can be computed as:

$$\max|u_i(t)| = u_{i,max} = |\Gamma_i \,.\, S_d(T_i, \xi_i)| \tag{2.39}$$

where $S_d(T_i, \xi_i)$ is the ordinate of displacement response spectrum for (T_i,ξ_i). If the seismic input is given in the form of a pseudo-acceleration response spectra, $S_d(T_i, \xi_i)$ shall be replaced with $S_a(T_i, \xi_i)$ /$\omega_i{}^2$.

Thus, by knowing the solution in terms of modal displacement response computed using the design response spectrum, it is possible to calculate the response due to this particular mode in the real coordinates as below:

$$\max|x_i(t)| = x_{i,max} = |\phi_i \,.\, u_{i,max}| = |\Gamma_i \,.\, \phi_i \,.\, S_d(T_i, \xi_i)| \tag{2.40}$$

Once the displacement response in the real coordinate system has been computed, the forces acting at a certain degree of freedom j, corresponding to a certain mode i, can be calculated as per the procedure explained below:

1) Calculation of the vector of forces per mode,

$$F_i = K \cdot x_{i,max} = \Gamma_i \cdot S_d(T_i, \xi_i) \cdot \boldsymbol{K} \cdot \phi_i \tag{2.41}$$

Using the characteristic equation: $\boldsymbol{K}\phi_i = \omega_i{}^2 \boldsymbol{M}\phi_i$, we get,

$$F_i = \Gamma_i \cdot S_d(T_i, \xi_i).\omega_i{}^2.M \,.\, \phi_i = \Gamma_i \cdot S_a(T_i, \xi_i) \cdot \boldsymbol{M} \cdot \phi_i \tag{2.42}$$

In a scalar form, the same equation for force acting at the degree of freedom "j" for mode "i" reads:

$$F_{ji} = \Gamma_i \cdot S_a(T_i, \xi_i) \,.\, m_j \,.\, \phi_{ji} \tag{2.43}$$

2) The force thus calculated above is finally applied to the structural modal mass at "j" and peak stresses are calculated following a static analysis of the structure.

Modal combination rules

The response spectrum approach described above provides the peak response for each corresponding vibration mode i, i.e. $x_{i,max}$. However, it is of interest to determine the total maximum response at a degree of freedom j which considers the contribution of response from different modes using statistical methods described in this section. This is so because the individual modal response obtains their peak at different time instants. Thus, these combination rules, does not yield the exact response, estimate the likelihood of a peak response. The most commonly used statistical combination rules are elaborated briefly:

1) Absolute Sum (ABSSUM)
It is assumed that all the maxima (absolute value) corresponding to different modes occur simultaneously i.e.

$$x_{max} = \sum |x_{i,max}| = \sum |\Gamma_i \,.\, \phi_i . S_d(T_i, \xi_i)| \tag{2.44}$$

This method specifies an upper bound of maximum response since it is highly unlikely that all the modes peak at the same time, i.e. x(t) ≤ x_{max}. It is rarely applied in practice due to its conservatism.

2) Square Root of Sum of Squares (SRSS)
The rule can be explained with the following expression:

$$x_{max} = \left(\sum (x_{i,max})^2\right)^{0.5} = \left(\sum (\Gamma_i \,.\, \phi_i . S_d(T_i, \xi_i))^2\right)^{0.5} \tag{2.45}$$

Accurate estimates of the actual maximum response are obtained using this method with well-separated eigenfrequencies.

3) Complete Quadratic Combination (CQC)
For closely spaced eigen frequencies, this rule can be explained as:

$$x_{max} = \left(\sum_{i=1}^{N}\sum_{j=1}^{N} \rho_{ij}\, x_{i,max} x_{j,\max}\right)^{0.5} \tag{2.46}$$

where ρij is a correlation coefficient. Variour researchers have contributed to the calculation of this coeffiecient, Rosebleuth-Elorduy equations (1971), Der Kiureghion equations.

Section 2.5.2 outlines the Modal Response Spectrum Analysis method to determine the response of MDoF systems subjected to seismic input in the form of response spectrum. The analysis is reduced to a series of static analysis corresponding to each vibration mode to obtain the response spectrum quantities $x_{i,\ max}$ which are subsequently combined statistically to obtain x_{max}. The required dynamic analysis is carried out in the form of obtaining response spectra for all possible values of (T_i, ξ_i) which is then used to calculate the modal response. It is important to stress on the fact that this method is applicable to linear-elastic systems (force-displacement relationship is linear) and non-linear behaviour of the system is considered using a behaviour factor (q-factor in EN1998). While it becomes necessary to consider non-linear behaviour of the structural system when one shifts the focus to performance-based design which is discussed in the next section.

2.5.3 Non-Linear Static Pushover Analysis

Non-linear Static Pushover Analysis (for brevity, called POA) has gained considerable attention in the recent past due to its fast and easy implementation in predicting the seismic performance of existing structures as well as new constructions designed for a specified level of ground motion as compared to non-linear time history analysis (NLTHA) although latter is the most accurate approach. Linear methods discussed in the previous sections are based on the linear elastic structural behaviour and fail to capture the structural performance in the non-linear regime. Also, the expected damage in quantitative terms cannot be predicted. POA

offers the ability to provide estimates of the expected inelastic deformation demands and to help identify design flaws that otherwise are not captured by linear methods [28].

The non-linear seismic performance can be predicted in its simplied form by using a simplified structural model, a generalized SDoF system, combined with the seismic input in ADRS (Acceleration Displacement Response Spectrum) format. It assumes that the response of a structure is governed primarily by its fundamental mode (neglecting the effects of higher modes of vibration) and a MDoF can be converted to an equivalent SDoF system having generalized parameters, followed by subjecting it to a monotonically increasing load representing seismic inertial forces experienced by the structure. At each incremental load step, roof lateral displacement (Δ) and corresponding base shear (V) is recorded and the output of POA is a V-Δ plot. A bi-linear form of this plot is converted to S_a-S_d (spectral acceleration-spectral displacement) format, known as capacity spectrum, and the performance of a structure is directly compared with ADRS to obtain seismic effects imposed on the structure. Figure 2.24 shows a step-by-step procedure of carrying out POA analysis.

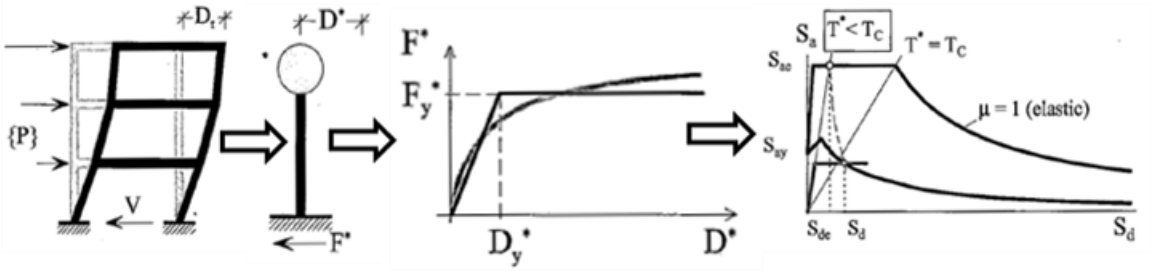

Figure 2.24 Simplified procedure to perform non-linear static pushover analysis

As much as the advantages of carrying out POA, the reliability of this method can be reduced by certain limitations. The first one being the choice of static load pattern. It is likely that the chosen load pattern favors certain deformation modes triggered by the load pattern and miss out others that are initiated by ground motion and inelastic dynamic response characteristics of the structure [29]. An example being a weak top story for which an invariant load pattern will lead to concentration of inelastic deformations in that story and may not initiate deformations in other stories of the structure. A good judgement is needed in selecting an appropriate load pattern. The second one being assumption of fundamental mode response of the structure. For a low-rise structure, this assumption would be correct, but the reliability reduces when higher modes of vibration also contribute to the dynamic behaviour of the structure. Also, during incremental lateral loads, changes in the structure properties (stiffness) is not explicitly taken into account.

The N2 method of pushover analysis to determine the non-linear performance of the structure, developed by [29] and also implemented in EN1998 consists of the following procedure:

- A pushover analysis is performed based on a chosen lateral load pattern (either a uniform load or based on fundamental mode of vibration) to obtain base shear-roof displacement plot.
- The obtained pushover curve is transformed to a bi-linear capacity curve and the time-period corresponding to elastic leg of the curve is determined (T^*). The procedure to bi-linearize the curve is that elastic leg of the curve should intersect the pushover curve at ~0.6 times the proposed yield point and the area under the curves should be

same to follow equal energy principle. Figure 2.25 shows the application of these rules.

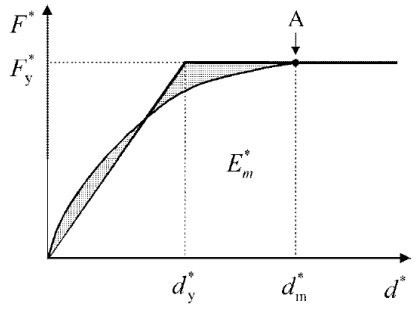

Figure 2.25 Procedure to bi-linearize the capacity spectrum

- Calculation of target elastic displacement using $d_{et}^* = S_e(T^*) \cdot \left[\frac{T^*}{2\pi}\right]^2$ in which $S_a(T^*)$ is the elastic spectral acceleration corresponding to the time-period T_e of the equivalent SDoF system.

  a) For $T^* < T_c$ (short-period): if $\frac{F_y^*}{m^*} \geq S_e(T^*)$, the response of equivalent SDoF is elastic and $d_t^* = d_{et}^*$ else;

  if $\frac{F_y^*}{m^*} \leq S_e(T^*)$, the system response non-linear and

  $d_t^* = \frac{d_{et}^*}{q}\left[1 + (q-1)\,\frac{T_C}{T^*}\right] \geq d_{et}^*$

  b) For $T^* > T_c$ (medium and long-period): $d_t^* = d_{et}^*$

- The performance of the structure is determined by comparing the target displacement d_t^* with d_m^* which is the point of formation of a plastic mechanism.

2.5.3.1 Performance Levels for Assessment

The performance of a structure during seismic action is based on assessment of limit states of damage for a specific return period (probability of exceedance in a certain period of time), thus achievement of a seismic capacity target. The three limit states as defined for this purpose in EN1998-3 are the Near Collapse (NC), Significant Damage (SD) and Damage Limitation (DL) analogous to the ones defined in FEMA356 [31] guidelines Collapse Prevention (CP), Life Safety (LS) and Immediate Occupancy (IO) respectively. These limit states are explained briefly below:

Limit State of Near Collapse (NC): The structure is heavily damaged with low residual strength and stiffness. Vertical elements are still capable of sustaining gravity loads and most non-structural elements have collapsed. Large permanent drifts are present. This level is achieved corresponding to a seismic action with probability of exceedance of 2% in 50 years (i.e. a return period T_r = 2475 years)

Limit State of Significant Damage (SD): The structure is significantly damaged with some residual strength and stiffness. Vertical elements are capable of sustaining gravity loads and moderate permanent drifts are present. The structure is likely to be uneconomic to repair. Seismic action corresponding to a 10% probability of exceedance (T_r = 475 years) is considered to achieve this LS.

Limit State of Damage Limitation (DL): The structure is lightly damaged with significant yielding of elements in the structure and still retain strength and stiffness properties. Non-structural elements like infill and partitions, may show distributed cracking but it is possible to economically repair the structure. There are no permanent drifts. This level is achieved corresponding to a seismic action with probability of exceedance of 20% in 50 years (i.e. a return period T_r = 225 years)

The following tables adopted from EN1998-3, Appendix B recommends rotation and deformation capacities for beams/columns and braces in tension and compression corresponding to achievement of a particular level of limit state.

Table 2.1 Plastic rotation capacity at the end of beams or columns

	Limit State		
Cross section class	DL	SD	NC
1	1.0 θ_y	6.0 θ_y	8.0 θ_y
2	0.25 θ_y	2.0 θ_y	3.0 θ_y

Table 2.2 Axial deformation capacity of braces in compression

	Limit State		
Cross section class	DL	SD	NC
1	0.25 Δ_c	4.0 Δ_c	6.0 Δ_c
2	0.25 Δ_c	1.0 Δ_c	2.0 Δ_c

Table 2.3 Axial deformation capacity of braces in tension

Limit State		
DL	SD	NC
0.25 Δ_t	7.0 Δ_t	9.0 Δ_t

where:

θ_y: chord rotation at yielding for steel members [31]

$\theta_y = \frac{W_{pl} f_y l_b}{6EI_b}$ for beams

$\theta_y = \frac{W_{pl} f_y l_b}{6EI_b}\left(1 - \frac{P}{P_y}\right)$ for columns

The performance of a structure can be evaluated based on limiting values of plastic rotations and axial deformations corresponding to achievement of a target limit state.

3. Analysis of Seismic Input

The present chapter in this report necessitates from the importance in understanding how the seismic input for carrying out analysis using different methods outlined before is generated which is of significance to structural engineers. The seismic signals recorded in the form of accelerograms (ground acceleration versus time) serve as an input along with solving the basic dynamic equation of motion of a single degree of freedom system at each instant of time forms the basis of elastic response spectrum which fundamentally is provided by design codes in its simplified form for a specified level of hazard. The following sections starts with the response spectrum in its fundamental form.

3.1 Development of Response Spectrum

The concept of response spectrum stems from the need to provide seismic input in a clear and concise form without having to deal with analyzing complex ground motion records every time for performing linear analysis for e.g. lateral force method and modal response spectrum analysis. Since each seismic event is unique (in terms of frequency content, time period, peak ground acceleration), the use of response spectrum for a recorded ground motion in the past for seismic assessment or design of new constructions is inappropriate. The jagged response at a particular site is essentially characteristic of a unique event and may not necessarily match another event recorded at the same site in terms of peaks and valleys at same time periods. This is an apparent observation in figure 3.1 [13] which shows the response spectra (normalized to PGA) for the horizontal component of ground motions recorded at same seismic station, El Centro, California.

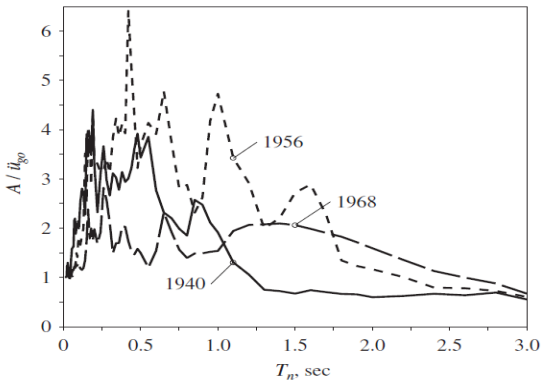

Figure 3.1 Response spectra for different events recorded at same site

So, it is practically impossible to predict the jagged response spectra for a ground motion that may occur in the future based on individual responses recorded. Therefore, the characteristics of design spectra should be such that it consists of a set of smoothened lines for a particular level of damping and should in a general way, be representative of the ground motions recorded for past earthquakes. In the event of non-availability of such records, ground motions representative of a similar site condition at other site could be used provided factors such as magnitude, seismic fault-site distance (near/far), faulting mechanism and local soil conditions should be matched.

The first step in obtaining a design response spectrum is selection of an ensemble of response spectra for ground motions with similar characteristics. For a particular ground motion record,

one can obtain the response in the following way starting with the equation of motion and corresponding response using Duhamel's integral of a SDoF system:

$$\ddot{u} + 2\xi\omega_n\dot{u} + \omega_n^2 u = -\ddot{u}_g \tag{3.1}$$

$$u(t) = -\frac{1}{\omega_D}\int_0^t \ddot{u}_g(\tau)\exp(-\xi\omega_n(t-\tau))\sin(\omega_D(t-\tau))d\tau \tag{3.2}$$

Closely observing eq. 3.2 shows that except for the ground motion amplitude $\ddot{u}_g$, the response u(t) depends on the system damping ratio ξ and time-period of vibration ($T_n = 2\pi/\omega_n$) which are characteristic for a system. Following this, the concept of response spectrum evolved which is defined as a plot of peak value of a response quantity as a function of natural vibration period [13]. It provides a means to summarize the peak response quantity of all possible SDoF systems subjected to a particular component of ground motion.

A plot of maximum obtained response using above steps as a function of T gives a response spectrum for the given damping ratio. Repeating the previous steps for a varying ξ now, one can obtain a series of such curves with varying level of damping. Figure 3.3 and 3.4 shows respectively the displacement response spectrum and pseudo-acceleration response spectrum for a horizontal ground motion component of El Centro earthquake (figure 3.2), plotted for various levels of damping ratio. An expected trend can be observed in the response that highly damped systems respond less as compared to lightly damped systems. A MATLAB script written to obtain the response spectrum was used and is attached in Appendix I. The response spectrum concept can be extended, in a similar way, to obtain pseudo-velocity and pseudo-acceleration response spectrum, the difference lies in the plotted response quantity against time-period. These quantities can be obtained from spectral displacement (S_d) using the following relations:

$$S_a = \omega_n^2 \cdot S_d \tag{3.4}$$

$$S_v = \omega_n \cdot S_d \tag{3.5}$$

The reason behind plotting response spectrum in different formats is that different response quantities can readily give peak deformation (S_d), peak strain energy stored in the system (S_v) and equivalent static inertial forces (S_a) acting on the system. The spectral quantity of interest can be determined from above plots corresponding to relevant time-period and the structural system can be solved just like a system imposed to static loads. The complex dynamic analysis has already been performed in computation of spectral response parameters and structural modal characteristics. This is the essence of linear-dynamic analysis methodology (response spectrum analysis).

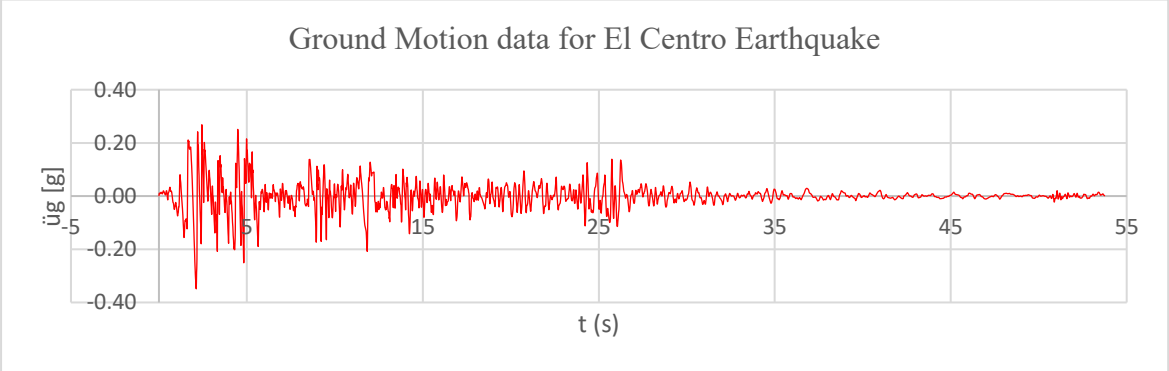

Figure 3.2 Horizontal ground motion component of El Centro earthquake, California

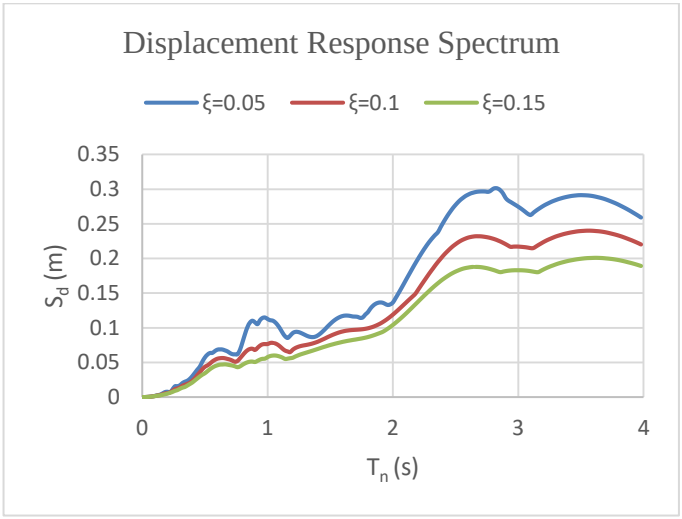

Figure 3.3 Displacement response spectrum for El Centro Earthquake

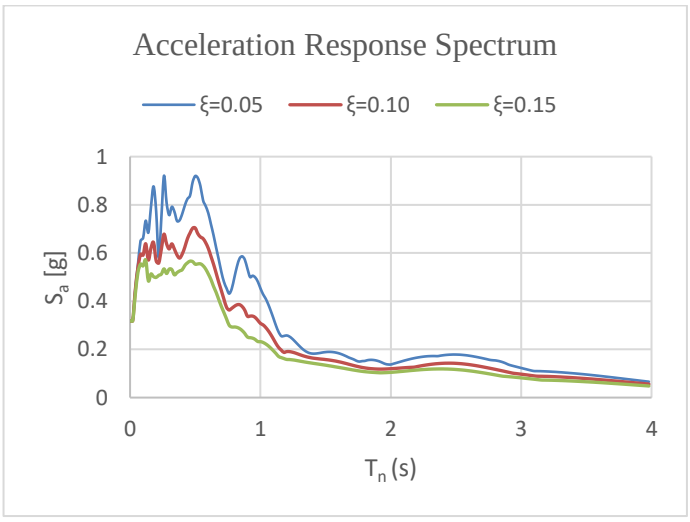

Figure 3.4 Pseudo-acceleration response spectrum for El Centro earthquake

Observing figure 3.4, it is seen that for all levels of damping, pseudo-acceleration approaches PGA at T~0 s. The trend can be seen to follow the reasoning that for a fixed mass system, time period in the vicinity of zero means that the system is extremely stiff because of which the deformation is small, and the mass moves rigidly with the ground; i.e. the response

acceleration is equal to PGA of the ground motion. On the contrary, for a long period structure, the system is extremely flexible for a fixed mass. While the ground moves, the system is expected to remain stationary; i.e. response acceleration is close to zero and structure is expected to follow the peak ground displacement.

Once jagged response spectra for a set of ground motions is obtained using the procedure elaborated above, probability distribution corresponding to each time period is calculated with its mean and standard deviation (σ) values. Connecting these mean spectral values provide mean response spectrum and with mean plus one standard deviation, one obtains mean+1σ response spectrum as seen in figure 3.5 based on data from an ensemble of shallow events scaled to a common PGA of 0.32g recorded in Italy, provided by European Strong Motion database. The design spectrum thus obtained is much smoother as compared to the response spectrum of individual ground motions. It is easier to idealize such spectrum in to a series of straight lines which forms a basis for equations provided in design codes. Various researchers have provided procedures to linearize the design spectrum [30] considering amplification based on local soil factors.

This section outlined the construction of elastic design spectra based on the principles of structural dynamics however, modern methods involve probabilistic seismic hazard analysis (PSHA) considering the rate of seismic activity in a region, zonation of the field based on concentration of earthquakes in a region and development of Ground Motion Prediction Equations (GMPE) resulting in a uniform hazard spectrum. Such approach is adopted for

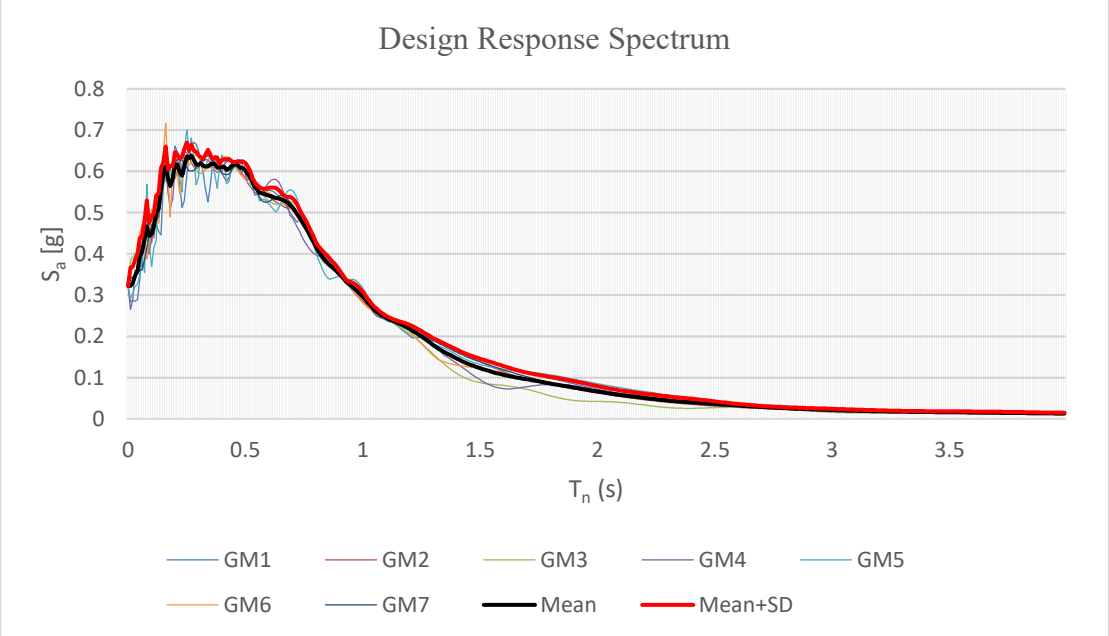

Figure 3.5 Design response spectra from an ensemble of ground motions for near-fault ground motions [European Strong Motion Database]

derivation of site-specific response spectra in the Groningen gas field. The latest GMPE v2 model developed by KNMI introduces a laterally varying site response model which includes non-linear site amplification functions [Probabilistic Seismic Hazard Analysis for Induced Earthquakes in Groningen, Update June 2016, Jesper Spetzler and Bernard Dost, KNMI, de Bilt]. Following the shallow geology of the region, non-linear site amplification effects were

accounted for by considering a lateral varying shear-wave model for the upper 350m based on soil topography.

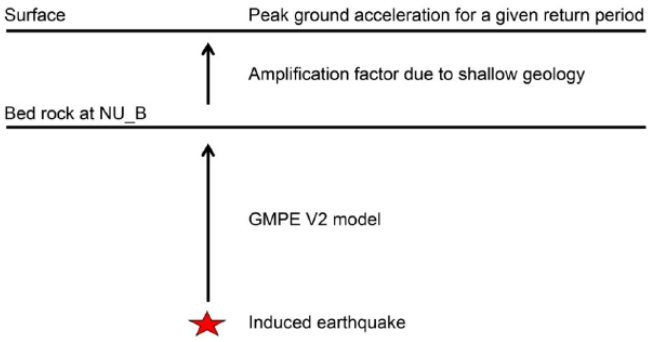

Figure 3.6 Methodology adopted for development of ground motion spectrum in Groningen region [KNMI]

The methodology adopted for obtaining ground motion corresponding to a certain level of hazard adopted by KNMI a two-step as illustrated in figure 3.6. First, the hazard curve at ~350 m reference bedrock depth is calculated considering the contribution of induced earthquake over a certain zone and magnitude group. As a second step, the peak spectral acceleration at the surface level is obtained by convolution of probability density function of spectral accelerations at reference level with the corresponding probability density function of site amplification factor. The result is a seismic hazard curve obtained at the ground surface for spectral acceleration including the non-linear site amplification factor.

3.2 PGA based design approach

Modern seismic design codes and regulations provide seismic input in the form of equations representing various parts of the spectra viz. constant acceleration, constant velocity and constant displacement normalized to PGA of the seismic signal with an explicit term to account for local soil conditions in the region. A comparison of such approach between NPR9998 and EN1998-1 is made in table 3.1 and a dimensionless elastic response spectrum is shown in figure 3.7.

Table 3.1 Elastic Spectral Acceleration Spectra definition

Time Period	NPR9998: 2017	EN1998-1
$0 \le T \le T_B$	$a_g S \cdot \left[1 + \frac{T}{T_B}(\eta \cdot p - 1)\right]$	$a_g \cdot S \cdot \left[1 + \frac{T}{T_B}(\eta \cdot 2.5 - 1)\right]$
$T_B \le T \le T_C$	$a_g S \cdot \eta \cdot p$	$a_g \cdot S \cdot \eta \cdot 2.5$
$T_C \le T \le T_D$	$a_g S \cdot \eta \cdot p \cdot \left[\frac{T_C}{T}\right]$	$a_g \cdot S \cdot \eta \cdot 2.5 \cdot \left[\frac{T_C}{T}\right]$
$T_D \le T \le 4s$	$a_g S \cdot \eta \cdot p \cdot \left[\frac{T_C \cdot T_D}{T^2}\right]$	$a_g \cdot S \cdot \eta \cdot 2.5 \cdot \left[\frac{T_C \cdot T_D}{T^2}\right]$

where
T: time-period of vibration of linear SDoF system;
$a_g S$: peak ground acceleration at surface level (including soil factor);
a_g: peak ground acceleration;
S: soil factor

η: damping correction factor defined as $\sqrt{\frac{10}{(5+\xi)}} \geq 0.55$ where ξ is defined in % of critical damping
T_B: lower limit of period for which spectral acceleration is constant;
T_C: upper limit of period for which spectral acceleration is constant;
T_D: time period defining the beginning of constant displacement region of the spectra;
p: ratio of spectral acceleration at constant plateau to peak ground acceleration including soil factor.

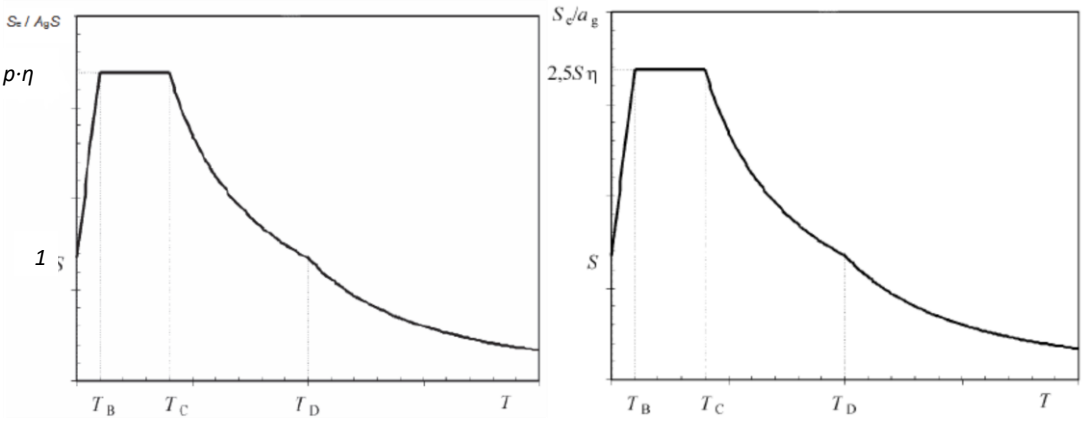

Figure 3.7 Comparison of dimensionless elastic response spectra as per NPR9998 and EN1998-1

An important observation in the two approaches to define elastic response spectrum is that whereas EN1998 specifies spectral factor of 2.5 for constant acceleration plateau, it is a variable in NPR9998 which is specific for a site under consideration ranging from ~1.6-2.3 as observed in the online webtool defined. It would be interesting to understand the origin of this variable factor but the background information towards development of NPR9998 proposed equations was not available. Secondly, soil factor is explicitly considered as factor S in EN1998 equations based on defined categories of soil whereas, the a_gS implicitly takes into account amplification effects due to local geology.

4. Case Study: Seismic Analysis & Design of a Steel Building

The outcome of this present research is the interpretation of seismic analysis results of an office steel building located in an area affected by the induced earthquakes in Groningen area of the Netherlands, to demonstrate the state-of-the-art seismic analysis methods as discussed in the previous chapters. The structure has been preliminary designed for non-seismic actions and the action effects from earthquakes have been applied to check the adequacy of this building to seismic design situation. The following sections describe in detail, description of the structure and the analysis carried out.

4.1 Description of Structure

As outlined above, the hypothetical case study structure adapted for this section is in the form of a regular steel structure office building, category B as per EN1991-1-1:2002 located near Oosterdijkshorn region of the Netherlands with a GPS (lat, lng) [°] location of 53.287405, 6.718785. Figure 4.1 shows the basic geometry of the adapted for this chapter.

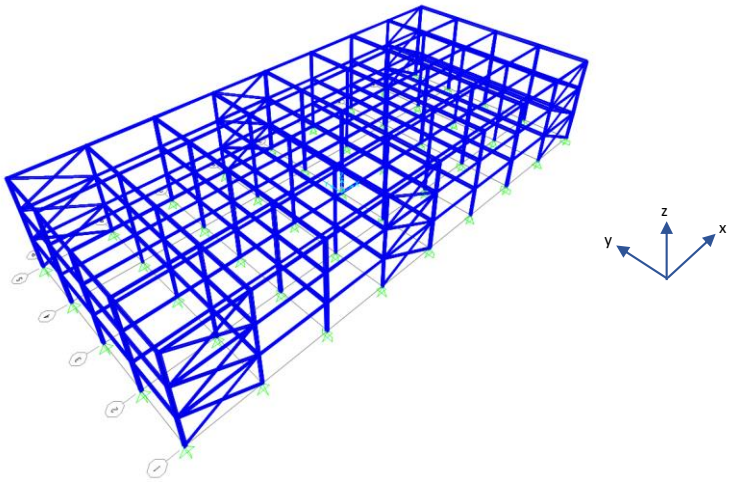

Figure 4.1 3D model of Steel Office Building (from SAP2000)

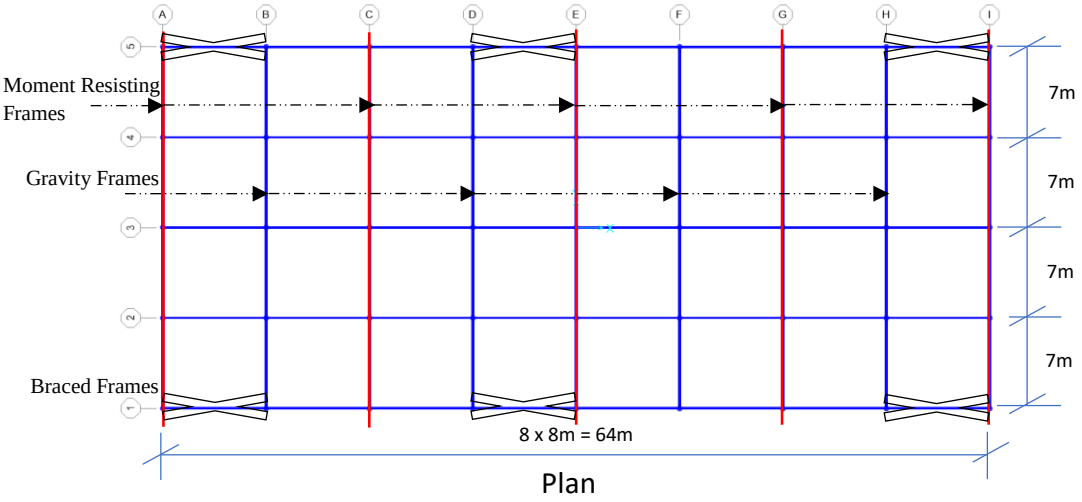

Figure 4.2 Plan of Steel Office Building

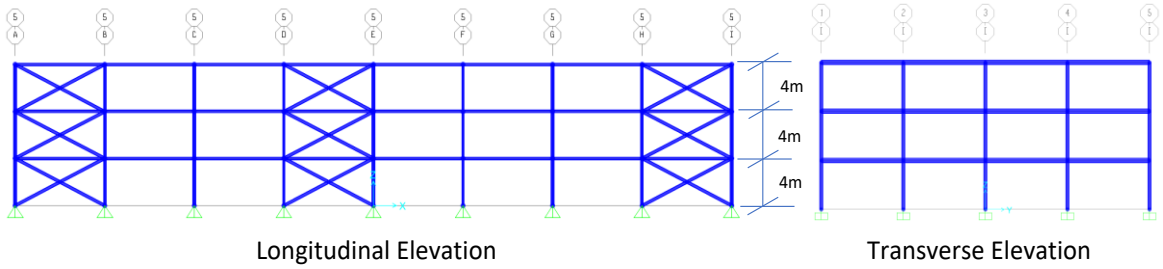

Figure 4.3 Longitudinal and Transverse Elevation

The building geometry is selected such that lateral resistance to seismic forces is provided by moment resisting frames (MRF) in the transverse direction, y and by concentric braced frames (CBF) in the longitudinal direction, x of the geometry. The structure is fixed at the foundation level in the transverse direction of MRF's and is pinned longitudinal direction. All gravity frames are pinned at the foundation level. Table 4.1 shows the summary of lateral and gravity force resisting system adopted. The structure spans 64m (8@8m) in the longitudinal and 28m (4@7m) in the transverse direction. The storey height is 4m and total height adds up to 12m above the ground level.

Table 4.1 Type of load bearing system

	Longitudinal	Transverse
Lateral Force Resisting System	Braced Grid 1: A-B, D-E, H-I Grid 5: A-B, D-E, H-I	Moment Resisting Frames Grid A, C, E, G, I
Gravity Load System	Grid B, D, F, H	

4.1.1 Loads

It is assumed that a composite concrete slab with normal weight concrete supported by a metal deck serves as the floor system. For practical purpose, ComFlor® 60 composite slab by Tata Steel construction with a slab depth of 130mm is selected supported by secondary beams spanning 8m in the x-direction and spaced 2.33m center to center on primary beams in the y-direction.

The structural dead load from this floor arrangement is estimated at 2.56 kN/m^2 with an additional 0.2 kN/m^2 for ceiling and installations. A 30mm concrete overlay with a weight of 0.75kN/m^2 is used for surfacing at the floor and roof level. The total dead load at each level is 3.51 kN/m^2.

A basic imposed load of 3 kN/m^2 is applied on level 1 and 2 and reduced to 1 kN/m^2 for roof considering accessibility for normal maintenance and repair. The reduced imposed load in seismic situation based on the factor $\psi_{E,i}$ is 0.18·3 = 0.54 kN/m^2 (EN1998 propose φ factor of 0.5 whereas NPR9998 recommends 0.6) . Glass façade elements with a dead load of 1.2 kN/m and movable partitions 2 kN/m have been considered. Based on these loads, the total dead, reduced imposed and total gravity load acting at each level is summarized in Table 4.3 for the whole building. Table 4.2 sums up gravity loads acting on the building for non-seismic design situation.

Table 4.2 Gravity Loads for the whole building in non-seismic design situation

	Dead Load (kN)		Live Load (kN)		Total Load	
Level	Story	Cumulative	Story	Cumulative	Story	Cumulative
Roof	6438	6438	1792	1792	8230	8230
2	6510	12948	6152	2715	12662	20892
1	6510	19458	6152	8867	12662	33554

Table 4.3 Gravity Loads for the whole building in seismic design situation

	Dead Load (kN)		Reduced Live Load (kN)		Total Load	
Level	Story	Cumulative	Story	Cumulative	Story	Cumulative
Roof	6438	6438	323	323	6761	6761
2	6510	12948	1108	1431	7941	14702
1	6510	19458	1108	2539	7941	22643

An important aspect to be mentioned here is the consideration of weight for movable partitions as a live load and subsequently using it with a reduced factor. Although EN1991-1-1 recommends adding movable partition weight to the imposed floor loading, it is to be acknowledged that during a seismic event, the partition itself contributes to the inertial mass of the building and therefore, should be considered as a dead load. For the present case study, recommendation from EN1991-1-1 is adopted.

4.1.2 SAP2000 Model

The office building defined in the previous section was analyzed using SAP2000 v. 20.0.0 (evaluation copy) provided by CSI America. The following considerations were made while modeling the structure:

- The columns for MRF were supported at the base which were idealized as fixed connection in the transverse direction and pinned in the longitudinal direction. All gravity frame columns were pinned at the base.
- All beams and columns were modeled as frame elements with centerline dimensions without any rigid offsets.
- The composite action of floor system with the beams was not explicitly modeled for the analysis. Load reaction resulting from secondary composite beams was applied on the primary beams considering equivalent tributary area supported.
- The rigid diaphragm action of the composite floor was ensured by constraining the nodes at a story level in the vertical direction of the model.
- A default material damping of 5% was assumed for the model.

For the planar analysis, two of the MRF's were modeled to reflect an exterior and interior frame respectively. A leaning column rigidly connected to the floor diaphragm level laterally through rigid massless truss elements was added to the frame to simulate P-Δ effects. The leaning column nodes support additional inertial mass on account of lateral support to the gravity frames during seismic motion. As it will be evident in the analysis later, this arrangement reflects the true structural behavior in a sense that stiffness modification due to P-Δ effects increase the structural modal vibration period. A simple model with leaning column added to the model is shown in figure 4.4 below.

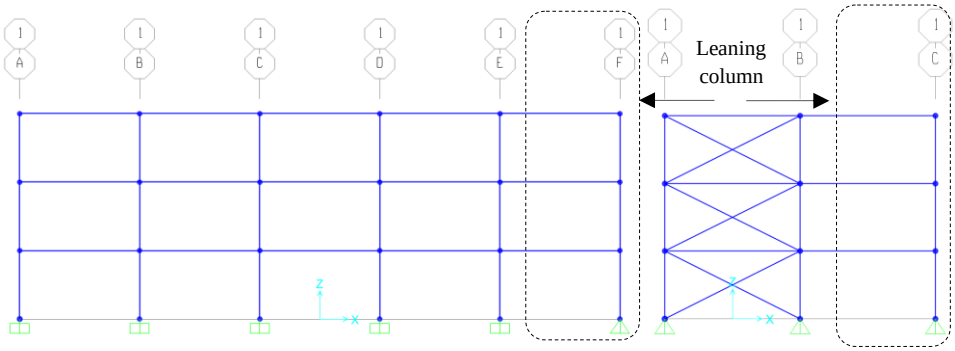

Figure 4.4 Planar analysis model with P-Δ effects included for a) MRF b) CBF

With a similar approach, one of the X-braced frames was modeled to include the P-Δ effects in the longitudinal direction of the structure. A non-linear model was run to utilize only the tension capacity of the brace when subjected to seismic loading since compression in one of the braces makes it redundant with a drop-in stiffness and strength on account of buckling. The CBF is stiff when compared to the MRF leading to a reduced time-period in the longitudinal direction and attracting much higher seismic forces.

4.1.3 Preliminary Design of the Structure

The structure was preliminary designed for the loads outlined in section 4.1.1. Figure 4.5 shows the adopted sections as a result and summarized in table 4.4. The selected sections conform to the guidelines recommended to ensure that the structural configuration possess adequate ductility justified by its behavior factor. For multi-story buildings, it has to be ensured that a soft story mechanism (shown in figure 4.6) is prevented i.e. it is required that flexural plastic hinges form in the beam element and not in the column at the joint. The same is verified from the plastic mechanisms obtained by pushover analysis. To sum up, EN1998-1 sec. 4.4.2.3 required that at all joints of primary seismic girders with primary seismic columns:

$$\sum M^{c}_{pl,Rd} \geq 1.3 \sum M^{b}_{pl,Rd} \tag{4.1}$$

Where the expression on left side of the inequality is the sum of plastic moment of resistance of the columns framing in the joint whereas the expression on the right is the sum of design values of moments of resistance of the beams framing therein. For the same material grade, the expression reduces to equation 4.2, where W_{pl} is the plastic section modulus.

$$\sum W^{c}_{pl} \geq 1.3 \sum W^{b}_{pl} \tag{4.2}$$

Table 4.4 Member profiles used in the analysis

	Column		Beam		Brace
Level	MRF	Gravity	MRF	Gravity	
R	HE300B	HE240A	IPE400	IPE240(C)	CHS168.3X4
2	HE300B	HE240A	IPE400	IPE240(C)	CHS168.3X6.3
1	HE300B	HE240A	IPE400	IPE240(C)	CHS 193.7X6.3

IPE240 (C) refers to composite beams with the deck supported slab

The framing arrangement along the transverse and longitudinal direction with above member profiles is shown in figure 4.5 below.

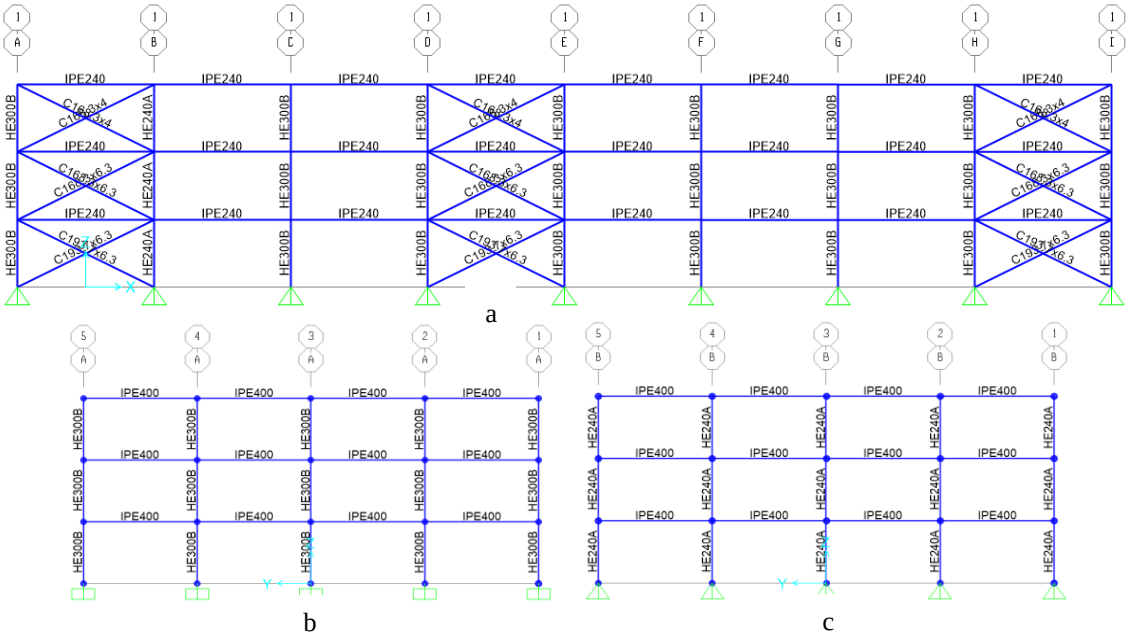

Figure 4.5 Framing member profiles for a) longitudinal frame b) moment resisting frames c) gravity frames

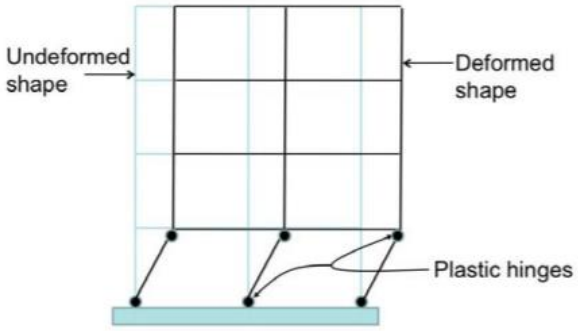

Figure 4.6 Soft story mechanism

4.2 Description of Seismic Action

Based on the location of structure as defined in section 4.1, the seismic input was chosen from NPR 9998 webtool, *http://seismischekrachten.nen.nl/webtool.php*, for a horizontal ground motion corresponding to a mean return period of 475 years represented by the following parameters:

$a_g S$ [g] 0.2259
p 1.995
T_B [s] 0.191
T_C [s] 0.372
T_D [s] 0.823

where the symbols refer to parameters defined in section 3.2 of this report. Since the actual time history of these seismic signals from this region have not been made available in the public domain, spectrum compatible ground motions can be generated based on near-fault

ground motions adopted from European Strong Motion (ESM) database. These ground motion can be spectrally matched to the pseudo-acceleration spectrum proposed by NPR9998 for this site. This step is necessary for carrying out complete time history analysis of the structure under consideration. Figure 4.7 shows the design response spectrum adopted for this study in the elastic form as well the inelastic spectrum corresponding to a behavior factor of 6.5 and 4 for MRF and CBF respectively. The q-factor approach for framing type is based on the recommendations of EN1998-1-1, table 6.2 for DCH (Ductility Class High) which is

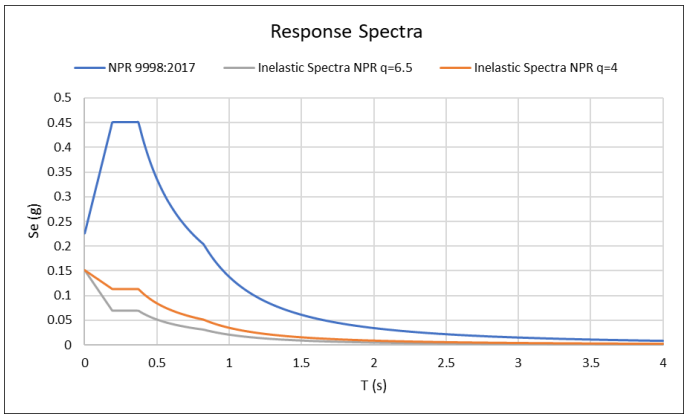

Figure 4.7 Design response spectrum for the considered site

recapped in table 4.5 below.

Table 4.5 Structural behavior factors

Structural Type	q (behavior factor)
a) Moment resisting frames	5 α_u/α_1
b) Frame with concentric bracings	4

The recommended value of α_u/α_1 is 1.3 which is used for the analysis and verified by global nonlinear static (pushover) analysis in the further sections.

For a conservative estimation of seismic forces acting on the structure, the minimum threshold of design spectral acceleration for periods of vibration, $T_C \leq T \leq T_D$ and $T_D \leq T$ is given as $\beta \cdot a_g$, which is estimated as 0.03g, where β = 0.2 is the lower bound factor for horizontal design spectrum recommended by EN1998-1.

4.3 Lateral Force Analysis

The considered building can be categorized as being regular in plan and elevation in terms of mass and stiffness distribution. It satisfies the provisions of section 4.2.3.2 of EN19998-1-1, therefore a planar structural analysis in the two considered directions of framing is permitted for the simplification purpose. However, the dynamic characteristics of the frame were verified with a 3D model of the whole structure at a later stage.

Two planar models were analyzed, one for each direction of framing, to determine the fundamental time period of vibration with and without considering a leaning column approach to demonstrate that it leads to elongation of the structural period. The results are shown in table 4.6 below including a comparison with the fundamental time determined from NPR9998 (or EN1998-1) equation 4.6, dependent on height. It can be observed that the difference is significant and leads to an over-estimation of base shear demands on the structure. The

seismic mass of the structure is based on the combination ($G + \psi_{Ei} \cdot Q$) which adds up to $2517.79 \cdot 10^3$ kg to be used for calculation of lateral force demands.

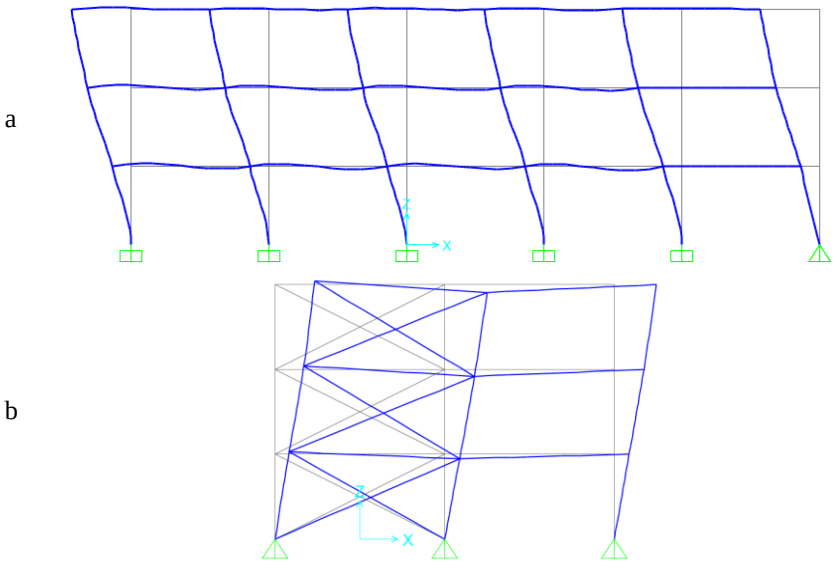

Figure 4.8 Fundamental mode shape for a) MRF b) CBF

Table 4.6 Comparison of fundamental mode time period (s)

Planar Analysis	NPR 9998 / EN1998	P-Δ excluded	P-Δ included
a) Transverse (MRF)	0.548	0.995	1.333
b) Longitudinal (CBF)	0.484	0.094	0.487

4.3.1 Base Shear force

The base shear force acting on the structure in each horizontal direction considered was determined using equation 4.5 of NPR9998 (and EN1998-1) as shown below:

$$F_b = S_d(T_1) \cdot m \cdot \lambda$$

where λ is a correction factor on accounting for the fact that the effective modal mass of fundamental mode of vibration is smaller on an average by 15% than the total seismic mass of the building. The results of calculated base shear forces are summarized in table 4.7 and compared in figure 4.9.

Table 4.7 Summary of base shear forces (kN)

Planar Analysis	NPR 9998 / EN1998	P-Δ excluded	P-Δ included
a) Transverse (MRF)	1180	741	741
b) Longitudinal (CBF)	2157	3279	2203

Note that for MRF, the seismic base shear force has the same value (741 kN) due to the lower bound spectral acceleration $\beta \cdot a_g$ adopted in section 4.2 (recommended by EN1998-1) while assessing demands using q-factor approach.

As observed from the summary of base shear forces above, it is of significance the way an

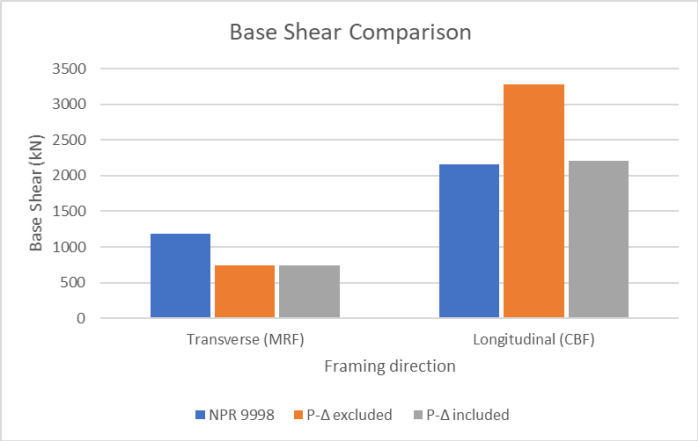

Figure 4.9 Comparison of seismic base shear forces

analysis is carried out to have a correct estimation of forces. The seismic base shear is distributed along the height of the structure by approximating the horizontal displacements increasing linearly along the height, the basis which was made in section 2.4.1 of this report. Since the analysis was made for one of the MRF and CBF for two mutually perpendicular directions, one-fifth of the force corresponding to MRF and one-sixth of the force calculated for CBF is considered, i.e. 148.2 kN and 367 kN respectively.

Table 4.8 Distribution of seismic forces along height (Internal MRF)

Level	w_i (kN)	h_i (m)	$w_i \cdot h_i$ (kN·m)	F_i (kN)	δ	$F_i \cdot \delta$ (kN)
R	6761	12	81132	68.15	1.3	88.60
2	7941	8	63528	53.37	1.3	69.40
1	7941	4	31764	26.68	1.3	34.70
∑	*22643*		*176424*	*148.20*		

Table 4.9 Distribution of seismic forces along height (External MRF)

Level	w_i (kN)	h_i (m)	$w_i \cdot h_i$ (kN·m)	F_i (kN)	δ	$F_i \cdot \delta$ (kN)
R	6761	12	81132	68.15	1.6	109.05
2	7941	8	63528	53.37	1.6	85.40
1	7941	4	31764	26.68	1.6	42.70
∑	*22643*		*176424*	*148.20*		

Table 4.10 Distribution of seismic forces along height (CBF)

Level	w_i (kN)	h_i (m)	$w_i \cdot h_i$ (kN·m)	F_i (kN)	δ	$F_i \cdot \delta$ (kN)
R	6761	12	81132	168.80	1.6	270.10
2	7941	8	63528	132.15	1.6	211.45
1	7941	4	31764	66.05	1.6	105.70
∑	*22643*		*176424*	*367*		

In the above tables, F_i is lateral base shear force per storey and $F_i \cdot \delta$ is the storey base shear amplified to account for accidental torsional effects. The same has been incorporated in the spatial model for response spectrum analysis in the form of a torsional moment corresponding to 5% eccentricity in a particular direction at the story center of stiffness which shall be elaborated in section 4.4.

4.3.2 Assessment of structural safety

While NPR 9998 emphasizes on the assessment of near collapse (NC) limit state, it is considered to be fulfilled following the verification of cross-section capacity, prevention of brittle failure, stability of the building, strength of horizontal diaphragms, foundation stability and strength of seismic joints. For the present case study, these requirements translate to verification of cross-section resistance for critically loaded members, prevention of brittle failure by ensuring the capacity design principles as outlined before, stability of the building in terms of limiting interstorey drift coefficient (θ) and fulfillment of damage limitation requirements in terms of interstorey drift. It has to be ensured that beam to column connection possess required degree of overstrength to dissipate energy in the connected beams.

A. Check for Interstorey drift coefficient

The effects of second-order (P-Δ) need not be considered if the interstorey drift coefficient (θ) is ≤ 0.10, and if $0.1 < \theta \leq 0.2$, the approximate effects can be taken into account by multiplying the relevant seismic action effects, for e.g. bending moments and shear forces by a factor equal to 1/(1-θ) as will be done for this structure. When $\theta > 0.2$, a more complicated non-linear analysis needs to be performed for evaluating the P-Δ effects and in no case, θ should be greater than 0.3. It is for these limitations that govern the member sizes while designing a structure to resist seismic actions. At first, it may seem that the member sizes adopted for this case study structure are greater than what is required for such a structural configuration, it is for the above analysis and drift limitations that justifies the selection obtained after an iterative procedure. Member sizes in MRF's are governed by these limitations.

Table 4.11 Check for P-Δ effects (Internal MRF)

Level	d_s (m)	d_r (m)	V_{tot} (kN)	P_{tot} (kN)	h (m)	θ	Amplified effect 1/(1-θ)	Drift Check (DL)	
								$d_r \cdot \nu / h$	≤ 0.01
1	0.0539	0.0539	192.70	2830.38	4	0.198	1.25	0.006	Ok
2	0.1223	0.0684	158.00	1837.75	4	0.199	1.25	0.008	Ok
R	0.1660	0.0437	88.60	845.13	4	0.104	1.11	0.005	Ok

Table 4.12 Check for P-Δ effects (External MRF)

Level	d_s (m)	d_r (m)	V_{tot} (kN)	P_{tot} (kN)	h (m)	θ	Amplified effect 1/(1-θ)	Drift Check (DL)	
								$d_r \cdot \nu / h$	≤ 0.01
1	0.0660	0.0660	237.15	2830.38	4	0.196	1.24	0.008	Ok
2	0.1505	0.0845	194.45	1837.75	4	0.199	1.25	0.010	Ok
R	0.2052	0.0547	109.05	845.13	4	0.106	1.12	0.007	Ok

Table 4.13 Check for P-Δ effects (CBF)

Level	d_s (m)	d_r (m)	V_{tot} (kN)	P_{tot} (kN)	h (m)	θ	Amplified effect 1/(1-θ)	Drift Check (DL)	
								$d_r \cdot \nu / h$	≤ 0.01
1	0.0602	0.0602	587.25	3773.83	4	0.097	1.00	0.0060	Ok
2	0.1175	0.0573	481.55	2450.33	4	0.073	1.00	0.0057	Ok
R	0.1639	0.0464	270.10	1126.83	4	0.048	1.00	0.0046	Ok

B. **Estimation of Seismic Action Effects for Moment Resisting Frames**

B.1 Summary of action effects for beams

Seismic action effects corresponding to dead load plus reduced imposed loads ($G + \psi_{E,i} \cdot Q$) and lateral loads based on seismic base shear forces (E) were evaluated. The summary of forces for the critically loaded members is shown below by taking into consideration an overstrength factor (Ω) resulting from reserve of forces ($M_{pl,Rd} / M_{Ed,i}$) on the girders to ensure that the columns are designed for sufficient overstrength to prevent the formation of plastic hinges in the column sections. Detailed calculations are shown in 'Appendix II' of this report. The limits imposed on axial and shear forces under design seismic combination is to verify that full plastic moment of resistance and rotation capacity of beams are not decreased by compression and shear forces to ensure flexure plastic hinges in the beams (6.6.2 (2), EN1998-1)

Table 4.14 Section resistance verification for beams (Internal MRF)

	Action	Resistance	U.C.	Limit
Bending Moment, (kNm)	256.00	463.99	0.55	≤ 1.00
Axial Forces (kN)	124.40	2999.75	0.04	≤ 0.15
Shear Forces (kN)	251.27	875.16	0.29	≤ 0.50

The shear force in the beam (V_{Ed}) is calculated as: $V_{Ed} = V_{Ed,G+\psi \cdot Q} + V_{Ed,M} \cdot (1/(1-\theta))$ where VEd,M is the design shear force due to application of plastic moments with opposite signs at the end sections of the beam i.e. $2 \cdot M_{pl,Rd} / L$ in this case. A sample calcuation is shown in Appendix II towards the end (refer page 88).

Table 4.15 Section resistance verification for beams (External MRF)

	Action	Resistance	U.C.	Limit
Bending Moment, (kNm)	194.23	463.99	0.42	≤ 1.00
Axial Forces (kN)	125.90	2999.75	0.04	≤ 0.15
Shear Forces (kN)	209.33	875.16	0.24	≤ 0.50

B.2 Summary of action effects for columns

Based on the overstrength factor (Ω) calculated for beams in the moment resisting frames, columns are verified in compression considering the most unfavorable combination of axial for and bending moments. The design action effects, N_{Ed}, M_{Ed}, V_{Ed} for columns are computed as below with further amplification on account of P-Δ effects (6.6.3 (1), EN1998-1):

$N_{Ed} = N_{Ed,G} + (1.1 \cdot \gamma_{ov} \cdot \Omega \cdot N_{Ed,E}) \cdot k_\theta$

$M_{Ed} = M_{Ed,G} + (1.1 \cdot \gamma_{ov} \cdot \Omega \cdot M_{Ed,E}) \cdot k_\theta$ where $k_\theta = \frac{1}{(1-\theta)}$

$V_{Ed} = V_{Ed,G} + (1.1 \cdot \gamma_{ov} \cdot \Omega \cdot V_{Ed,E}) \cdot k_\theta$

where:
$N_{Ed,G}$ ($M_{Ed,G}$, $V_{Ed,G}$) are the compression forces (bending moment and shear force, respectively) in the column due to non-seismic actions (i.e. $G+\psi_{E,i}\cdot Q$) included in the combination of actions for seismic design situation;
$N_{Ed,E}$ ($M_{Ed,E}$, $V_{Ed,E}$) are the compression forces (bending moment and shear force, respectively) in the column due to design seismic action;
γ_{ov} is the overstrength factor which takes into account the possibility of actual yield strength of steel being higher than the nominal yield. In the absence of measured data, the recommended value is 1.25 further amplified by the factor 1.1 to account for material effects such as strain hardening;

The following tables summarize design forces for the columns to be used for verification. Detailed calculations are furnished in 'Appendix II' of this report and a sample calculation is shown as well. The U.C. in below table shows the plastic resistance capacity check. Calculations for interaction of axial and bending are shown in 'Appendix IV' of this report including the stability.

Table 4.16 Design action effects for columns (Internal MRF)

	Action	Resistance	U.C.	Limit
Bending Moment, (kNm)	332.73	663.50	0.50	≤ 1.00
Axial Forces (kN)	742.13	5293.05	0.14	≤ 1.00
Shear Forces (kN)	133.49	972.12	0.14	≤ 0.50

Table 4.17 Design action effects for columns (External MRF)

	Action	Resistance	U.C.	Limit
Bending Moment, (kNm)	536.12	663.50	0.81	≤ 1.00
Axial Forces (kN)	416.10	5293.05	0.08	≤ 1.00
Shear Forces (kN)	214.55	972.12	0.22	≤ 0.50

C. Estimation of Seismic Action Effects for Concentrically Braced Frames

C.1 Summary of action effects for braces

In a similar way as for MRF, the lateral seismic base shear evaluated above was applied to the planar model taking into account the accidental torsional effects. As evident from the estimation of time-period, CBF are much stiffer than MRF due to the presence of tension/compression braces. However, the hysteretic behavior of CBF is less reliable because of the buckling of compression brace under cyclic loading and once it buckles, it is not assumed to carry lateral forces. Whole of the seismic forces are transferred to the columns by the brace in tension. This behavior is implemented in the model by defining a 'compression limit' of zero for the braces acting in compression and modifying the lateral load case as nonlinear. As a result, the brace in tension carries axial load whereas the compression brace acts as redundant for lateral forces.

Following the capacity-based design requirements for braced frames, it has to be ensured that yielding of tension brace occurs before yielding/buckling of columns and beams. The axial forces in the brace (N_{Ed}) should be less the design plastic resistance ($N_{pl,Rd}$) of the member. Further, EN1998-1 limits the non-dimensional slenderness $\bar{\lambda}$ to $1.3 \leq \bar{\lambda} \leq 2.0$. The lower limit of 1.3 is to avoid overloading of columns in the prebuckling stage when both the compression/tension braces are active beyond the action effects at ultimate limit state where

only tension brace is active. The upper limit is to achieve a satisfactory hysteretic behavior and avoid shock loading under cyclic conditions [34].

To achieve the capacity requirements, similar to the case of MRF, in CBF an overstrength factor Ω is defined such that it is the minimum value $\Omega_i = N_{pl,Rd,i} / N_{Ed,i}$ of all the diagonals of the braced system where the numerator is the plastic resistance and denominator represents the design axial force for i^{th} diagonal member. The calculated value of Ω is then used to evaluate overstrength axial demand for beams and columns and determined as:

$$N_{Ed,m} = N_{Ed,G} + 1.1 \cdot \gamma_{ov} \cdot \Omega \cdot N_{Ed,E}$$

Where the symbols have usual meanings as before. Similar to the analysis of MRF, braced frames were checked for interstory drifts and P-Δ effects however, the effects are not as pronounced as in the former due to high lateral stiffness of braced frames as observed in table 4.13. Analysis of CBF require specific attention to ductility. Once yielding of the brace occurs at a story level, the ductility demand concentrates and there are chances of formation of soft-story mechanism. To prevent such situation, EN1998-1 recommends balancing the Ω (i.e. capacity / demand) over the height, by limiting the difference in overstrength factor across all storeys within a frame to 25%. Equivalently, 6.7.3 (8) states that 'in order to satisfy a homogeneous dissipative behavior of the diagonals, it should be checked that maximum overstrength Ω_i does not differ from the minimum value by more than 25%' [EN1998-1]. To fulfil such limitations in addition to limitations on $\bar{\lambda}$ described above, it becomes practically difficult to select brace sizes and subsequent reduction in section sizes for brace elements becomes unavoidable. Table 4.19 shows calculation of Ω for the analyzed frame and 4.18 shows the relative slenderness check performed for CBF analysis. Section class 1 requires limiting d/t ratio of the brace to $\leq 50\varepsilon^2$, which is 42.75 for S275 grade steel used for bracings. The adopted section sizes conform to both the requirements.

Table 4.18 Check for relative slenderness of brace elements ($\bar{\lambda}$)

Brace ID	10	12	14
Brace Section	CHS193.7x6.3	CHS168.3x6.3	CHS168.3x4
d/t	30.75	26.71	42.07
Section Class	1	1	1
Length, L (mm)	8940	8940	8940
Area, A (mm^2)	3710	3210	2060
I (mm^4)	1.63E+07	1.05E+07	6.97E+06
E (N/mm^2)	210000	210000	210000
f_y (N/mm^2)	275	275	275
N_{cr} (N)	422699	273069	180749
$\bar{\lambda}$	1.56	1.65	1.87

Table 4.19 Design action effects for brace (CBF)

Brace ID	$N_{pl,Rd}$ (kN)	N_{Ed} (kN)	1/(1-θ)	Ω	U.C.
10	1020.250	657.530	1.000	1.552	0.641
12	882.750	535.640	1.000	1.648	0.606
14	566.500	303.760	1.000	1.865	0.536
			Ω_{min}	1.552	
			$\Omega_{max} / \Omega_{min}$	1.197	∴ OK

C.2 Summary of action effects for beams and columns

The beams and columns in a CBF are designed for overstrength axial forces considering the Ω_{min} factor calculated above and are checked for possible buckling/yielding based on interaction with bending moments co-existing in the seismic design situation. Table 4.20 summarize the design axial forces for beams and columns for the considered frame.

Table 4.20 Design action effects for beams and columns (CBF)

Member	Member ID	$N_{Ed,G+\psi \cdot Q}$ (kN)	$N_{Ed,E}$ (kN)	Ω	1/(1-θ)	$N_{Ed,m}$ (kN)
Column	1	-63.110	316.710	1.552	1.000	612.592
Column	4	-63.110	-728.130	1.552	1.000	-1616.579
Beam	7	3.700	-585.810	1.552	1.000	-1246.129

The column member ID 1 forms a part of MRF in the transverse direction. In that case, the directional combination rules apply as specified by 4.3.3.5.1 of NPR9998 (and EN1998-1) as E_{Edx} "+" $0.30E_{Edy}$ and $0.30E_{Edx}$ "+" E_{Edy} whichever produces the maximum action effects. In this case, the braced frames result in axial forces in the column. For an external MRF column with bracing connected, this translates to max (416.10+0.30·612.592; 0.30·416.10+612.592) = 737.50 kN. Hence, the column has to be verified for a design axial force in seismic situation is 737.50 kN. The same will be used for verifying the cross-section and stability checks in further sections.

4.4 Modal Response Spectrum Analysis

A response spectrum analysis was carried out for the structure using a spatial model generated in SAP2000 to evaluate the action effects on structural members accounting for effects from additional modes of vibration corresponding to a mass participation of more than 90% in each direction of analysis. The defined seismic loading was in the form of a response spectrum derived from NPR9998 webtool as outlined in section 4.2 with a behavior factor (q-factor) of 6.5 in the transverse direction and 4 in the longitudinal direction (for brevity, Y and X direction) of the spatial model. A modal analysis was run for the structural geometry with mass source defined corresponding to earlier discussed "$G + \psi_{Ei} \cdot Q$" non-seismic loads in the seismic load combination. The nodal degree of freedom at each floor level was constrained in the global Z direction (vertical) so that a rigid diaphragmatic behavior is realized, which is due to the presence of composite floor slab. The floor system itself was not modeled to avoid complexity, however the action effects due to dead and imposed loading were applied directly to the supporting members. For modal combination, SRSS rule was selected. The results of modal analysis are summarized below.

Table 4.21 Summary of modal results for spatial model

Mode ID	Period (s)	Participating mass, X	Participating mass, Y	Sum, X	Sum, X
1	1.308	4.159E-12	0.858	4.159E-12	0.858
2	0.614	9.496E-08	1.500E-04	9.497E-08	0.858
3	0.469	0.870	2.802E-12	0.870	0.858
4	0.403	3.798E-12	0.114	0.870	0.972
5	0.223	9.156E-12	0.028	0.870	0.999
6	0.207	1.753E-08	1.100E-04	0.870	0.999
7	0.163	0.117	2.684E-12	0.987	0.999

The above table shows that modal mass participation above the code required 90% is well achieved after 7th mode of vibration in both X and Y directions. A comparison of fundamental period of vibration from spatial model is made with the results from planar analysis in table 4.22 and results are in close agreement. This is an important observation in a sense that, for regular structures in plan and elevation with uniformly distributed mass and stiffness properties, planar structural models are equally powerful in capturing the dynamic behavior leading to simplification of the analysis. The relevant modes shapes are shown in figure 4.10 below contributing to significant modal mass.

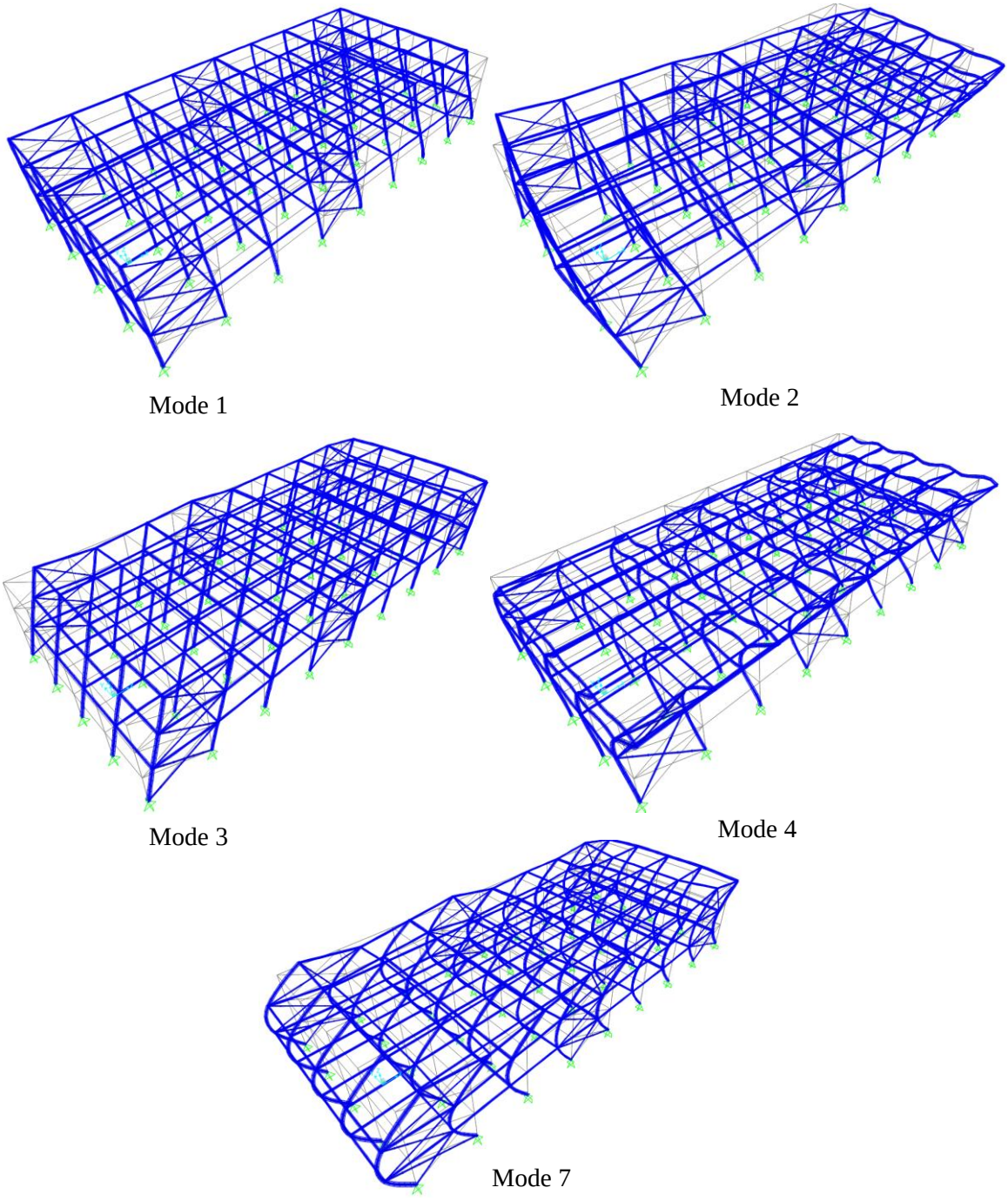

Figure 4.10 Predominant mode shapes contributing to mass participation for mode 1 (translation y), mode 2 (torsional), mode 3 (translation x), mode 4 and 7 (coupled modes)

Table 4.22 Comparison of fundamental time period (T1) with planar models

	Spatial Model		Planar Model		Δ (%)	
	Y-direction	X-direction	Y-direction	X-direction	Y-direction	X-direction
T_1 (s)	1.308	0.469	1.333	0.487	1.91	3.83

As evident from the previous table, the difference in estimation of the fundamental modal time period using two different analysis methodologies are in close agreement with an acceptable difference.

4.4.1 Base Shear force

Seismic base shear forces were evaluated for the model based on relevant time periods of vibration to achieve mass participation more than 90%. A similar comparison, as time periods, is made in the following table for corresponding estimation of total base shear force acting on the structure in the considered analysis directions.

Table 4.23 Comparison of estimated seismic base shear with planar models

	Spatial Model		Planar Model		Δ (%)	
	Y	X	Y	X	Y	X
Base Shear (kN)	662.20	1940.69	741	2203	11.90	13.52

Detailed calculation of seismic base shear from SAP2000 output results is shown in Appendix III following the basic theory of modal combination rules. The above difference in the computed base shear value can be explained as follows. The seismic base shear calculated using lateral force analysis takes into account that whole of the force is corresponding to fundamental mode time period in the considered direction. However, from modal analysis, it can be observed that it is not the correct assumption but an approximate one. It is for this reason that a correction factor, λ is introduced in the codes that takes into account that on an average, the participating mass in the fundamental mode of vibration is 15% lower than the total seismic mass of the structure. In response spectrum analysis, it is explicit in the calculations corresponding to participation factors for different modes which when statistically combined leads to a more realistic estimation of base shear forces. Nevertheless, lateral force method of analysis provides a good fit with the latter results as observed above and can safely be used for preliminary analysis provided fundamental time period of the structure is determined in a realistic way as discussed in the previous sections.

4.4.2 Accidental Torsional effects

For assessment of accidental torsional effects, the program offers input in terms of diaphragm eccentricity to be considered at different levels of the structure. NPR9998 andEN1998-1 (4.3.2 (1)) recommends an eccentricity of 5% considered in each direction to account for uncertainties in the location of mass and/or in the spatial variation of ground motion i.e.

$$e_{ai} = \pm 0.05 \cdot L_i$$

where L_i is the floor-dimension perpendicular to direction of seismic action. For a spatial analysis, the application of a static loading about vertical axis (torsional moment, M_{ai}) is recommended at the center of mass of story level diaphragm and the envelope of accidental torsional effects from two directions of application are combined with the relevant seismic action.

$$M_{ai} = e_{ai} \cdot F_i$$

The program SAP2000 allows user to input diaphragm eccentricity in the response spectrum load case definition. The action effects resulting from application of torsion were verified with the program generated forces using the two approaches. First, results from SAP2000 and second, by application of static load case for torsion moment as described above. The envelope of two directions fits quite well with output results from SAP2000 as shown in the figures below. Legend Y-direction refers to the forces generated when base shear is acting in transverse direction and X-direction refers to the forces generated in members when base shear acts in the longitudinal direction.

As observed from plots in figure 4.11, the action effects resulting in columns and braces on account of accidental torsion in SAP2000 is verified with the other approach using application of static load case accounting for 5% eccentricity in each direction. The forces add up to the member forces due to seismic action to determine the total action effects for which the member has to be verified. In addition, it is also observed that most of the additional forces are transferred through the bracings to the base.

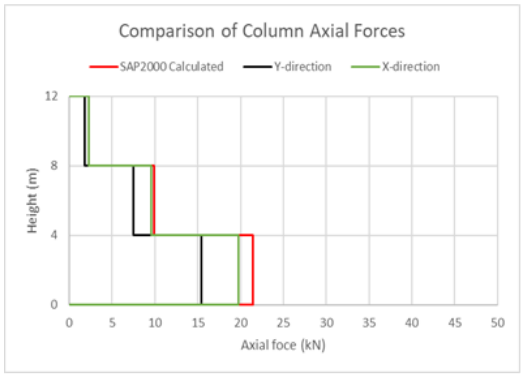

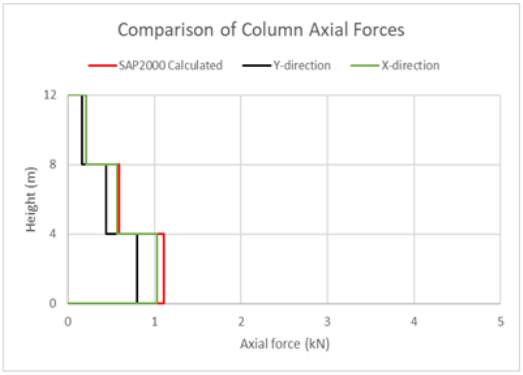

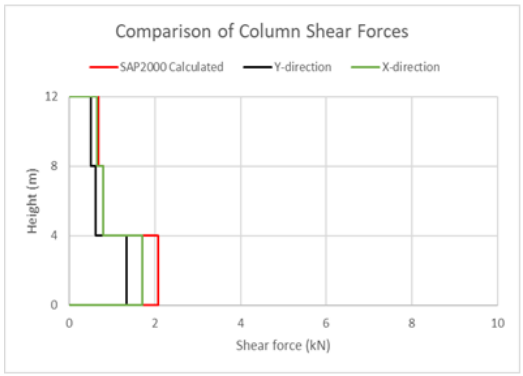

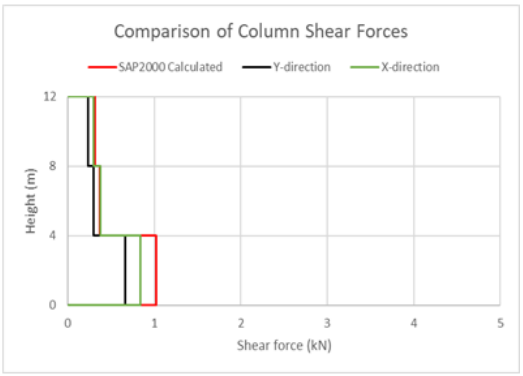

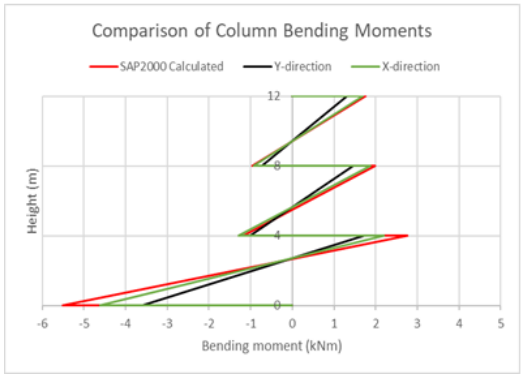

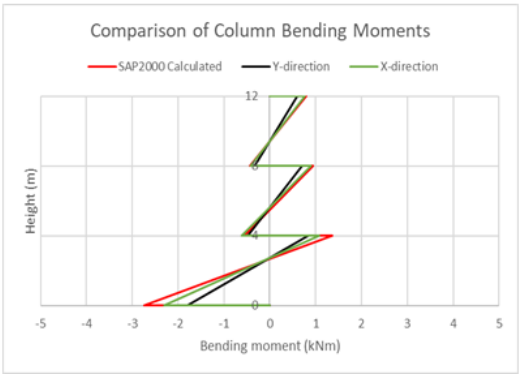

a) b)

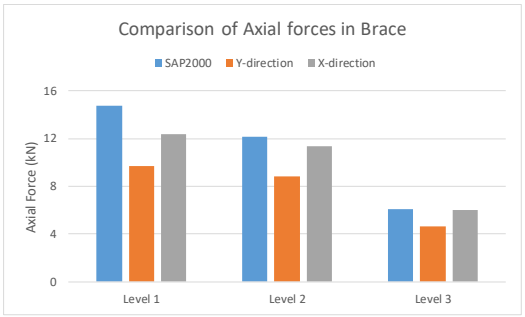

c)

Figure 4.11 Comparison of additional torsional eccentricity using different approaches in spatial model a) Forces due to torsion in external MRF, b) Forces due to torsion in internal MRF, c) Axial force in braces due to torsion

4.4.3 Assessment of Structural Safety

A. Check for Interstory drifts

As discussed in 4.3.2 A, interstory drift criteria needs to be satisfied for damage limitation requirement, for a seismic action which has a higher probability of occurrence than the design earthquake for no-collapse requirement by limiting the interstory drifts. In the table below, d_s is the displacement at a point due to design seismic action, d_e is the displacement of same point determined from linear analysis based on design response spectrum, d_r is the design interstory drift and ν is a reduction factor that takes into account a lower return period of the earthquake associated with damage limitation requirement.

Table 4.24 Check for P-Δ effects (Transverse direction)

Level	d_s (m)	d_r (m)	V_{tot} (kN)	P_{tot} (kN)	h (m)	θ	Amplified effect 1/(1-θ)	Drift Check (DL)	
								$d_r \cdot \nu / h$	≤ 0.01
1	0.0396	0.0396	1059.52	22643	4	0.213	1.27	0.005	Ok
2	0.0864	0.0468	868.768	14702	4	0.198	1.25	0.006	Ok
R	0.1178	0.0314	487.248	6761	4	0.109	1.22	0.004	Ok

Table 4.25 Check for P-Δ effects (Longitudinal direction)

Level	d_s (m)	d_r (m)	V_{tot} (kN)	P_{tot} (kN)	h (m)	θ	Amplified effect 1/(1-θ)	Drift Check (DL)	
								$d_r \cdot \nu / h$	≤ 0.01
1	0.0103	0.0103	323.40	22643	4	0.020	1.00	0.0013	Ok
2	0.0206	0.0103	265.16	14702	4	0.015	1.00	0.0013	Ok
R	0.0285	0.0079	148.69	6761	4	0.001	1.00	0.0010	Ok

As observed in the check for P-Δ effects above, it can be observed that θ for story 1 was marginally less than 0.2 for analysis in transverse direction, however detailed analysis using response spectrum reveals its value just over 0.2 which principally calls for a more detailed nonlinear analysis, but for this study, the further procedure is continued with the obtained values. In the stiff longitudinal direction, there is no need to amplify the action effects on account of P-Δ and the interstory drifts are in the allowable limits.

B. Estimation of Seismic Action Effects for Moment Resisting Frames

B.1 Summary of action effects for beams

Seismic action effects corresponding to dead load plus reduced imposed loads ($G + \psi_{E,i} \cdot Q$) and response spectrum based on seismic base shear forces (E) were evaluated. The summary of forces for the critically loaded members is shown below. One peculiar thing to be noticed when analyzing output results for response spectrum load case is that only positive values are shown for this particular load case, for the reason that these are SRSS combined modal results. One has to be careful when combining the results for ($G + \psi_{E,i} \cdot Q$) and RS load case. An example is shown below for clarity.

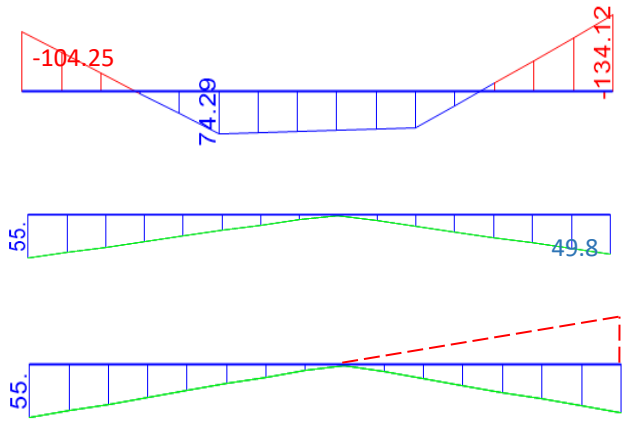

Bending moment output for member 16 ($G + \psi_{E,i} \cdot Q$)

Bending moment output for member 16 (RS)

Correct representation of bending moment output (RS)

Figure 4.12 Combination of response spectrum load case output from analysis

When making a linear combination of the load case ($G + \psi_{E,i} \cdot Q + RS$), left end of the beam will result in (-104.25+55) = -49.25 kNm and right end (-134.12+49.82) = -84.30 kNm. However, this is not the actual bending moment. The correct way to combine both components is (-104.25+55) = -49.25 kNm for left end and (-134.12-49.82) = -183.94 kNm for right end of the beam.

The summary of forces for the critically loaded members is shown below following the same procedure as outlined before in the lateral force analysis. Detailed calculations are shown in 'Appendix IV'. The action effects also include the factor k_θ as calculated above for Interstorey drift coefficient.

Table 4.26 Section resistance verification for beams (Internal MRF) from response spectrum analysis

	Action	Resistance	U.C.	Limit
Bending Moment (kNm)	233.24	463.99	0.50	≤ 1.00
Shear Forces (kN)	254.25	875.16	0.29	≤ 0.50

Table 4.27 Section resistance verification for beams (External MRF) from response spectrum analysis

	Action	Resistance	U.C.	Limit
Bending Moment (kNm)	157.80	463.99	0.34	≤ 1.00
Shear Forces (kN)	216.14	875.16	0.25	≤ 0.50

In the results from response spectrum analysis, since a rigid diaphragm was assigned to constraint the nodes at a story level in the program, the relative distance between two nodes did not change i.e. no axial strain in the beams giving rise to no axial stress. It is however observed from lateral analysis that calculated axial forces in the beam of MRF were well below the allowable limit of 0.15.

B.2 Summary of action effects for columns

The overstrength factor Ω from the strength reserve of beams in the internal and external MRF is calculated as 1.989 and 2.941 respectively. Based on this, the critical forces in columns are summarized in the following tables to be used for verification. Detailed calculations are furnished in 'Appendix IV' of this report.

Table 4.28 Design action effects for columns (Internal MRF) from response spectrum analysis

	Action	Resistance	U.C.	Limit
Bending Moment (kNm)	272.88	663.50	0.41	≤ 1.00
Axial Forces (kN)	744.03	5293.05	0.14	≤ 1.00
Shear Forces (kN)	111.22	972.12	0.12	≤ 0.50

Table 4.29 Design action effects for columns (External MRF) from response spectrum analysis

	Action	Resistance	U.C.	Limit
Bending Moment (kNm)	413.18	663.50	0.62	≤ 1.00
Axial Forces (kN)	1877.16	5293.05	0.36	≤ 1.00
Shear Forces (kN)	167.99	972.12	0.17	≤ 0.50

C. Estimation of Seismic Action Effects for Concentrically Braced Frames

Table 4.30 Design action effects for brace (CBF)

Brace ID	$N_{pl,Rd}$ (kN)	N_{Ed} (kN)	1/(1-θ)	Ω	U.C.
670	1020.250	628.864	1.000	1.622	0.616
672	882.750	484.173	1.000	1.823	0.548
674	566.500	308.150	1.000	1.838	0.544
			Ω_{min}	1.622	
			Ω_{min} / Ω_{min}	1.133	∴ OK

Table 4.31 Design action effects for beams and columns (CBF)

Member	Member ID	$N_{Ed,G+\psi \cdot Q}$ (kN)	$N_{Ed,E}$ (kN)	Ω	1/(1-θ)	$N_{Ed,m}$ (kN)
Column	1	-219.290	542.110	1.622	1.000	990.027
Column	16	-303.970	-541.590	1.622	1.000	-1512.127
Beam	136	-	-	-	-	-

4.5 Design of Connections

The capacity design procedure is based on the hierarchy of formation of plastic hinges in the structure to avoid a brittle global failure for e.g. soft-story mechanism. To dissipate energy in the beams of MRF, the moment connection between beam and column element should be designed for a required degree of overstrength taking into account moment of resistance as, $M_{pl,Rd,b}$ and shear force as $V_{Ed,G} + V_{Ed,M}$ calculated before and similarly for CBF, axial resistance of the tensile brace with an overstrength factor. The following expression from EN1998-1, 6.5.5 (3) summarized the discussion:

$R_d \geq 1.1 \cdot \gamma_{ov} \cdot R_{fy}$

where R_d is the resistance of connection and R_{fy} is the plastic resistance of the connected dissipative member. Other than this requirement, the design of a moment resisting connection should be such that the rotation capacity, θ_p of the plastic hinge region (beam ends) is not less than 35 mrad for DCH where

$\theta_p = \delta / 0.5L$

where δ is the beam deflection at midspan and L is the beam span.

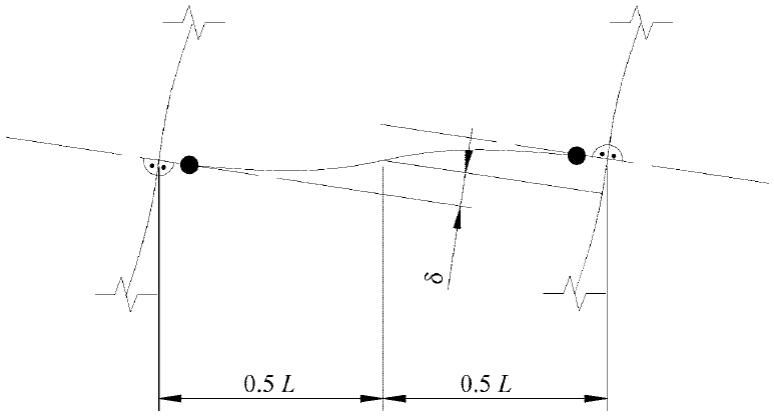

Figure 4.13 Beam deflection for calculation of θ_p

The following table summarizes the connection forces for design of a moment resisting connection based on overstrength above the moment resistance of connecting beam IPE400:

Table 4.32 Connection forces for MRF

Design Forces	
$M_{Rd,j}$ (kNm)	638
$V_{Rd,j}$ (kN)	382

The forces are calculated as below:

$$M_{Rd,j} = 1.1 \cdot \gamma_{ov} \cdot M_{pl,Rd,IPE400}$$
$$= 1.1 \cdot 1.25 \cdot (1.307 \cdot 355)$$
$$= 637.98 \text{ kNm}$$

$$V_{Rd,j} = 1.1 \cdot \gamma_{ov} \cdot (V_{Ed,G} + V_{Ed,M})$$
$$= 1.1 \cdot 1.25 \cdot (277.35)$$
$$= 381.36 \text{ kN}$$

where $M_{Rd,j}$ and $V_{Rd,j}$ refers to design moment resistance and shear resistance of the joint respectively.

A typical moment connection designed for an interior column is shown in figure 4.15. Although the designed solution, as confirmed with the findings from EQUALJoints research project [38], is the most expensive (~82% more expensive than unstiffened extended end-plate joint).

EQUALJOINTS (Europan pre-QUALified steel JOINTS) project addressed the needs to include pre-qualified joints in the design codes for bolted joints, typically used in the EU practice to provide seismic resistance, aimed to provide codified seismic pre-qualification charts for a set of standard joints, develop analytical and numerical models for predicting the behaviour of beam-column joints under cyclic loading based on wide experimental campaign and to define technological requirements for fabrication of thus codified joints and further to evaluate the economic benefits related to the costs and construction time for different solutions. Similar solutions have been recommended in US design codes (ANSI/AISC 358-05, 2005) and Japan. The same is expected to be included in the revised version of EN1998-1

as a result of this Equaljoints research project for the most commonly type used bolted joint configuration (haunched, extended stiffened and unstiffened end plate connections).

As a part of Equaljoints project, cyclic and monotonic loading tests were performed on haunched joint geometries which confirmed the concentration of plastic deformations in the portion of beam adjacent to haunch (predominantly in the beam flanges due to low-cycle fatigue, whereas negligible deformations in the column panel zone and connections. Figure 4.14 shows the moment-rotation response obtained from the experimental investigations with similar response on the hogging and sagging region. The same is ascertained due to the fact that overall behaviour depends on the beam section only without plastic engagement of the connection. The figure also shows non-degrading behaviour up to a 40 mrad rotation thus satisfying performance pre-qualification limits. All experimental specimens with 35° haunch exhibited chord rotations larger than 40 mrad satisfying the requirements for DCH whereas the ones with 45° qualified for DCM with lower than 35 mrad ultimate drifts.

Although EN1998-1 permits the application of dissipative semi-rigid or partial-strength connections, a set of following conditions needs to be fulfilled i) the connections have sufficient rotation capacity ii) framing members are demonstrated to be stable at ULS and iii) effects of connection deformation is considered in the calculation for global drift using pushover analysis or non-linear time history analysis [39]. In the event of considering these types of connections to enable them to contribute to dissipation of energy, the overstrength need not be applied.

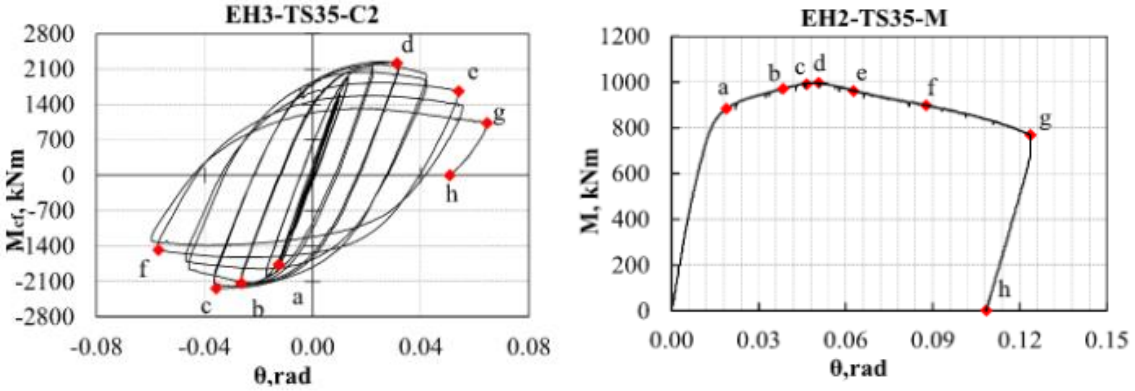

Figure 4.14 Experimental joint response for a haunched end-plate moment connection for a) cyclic test b) monotonic tests [38]

The concentrically braced frames (CBF's) provide an economical solution to seismic resistance of steel structures, the performance of diagonal members depends on the cyclic response during an earthquake. Dissipation of seismic energy is expected to occur in the tension brace whereas all other framing members are expected to remain elastic by designing for sufficient overstrength to ensure inelastic behaviour in the braces. The braces are generally connected to the frame using gusset plates and the buckling of brace in compression highly depends on the orientation of section shape and brace end restraints provided by the gusset plate [38]. The commonly used gusset plate connections are designed as either rotationally restrained or unrestrained. As per the design rules specified in AISC, 2005a, the design is based on unrestrained connection to accommodate brace end rotations in the minor axis bending of the gusset plates for out-of-plane brace buckling. A Standard Linear Clearance (SLC) model is adopted which incorporates a free length to permit formation of plastic hinges in the gusset plates at large interstorey drifts due to end rotation in post-buckled brace. Astaneh-Asl et al. (1981) and Cochran (2003) recommends a free length of $3t_p$, which was adopted in the experimental campaign SERIES-BRACES [45] to determine the performance

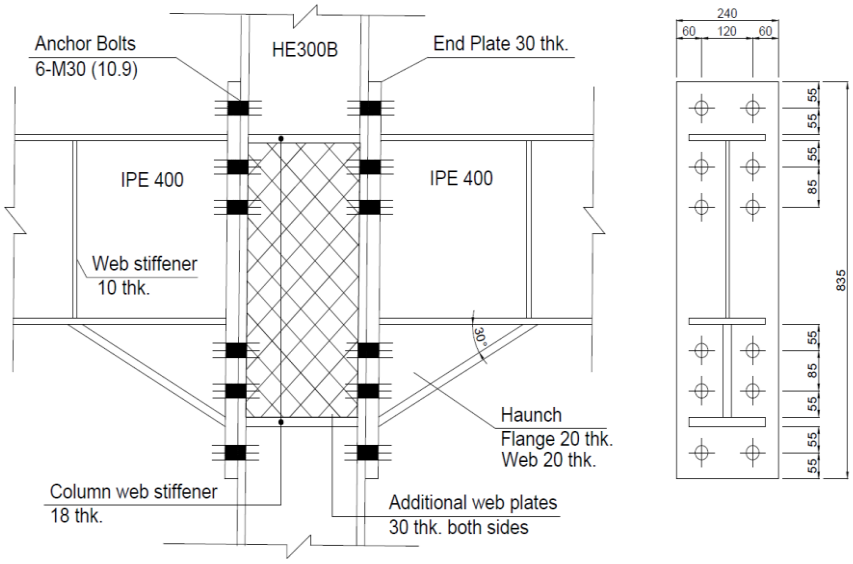

Figure 4.15 Typical full-strength haunched moment connection

of CBF's under monotonic and cyclic loading. Starting with an initial sizing of the gusset plate by aligning the centre line to the work-point of the connection, and subsequently determining the plate yield and buckling strength using Whitmore concept or Thornton model. However, these methods are based on the premise that dissipation of energy solely takes place in the brace member and the resistance of connection is much larger to remain elastic during cyclic loading. The requirements lead to a sub optimally large and stiff gusset plates which can lead to local damage at large inelastic deformations in the beams, columns and brace members reducing system ductility. A typical connection using this approach designed for brace at storey 1-2 between grid D-E is shown in figure 4.16. The design load based on overstrength on the plastic resistance of the brace member is $1.1 \cdot \gamma_{ov} \cdot N_{pl,Rd} = 1214$ kN.

Lehman et al. (2008) proposed balanced yielding approach permitting controlled yielding in the gusset plate by balancing gusset yield and brace yield strength by using a factor β_{ww} which indicates the ratio of the two.

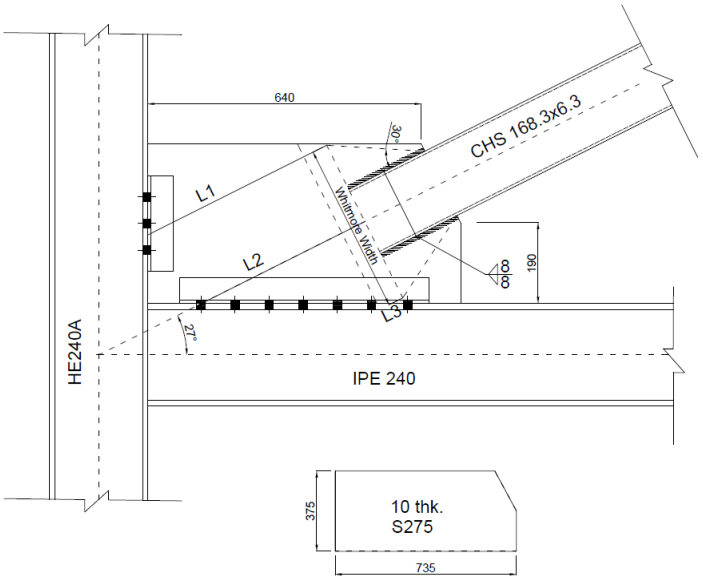

Figure 4.16 Typical full-strength Concentric Brace Connection at storey 1-2 between grid D-E

4.6 Non-Linear Static Pushover Analysis

In this section, the performance of above structure will be evaluated to ensure that intended behaviour as realized in the previous sections by subjecting it to a non-linear static pushover analysis (POA hereafter). The deficient zones when subjected to a lateral loading can be identified in terms of sequence of formation of plastic hinges in the structure and the performance in terms of collapse modes and verification of assumed behaviour factors to satisfy the validity of assumptions made previously.

4.6.1 Pushover Analysis for Moment Resisting Frames

The seismic performance of the building was evaluated using planar models corresponding to the longitudinal and transverse framing arrangements (CBF's and MRF's respectively). The formation of plastic hinges was allowed at the beam ends and column ends at each story of the analysed frame with hinge modelling definition as per i) FEMA 356, and ii) a bi-linear moment-rotation characteristics. Geometric non-linearity was included in the form of P-Δ effects and a leaning column (as defined before) to take into account destabilizing action from gravity frames. For beams, a flexural plastic hinge (M3 in SAP2000) was defined whereas, in columns, interaction between axial and moment (P-M3) was defined to represent the concentrated plasticity at member ends. Correspondingly, for bracings, an axial force-deformation relationship was defined to represent the hinges at a relative distance of 0.5 from member ends. Two different models were adopted for this purpose, where the first one incorporates FEMA 356 definition with a reduced load carrying capacity of the buckled brace in compression whereas the second one as per Eurocode which recommends performing analysis with a tension brace neglecting the contribution from brace in compression. The following figure 4.17 defines the FEMA 356 definition with parameters a,b and c discussed.

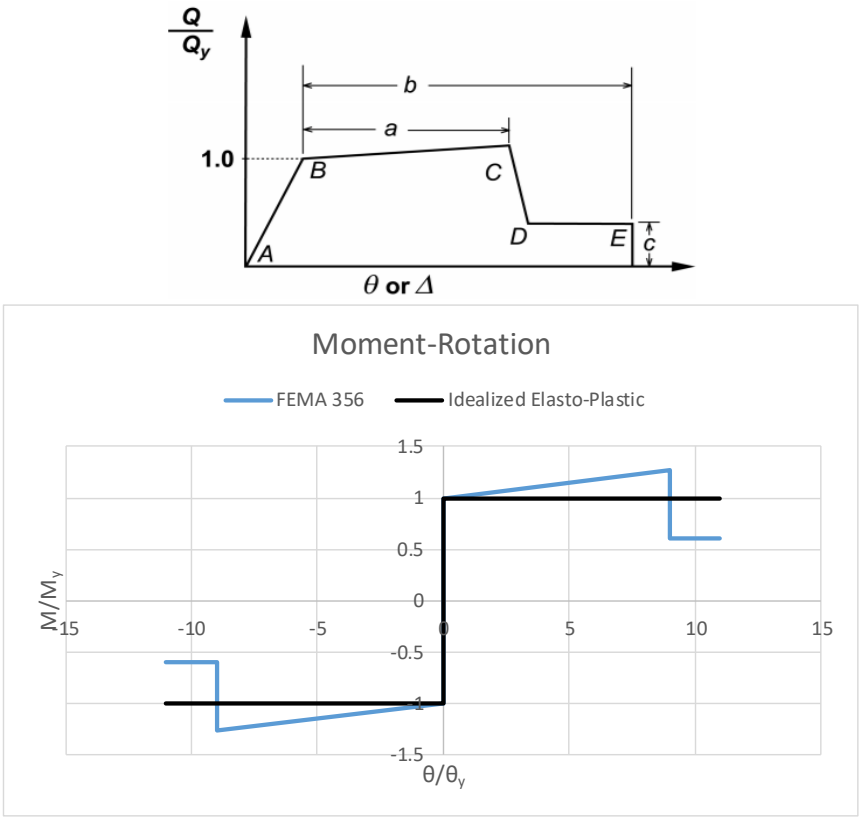

Figure 4.17 Generalized force-deformation relationship for steel elements [24]

The above backbone curve for beams in flexure is defined as per FEMA 356 provisions with strain hardening slope of 3% of the elastic slope. A corresponding EPP curve to compare the results is also defined in the same plot.

Figure 4.18 shows the pushover curve obtained by using i) uniform load pattern, and ii) modal pattern based on 1st mode of vibration. It is observed that the lateral load capacity drops at a global drift limit of ~4.5% of the structure's height. Similar recommendations are made by FEMA356 guidelines for near collapse limit state. Further, conservative estimates of capacity curve are obtained with modal pattern whereas uniform load pattern leads to a capacity on the higher side.

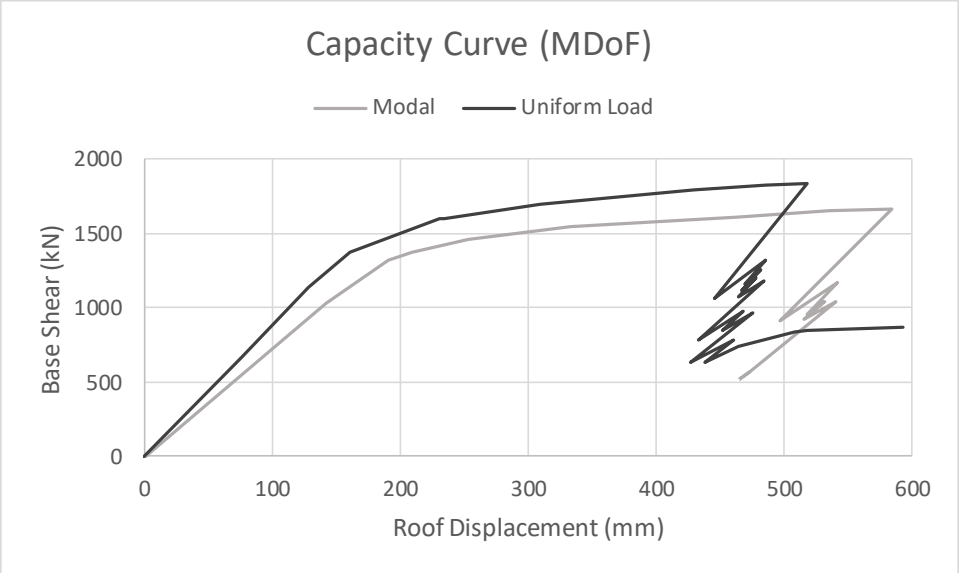

Figure 4.18 Pushover capacity curve obtained for MDoF MRF system for i) Modal, and ii) Uniform load pattern

Figure 4.19 shows the capacity curve obtained for an equivalent SDoF system and correspond bilinear idealization as per the rules defined in Annex B of EN1998-1. The structural system forms a global mechanism at point B (~4% global drift) in the above curve and there is a drop in the base shear beyond this point. Point A represents the formation of first plastic hinge in the structure. Interestingly, one would expect a structure to possess an overstrength (α_u/α_1) = 1841.73/1376.94 = 1.33 (for uniform pattern) and 1727.30/1318.54 = 1.31 (for modal pattern) which satisfies the recommendation of 1.3 adopted as per EN1998, but a careful observation on the pattern of formation of plastic hinges reveals that a story mechanism at ground floor level forms at step 9 (at collapse) which was not anticipated based on capacity design principles (figure 4.20). This could be due to HE300B just the first column section satisfying $\sum M^{c}_{pl,Rd} \geq 1.3 \cdot \sum M^{b}_{pl,Rd}$.

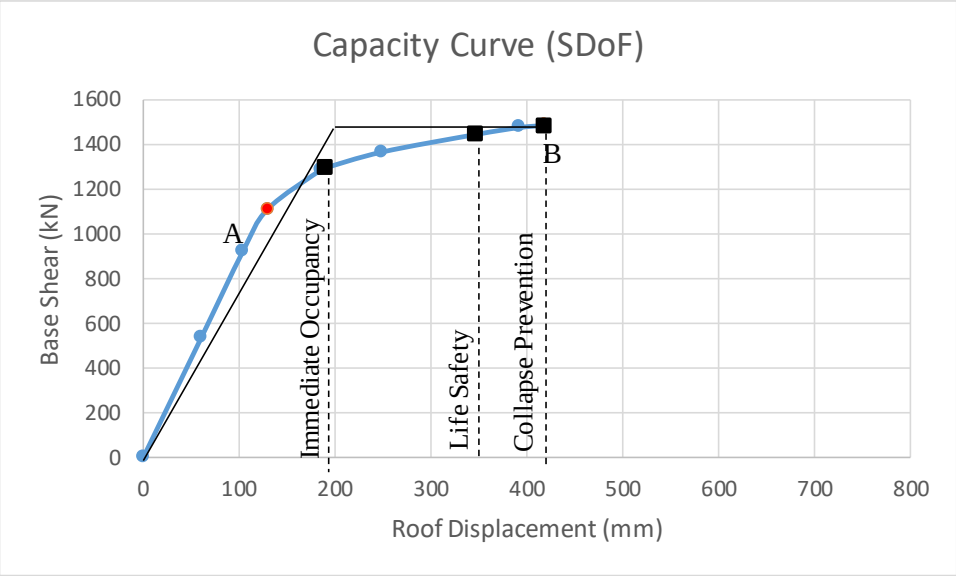

Figure 4.19 Pushover Capacity curve for equivalent SDoF system of Moment Resisting Frame

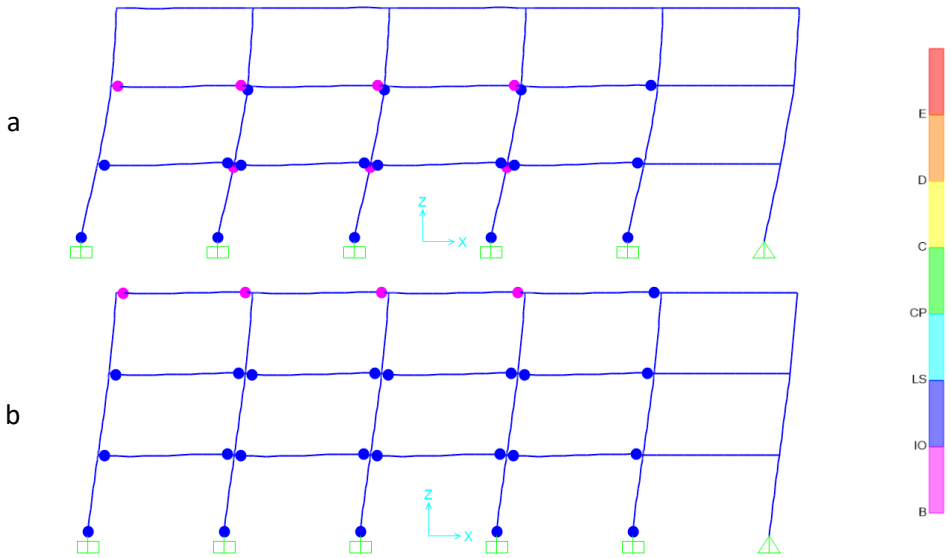

Figure 4.20 Formation of soft-story mechanism at step 9 with a) HE300B columns, b) HE300M columns

Whereas a similar analysis with HE300M column fulfils the strong column-weak beam principle of capacity design of steel frames where plastic hinges form at the designated beam ends and at the base of columns. Appendix VI shows the parameters adopted for obtaining target displacement and capacity spectrum corresponding to an equivalent SDoF system highlighted in figure 4.19.

In the next step, the seismic performance of the moment resisting frame with HE300B columns was evaluated in the ADRS spectrum format using graphical representation of seismic demand and the capacity spectrum as outlined in appendix B of EN1998 using N2 method.

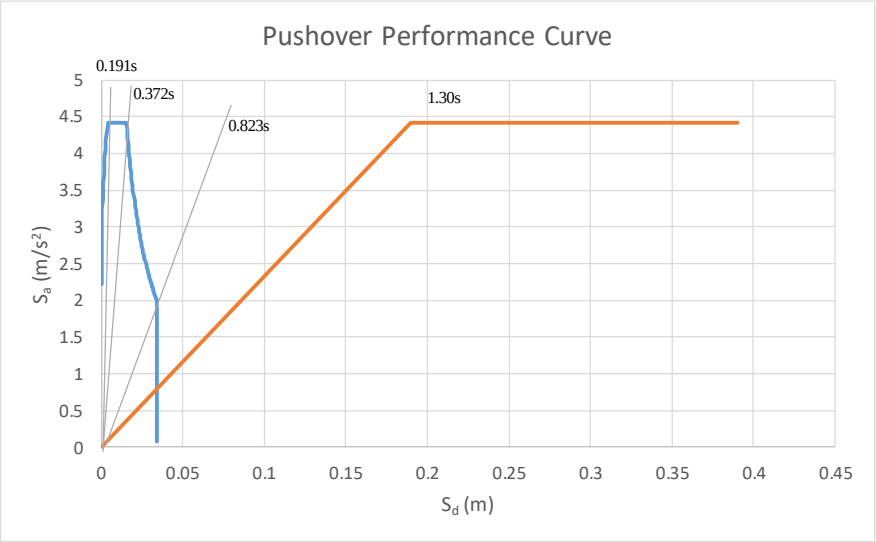

Figure 4.21 Determination of performance point for MRF frames

As observered from figure 4.21, the target displacement of the equivalent SDoF system is 33.35 mm imposed by the seismic input considered during which the structure is still is in elastic branch of the capacity spectrum. In other words, seismic action corresponding to this level does not lead to non-linear response of the structure in the transverse direction. Correspondingly, the target displacement for MDoF system is $\Gamma \cdot d^*_{et}$ = 41.38 mm and the structure remain elastic. Note that this is the target displacement for seismic input in the form of elastic response spectrum adopted in section 4.2.

A variation study was performed to assess the level of seismic motion that will cause the structure to perform inadequate corresponding to a specified limit state. Figure 4.22 suggests that seismic motion per EC8 type II 5% damped elastic spectra at a site with ground type C causes structure to perform inadequately for CP, LS and IO limit states for a PGA of 0.53g, 0.42g and 0.28g respectively. The corresponding target displacements of MDoF system ($\Gamma \cdot d^*_t$) for the above limit states are respectively 0.48 m, 0.39 m & 0.26 m. At these target displacements, the structure is considered inadequate for the associated performance limit state.

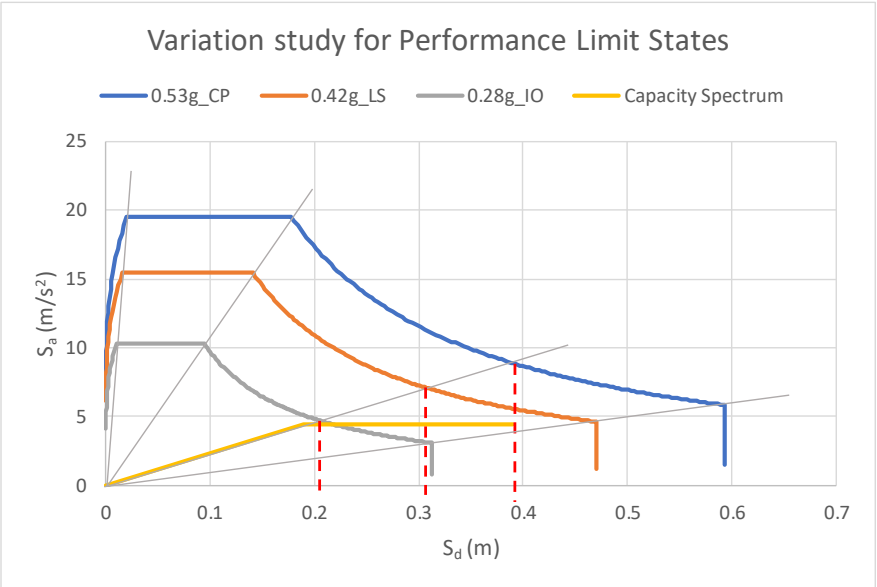

Figure 4.22 Variation of PGA corresponding to attainment of performance limit states (MRF)

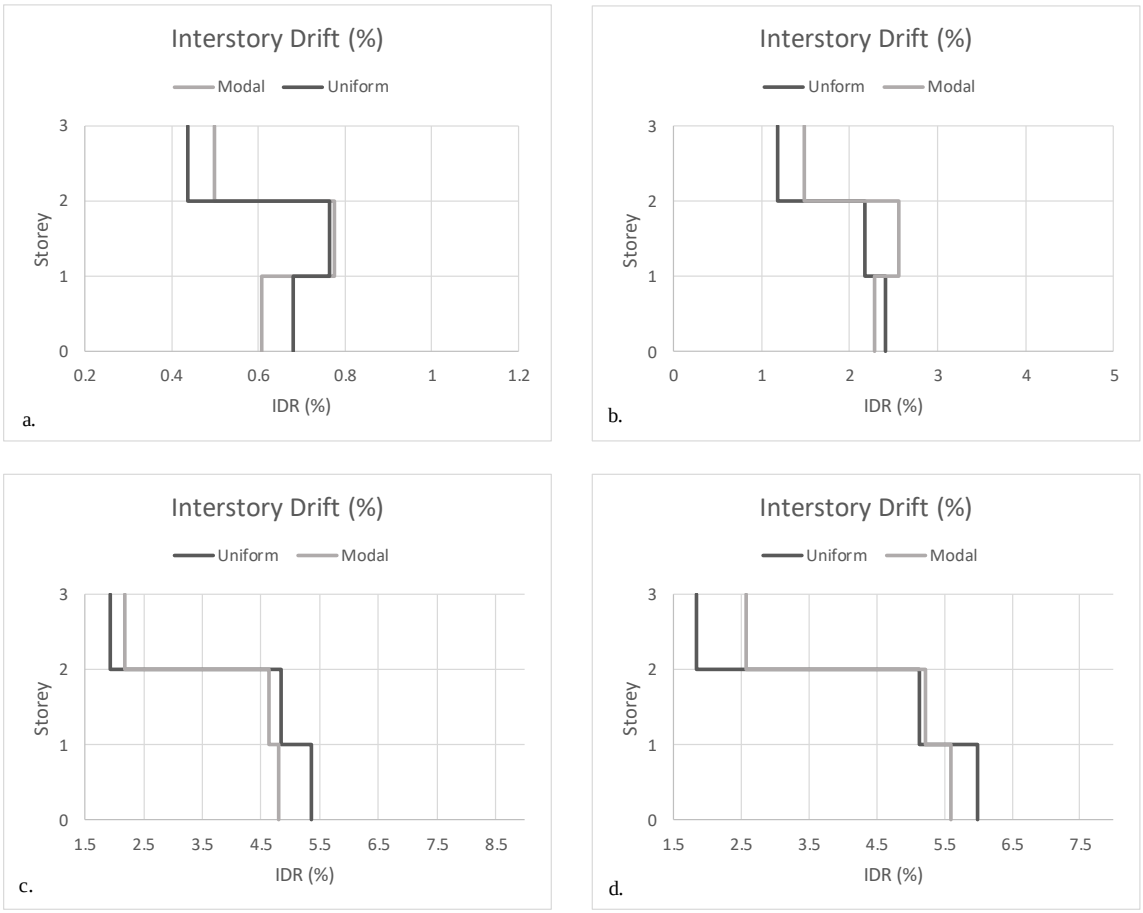

Figure 4.23 Interstory Drift Ratio (%) corresponding to target displacement at a) current seismic level, b) IO, c) LS and d) CP limit state for MRF

A comparison of interstory drift is shown in figure 4.23 at target displacements corresponding to attainment of different performance levels. The concentration of higher drifts in the lower story at LS and CP limit states is due to the formation of soft story mechanism as described in the previous observation whereas at IO, story 2 suffers the maximum interstory drifts. More so, in all the cases, a uniform load pattern leads to higher IDR's at lower stories whereas modal load pattern at the upper story. Although, the difference is not too significant, the loading pattern does have an impact on the determination of capacity curve as shown before and also on determination of IDR.

4.6.2 Pushover Analysis for Concentrically Braced Frames

A similar analysis was performed for the braced frame of the structure to analyse the anticipated behaviour when subjected to lateral seismic loading. There are two fundamental considerations when defining the behaviour of axial plastic hinges in the braces. Whereas EN1998-1 suggests taking into account only tension diagonals in the elastic analysis, the use of both tension and compression diagonals is allowed provided the behaviour of system is verified by non-linear analysis with pre-buckling and post-buckling situations of the compressed diagonal being considered. While modelling, this has been considered by defining hinges to drop load to zero at the critical buckling load. On the other hand, FEMA 356 recommends that the load carrying capacity of brace in compression drops to 0.4 times the buckling load. The analysis is performed for both the defined situations. Figure 4.24 shows the adopted behaviour of axial plastic hinges.

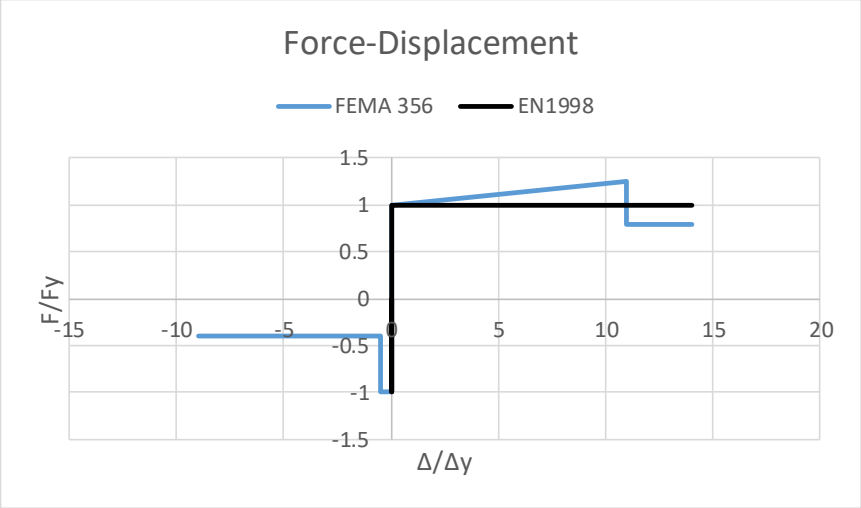

Figure 4.24 Generalized force-deformation relationship for braces

The principle consideration in capacity design of concentrically braced frames is to provide sufficient strength to the system so that bracing members yield in tension and buckles in compression, which is primarily the source of inelastic mechanisms, without failing of other components [34].

A pushover analysis was performed considering the above behaviour of axial plastic hinges located at a relative distance 0.5 along the brace length. The sequence of formation of plastic hinges is well in line with the anticipated behaviour i.e. the braces in compression buckles in a brittle manner whereas braces in tension yields consecutively starting from story 1 to story 3. The system is pushed to a global drift corresponding to recommendations from FEMA 356 which imposes a limitation of 2% for CP limit state. Figure 4.26 shows the pushover curve for the system subjected to i) Uniform load proportional to the storey mass and ii) 1st mode load pattern with FEMA 356 definition of plastic hinges and figure 4.27 is based on same parameters without a reserve of strength once a compression brace buckles whereas idealized elasto-plastic on the tension side without strain hardening effects and equivalent linearized curve for an equivalent SDoF system derived from the results of capacity curve of a MDoF system. The conversion parameters are summarized in Appendix VI of this report.

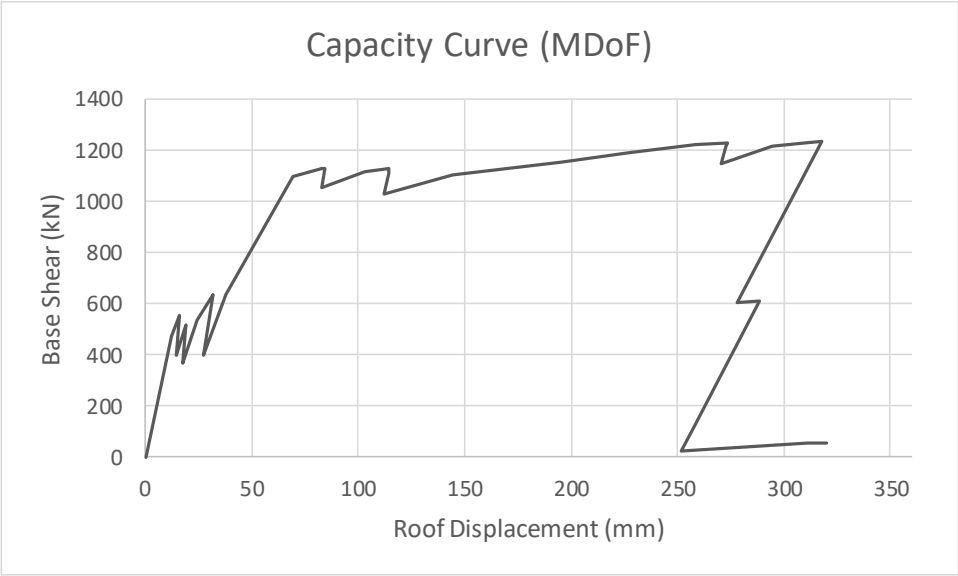

Figure 4.25 Pushover curve for a braced frame with drop in the load carrying capacity modelled with recommendations from FEMA356

Figure 4.25 reflects the typical characteristic curve for a CBF. The 'fork-type' kinks represent the drop in the lateral resistance after the first plastic event i.e. buckling of the compression brace as soon as the axial compression reached buckling resistance. It is followed by an increase in the resistance with reduced stiffness. A similar behaviour was observed in the report on Equaljoints research project [38] where a preliminary investigation on the behaviour of CBF's was made for 6 and 12 storied building.

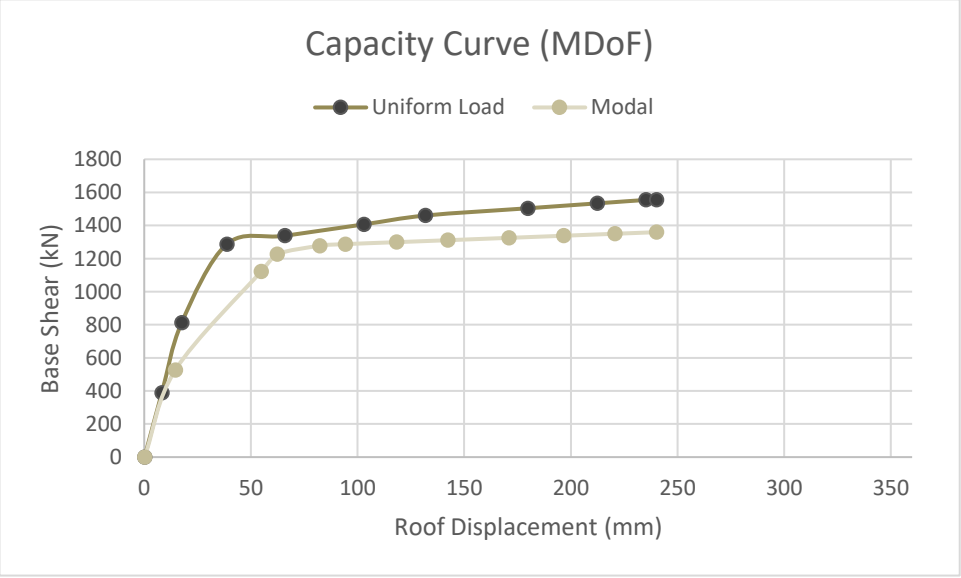

Figure 4.26 Pushover Capacity curve for MDoF system of Braced Frame with FEMA356 definition of plastic hinges

From the pattern of formation of plastic hinges, it is clear that the distribution of damage is uniform across the stroreys which was the basis to introduce selection criteria for braces as per EN1998-1 to avoid accumulation of ductility demands at a particular storey. Next, the

overstrength factor was determined corresponding to $q_s = \frac{F_y}{F_1} \cdot \frac{F_1}{F_d}$, where F_y is the ultimate collapse base shear, F_1 is the base shear corresponding to first non-linear event and F_d is the design base shear. EN1998-1 recommends minimum value of the overstrength factor calculated using the modal and uniform lateral load patterns. Table 4.33 shows the calculation of q_s factor as per EN1998-1 approach. Similar observations were made by da Silva, A.T., et al. [34]. Note that this q_s is not the q-factor considered in the design as per EN1998 which is $q_\mu \cdot q_s$

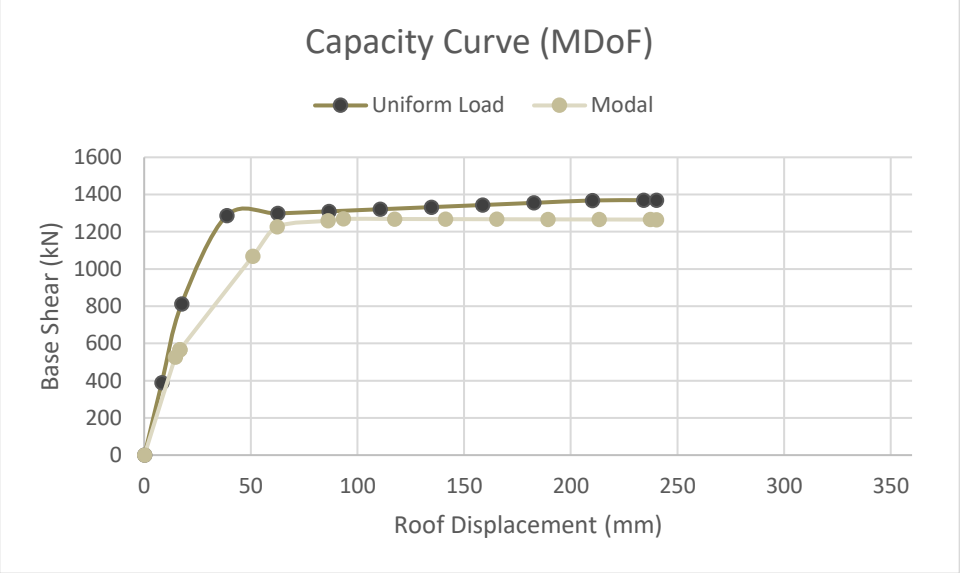

Figure 4.27 Pushover Capacity curve for MDoF system of Braced Frame with Idealized elasto-plastic definition of plastic hinges with no reserve capacity beyond buckling of compression brace

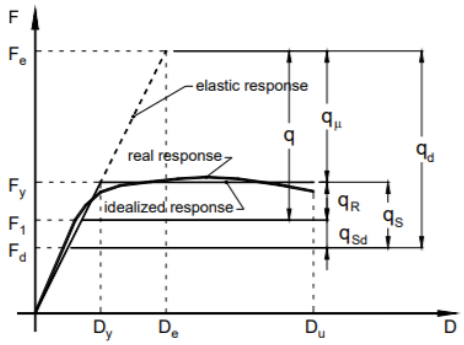

Figure 4.28 Definition of force reduction factors [35]

Table 4.33 Summary of behaviour factor from Pushover Analysis

Hinge Definition	F_y/F_1		F_1/F_d		$(F_y/F_1)_{min}$	$(F_1/F_d)_{min}$	q_s
	Modal	Uniform	Modal	Uniform			
FEMA356	1.109	1.208	2.087	2.192	1.109	2.087	2.315
EPP	1.032	1.065	2.088	2.192	1.032	2.088	2.155

Evident from the capacity curves of MDoF systems, the pushover curve for modal loads (inverted triangular) leads to a conservative estimate of structure's behaviour, figure 4.29 shows the capacity curve and equivalent linearization of the curve for corresponding SDoF system for determination of target displacement. The points marked on the same curve for performance limit states based on yield deformation (Δ_t or Δ_c) obtained from SAP2000 output comforms with the global drift limits based on FEMA 356 document i.e. 2% for CP, 1.5% for LS and 0.5% for IO limit states.

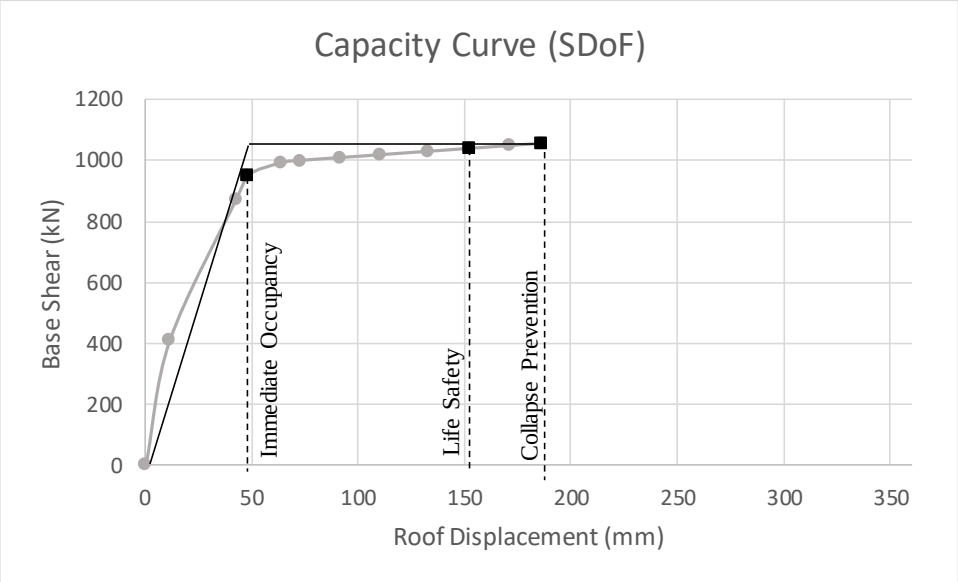

Figure 4.29 Pushover Capacity curve for SDoF system of Braced Frame

Next, the seismic performance of the concentrically braced frame was evaluated in the ADRS spectrum format using graphical representation of seismic demand and the capacity spectrum as per appendix B of EN1998 using N2 method. Figue 4.30 shows the determination of target

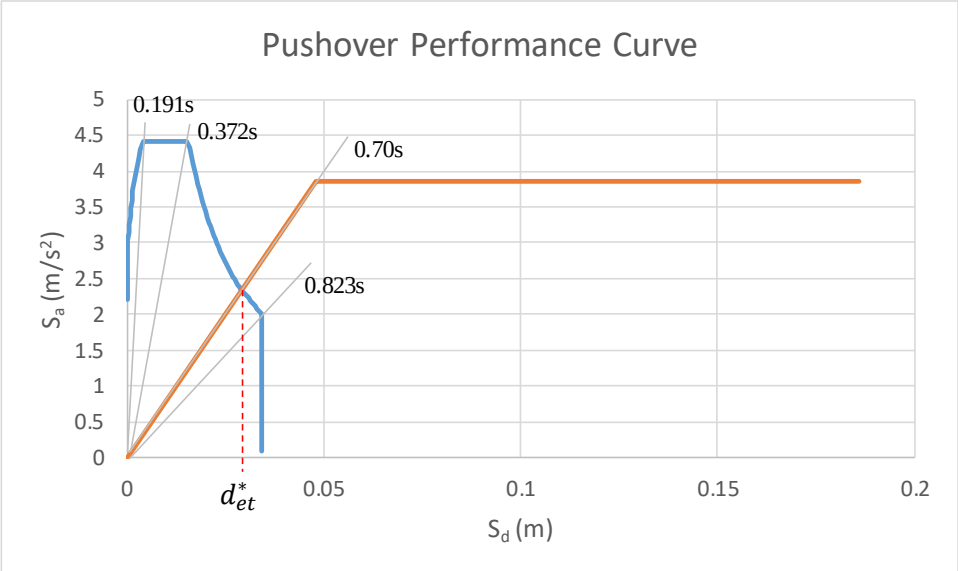

Figure 4.30 Determination of performance point for CBF frames

displacement imposed on the structure due to seismic action from the Groningen region.

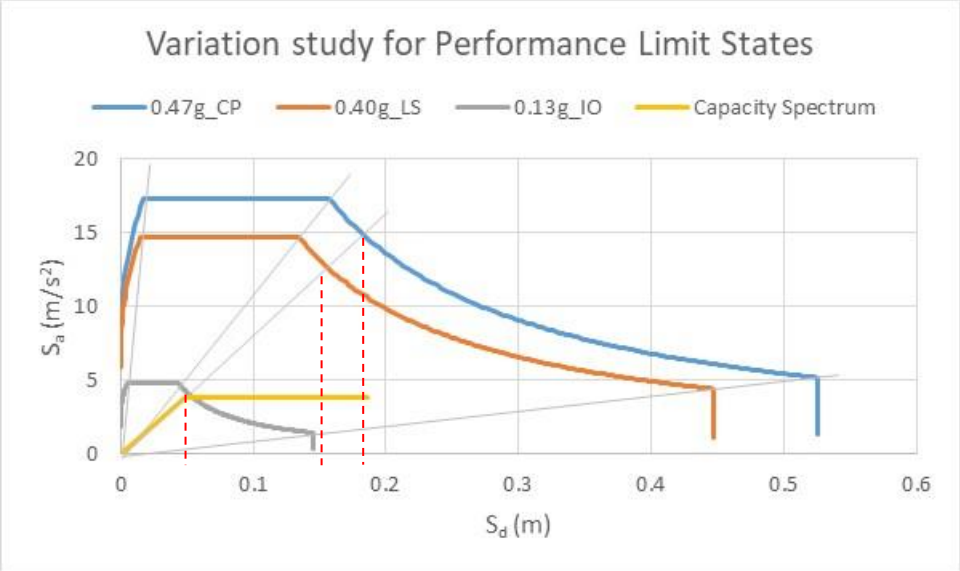

Figure 4.31 Variation of PGA corresponding to attainment of performance limit states (CBF)

The target displacement d^*_{et} for equivalent SDoF system as determined using N2 method is 29.20 mm which is less than the 0.5% global drift limit for IO limit state, the structure performs adequately. The corresponding displacement for MDoF system is $\Gamma \cdot d^*_{et}$=37.64 mm. A variation study to determine the level of seismic motion that will result in inadequate performance of structure was performed resulting in 0.47g, 0.40g and 0.13g for CP, LS and IO respectively for an ADRS reflecting EN1998 type II spectra at a site with type C soil conditions (figure 4.31). Figure 4.33 shows the distribution of interstory drifts (IDR, %) across the floors of the structure corresponding to i) target displacement at current seismic level, ii) IO, iii) LS, and iv) CP limit states for modal and uniform load patterns. The predominant accumulation of higher interstory drift at the 1st floor is attributed to plastification of tension brace starting at level 1 with subsequent increase in axial deformation (figure 4.32) as the target displacement is reached forming a storey like mechanism increasing the drifts.

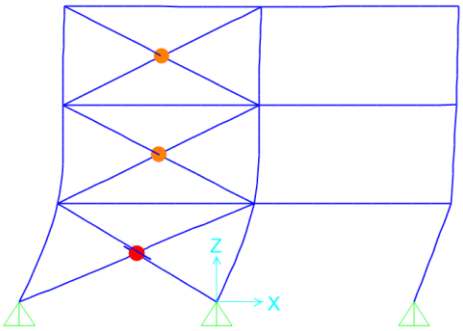

Figure 4.32 Deflected profile of CBF at CP limit state with higher interstorey drifts at storey 1

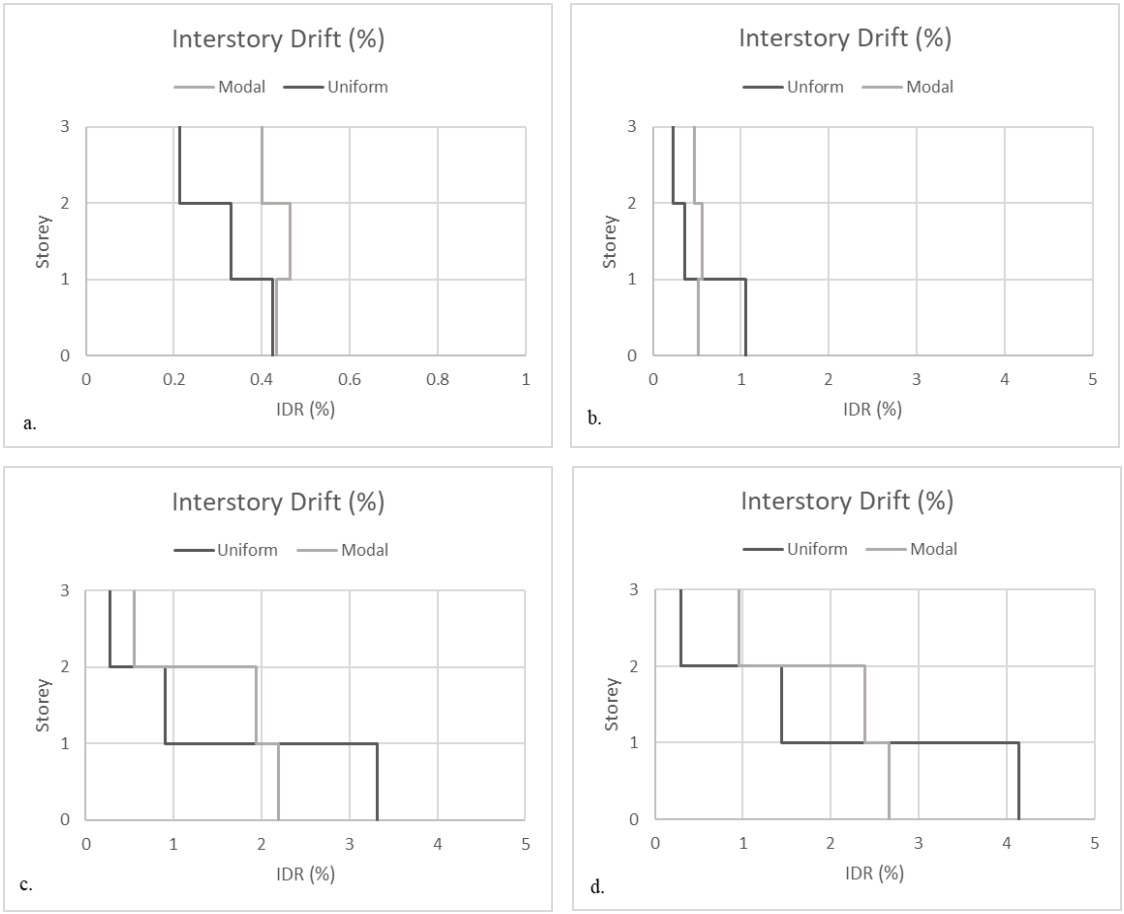

Figure 4.33 Interstory Drift Ratio (%) corresponding to target displacement at a) current seismic level, b) IO, c) LS and d) CP limit state for CBF

The comparison and discussion of results using the analysis methods used in this section is made in next chapter of report with further discussion on the applicability to other kind of structures.

5. Discussion

Based on the seismic analysis of case study structure performed in the previous chapter, this chapter is dedicated to comparison and discussion on the results obtained, applicability and further extension to structures other than regular typology of building structures. The case study structure was analysed globally for the seismic demands imposed due to seismic action corresponding to NPR9998 at Oosterdijkshorn region in the Groningen province of the Netherlands with PGA (a_gS) of 0.2259g with other parameters defined in section 4.2. Structural safety checks including inter-storey drift ratio, estimation of overstrength for capacity design procedures for MRF and CBF, discussion about the effects of brace slenderness limitations were performed by linear static (lateral force) and linear dynamic (response spectrum) analysis procedures. Non-linear static (pushover) analysis was performed to check anticipated progression of damage and to evaluate the performance of structure for this level of ground motion and also a variation study to assess the ground motion for which structure performs inadequate corresponding to performance levels defined in codes and guidelines.

The seismic analysis was performed for a steel structure, however, it is the fundamental understanding of the analysis methods which assess the structure on a global level to obtain the demands and assess the performance. The same procedures, in principle, are applicable to structures of different typology in terms of material behaviour viz. concrete, masonry, composite steel-concrete, with difference in strength, stiffness, constitutive relations and design methodology at the component level on one hand, and structural geometry viz. bridges, water-gates, quay-walls, water tanks on the other. The difference lies in the level of details to be included in the numerical or analytical model, for example, soil-structure interaction in the case of quay-walls, fluid-structure interaction in case of tanks which alter the dynamic behaviour of structures in terms of response time-period of vibration.

Whereas linear analysis based on force-based methods has been a traditional approach for seismic assessment to capture the force demands on the structure, displacement-based methods employing non-linear approach provides key insight in terms of quantification of damage to a specific performance level. Force-based methodology is generally based on a set of rules defined by guidelines which does not require the designer to understand the performance and structural behaviour but the component actions and corresponding resistance for example beam flexure, column interaction, connection strength, bracing behaviour etc based on capacity design rules. In contrast, displacement-based approach simulates the true non-linear behaviour of the structure in terms of imposed deformation demands and acceptance criteria based on experimental investigations to satisfy various performance levels, based on requirements of the owner and legislations. The performance levels intended to quantify damage are based on, for example, axial elongation/comrpession of braces, plastic rotation of plastic hinges in flexural members limited to accepted values as per EN1998-3, FEMA356, ATC40 [33]. Fundamental differences in the two methodologies generally adopted to satisfy structural behaviour is highlighted in detail in section 2.4 of this report.

In the next section, comparison of results obtained in the previous chapter is made with further discussion on the suitability of analysis methods and the level of insight they provide to understand the seismic behaviour.

5.1 Comparison of Results

This section compares the results in terms of force demands imposed on the structure due to the design earthquake in Groningen province of the Netherlands. Linear analysis was performed using lateral force analysis (linear-static) and response spectrum (linear-dynamic) methods using SAP2000. Capacity design rules were followed as recommended by EN1998-1 by considering an overstrength factor to enforce strong column-weak beam principles. Braces were adopted to avoid accumulation of ductility demands at a particular storey.

Structural time-period calculated using the simplified EN1998-1/NPR9998 expression resulted in deviation of natural period of vibration compared to the fundamental mode period calculated using modal analysis. This is an important consideration since estimation of seismic forces is solely based on time-period and system damping as far as linear methods are concerned. Consequently, the seismic base shear calculated may lead to over-estimation (or in some cases under-estimation). A numerical model taking into account inertial mass from gravity frames in the form of a 'leaning column' with mass lumped at storey joints correctly justifies the framing when one is interested in planar analysis in the form of 2D frames. A simple validation can be seen with time period calculated using this approach with the one calculated from 3D model of the entire structure in predominant modes.

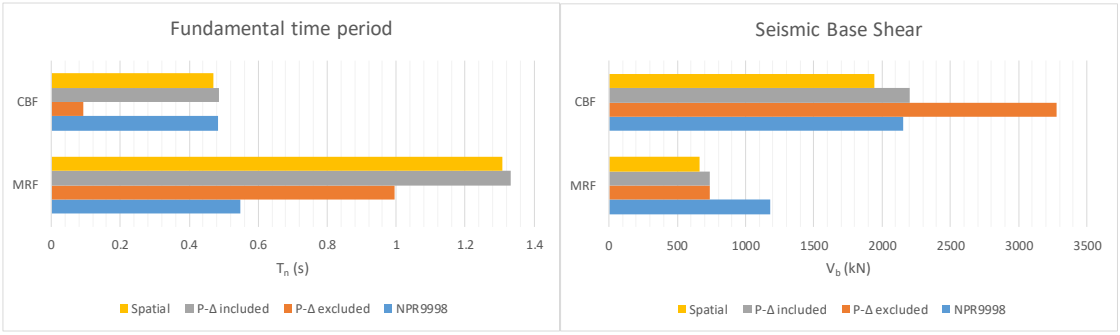

Figure 5.1 Comparison of fundamental time period and seismic base shear force using different numerical models

Next, the efficacy of planar models to capture the action effects for components was ascertained using calculation of critical forces for structural members using linear static (LS) approach and linear dynamic (LD) approach and the results were found to be in close agreement considering the lower seismic base shear in the LD methods which superimposes modal contributions as shown in figure 5.2. Note that axial forces in the girder from LD approach is not available since a rigid diaphragm was assigned at the floor level which resulted in a rigid body movement implying zero axial strains and correspondingly zero axial forces. However, this is not significant as observed from the results of LS approach where the utilization ratio for axial forces is less than 0.15 recommended by EN1998 to prevent plastic hinges due to axial force. Also, a shear force limit of 0.5 is imposed for beams of MRF's to ensure full plastic moment resistance is not decreased by shear forces. This limit was shown to be verified for the seismic design situation.

Figure 5.2 Comparison of critical element forces from linear static (LS) and linear dynamic (LD) procedures for a) MRF girders, b) internal MRF columns, c) external MRF columns and d) axial forces in braces

A pushover analysis was performed to check the check structural performance during the design earthquake, to verify the capacity design rules and to justify the overstrength (or redundancy) factor considered in the linear design methods. It was found that the structure deforms elastically under the design ground motion selected from the Groningen region and possess an overstrenth factor (α) of 1.31 as compared to 1.3 adopted in design however, the capacity-based consideration of strong column-weak beam was violated due to the formation of story mechanism at level 1 as opposed to the assumption of plastic hinges not being formed in the columns at a story level. In the event of a strong earthquake, this is not an appreciable behaviour as it may lead to a premature collapse of the structure in the form of soft storey. The analysis showed an intended configuration of inelasticity with a column size of HE300M.

It is for this reason that displacement-based non-linear analysis comes as a superior alternative to force-based analysis since the latter concludes an overstressed member due to additional forces being acted upon components due to an earthquake, whereas former leads to a conclusion on which one can quantify the damage based on degree on non-linearity induced by the ground motions in terms of rotation/displacement at a pre-authorised performance level. It should also be concluded that if a design earthquake leads a structure to respond elastically, as in this case, both the methodologies are expected to provide similar results.

Whereas FEMA 356 defines the attainment of a performance level at global level corresponding to a global drift limit (2% for CP, 1.5% for LS & 0.5% for IO) based on experimental investigations, EN1998-3 does not state the same at a global structure level. The corresponding performance limit states in EN1998-3 (CP, SD & DL) is pertained to component plastic rotations and displacements respectively for flexural members and axial members.

In the similar manner, pushover analysis was performed in the longitudinal direction of the framing considering two approaches with i) reserve capacity of compressional brace beyond buckling, ii) drop in the reserve capacity to zero, and pushover curves were obtained for both the cases with uniform and modal load application methods recommended generally by the guidelines. The ii) case provides a more conservative criteria in estimation of structural capacity as compared to the FEMA 356 approach. EN1998-1 makes the same recommendation as ii) above to neglect the resistance of compression brace beyond buckling. Target displacement for the design seismic action was calculated as per N2 method (Fajfar P. et. al) in the ADRS capacity spectrum format. A further variation of ground motion to predict the structural response corresponding to attainment of different performance levels in terms of induced target displacements was performed for IO, LS and CP limit states.

6. Conclusions and Recommendations

This chapter lists down conclusions derived from the present thesis starting from problem statement and the achieved objectives followed by recommendations for further studies and guidelines. The basic aim of this thesis was to lay down a fundamental understanding of earthquakes & guidelines in the field and behaviour of structures subjected to seismic loading in the region of Groningen, the Netherlands which is in the grip of induced earthquakes for a few years now due to extraction of gas in the shallow regions of the reservoir. Although the damage is pertained to cracks in the masonry structures, there has been a growing fear among the authorities and residents due to damage reports and there is a need to safeguard structures other than the masonry houses by making an assessment of potential weaknesses. The old structures have not been designed to sustain seismic loading and this calls for a need to assess the structural performance of existing structures as well as consideration of seismic loading for design of new structures since seismological studies have revealed the likelihood of an earthquake higher than the ones recorded historically till date.

The motivation to address seismic behaviour of steel structures stemmed from the consideration that apart from masonry structures, a city's infrastructure consists of framed steel industrial buildings, composite office buildings, bridges (either concrete, steel or composite although there is a predominant presence of concrete bridges in the Groningen province) as well as frames concrete structures. The global analysis for assessment of action effects and assessment of performance limit states by non-linear analysis performed in chapter 4 provides a detailed step-by-step procedure together with the underlying principles as well as differences in the analysis methodologies and comparison of results.

6.1 Conclusions

The case study, however made for a steel framed structure, can in principle serve the other typologies mentioned above. The difference lies in the expected structural behaviour at a material level, for example the non-linear behaviour for quasi-brittle masonry, concrete structures in which the crack initiation and propagation leads to a change in structural stiffness and induces non-linearity. Also, the potential regions for plasticity determines numerical modelling at the component level.

- An explanation on the understanding of design response spectrum is made in chapter 3 to enable a design engineer to interpret the form in which seismic loading is generated from a ground motion recorded by accelerograms by making use of response of a SDoF oscillator to each time step of an acceleration record. In the absence of accelerograms, suite of ground motion recordings from similar source, magnitude & site characteristics can be used and spectrally matched to the target spectra defined by guidelines which can then be used to perform advanced non-linear time history analysis.

- However, the generated mean spectra generated from a suite of ground motions from European Strong Motion (ESM) database and scaled to reference PGA corresponds closely to the one recommended by NPR9998 webtool, detailed investigation is required to understand how the non-linear soil response considered in the latter one is incorporated along with the a_gS term referred to in the document. The NPR committee was contacted but it was informed that they are expecting to release the background information by the end of year. It is important since the displacement induced by

elastic spectra from NPR on the structure is quite less as compared to similar spectra obtained from the EN1998-1 equations which explicitly consider soil factor.

- Although the characteristics of induced earthquakes in the Netherlands is different from the historic earthquakes for e.g. El-Centro, it is more on the response side that matters. The same analysis philosophy is in principle applicable to this situation. The difference lies in the input seismic loading in the form of design response spectra or ground motion time-history for advanced analysis.

- It was ascertained that fundamental time period calculation using the expression provided by NPR9998 and EN1998-1, which is a parametric function of height of a structure should be used with caution as it may lead to unrealistic demands on the structure. Instead, a modal analysis should be performed which reflects the participating mass and correct time period provided numerical model takes into account relevant parameters associated with lateral response of the structure, which in the case study was addition of a 'leaning column' to laterally support the gravity frames.

- Capacity-based design approach adopted during linear assessment of the structure should be verified with non-linear analysis to ascertain the assumption. In the case above, although the condition specified in EN1998-1 ($\Sigma M_{pl}^{c} \geq 1.3 \cdot \Sigma M_{pl}^{b}$) was satisfied while making force assessment, it was only concluded by a non-linear static pushover analysis that this condition was violated forming a soft storey mechanism after dissipation of energy in plastic hinges in the beams at the story level 1 leading to large interstorey drift. The pushover method also provides a means to verify the overstrength adopted in design using q-factor approach. The same was verified to satisfy the assumption of $\alpha = 1.30$ recommended by EN1993-1.

- Displacement-based non-linear static pushover analysis was performed with a lumped plasticity model with two different non-linear definition of plastic hinges and two invariant load patterns i.e. uniform and modal. However, for the case study building under consideration which vibrates predominantly in the fundamental mode (~85% mass participation), this method provides acceptable results, it is expected that when a single mode invariant load pattern is used for structures where higher mode effects are significant, it will not capture the real response. A modal pushover analysis is the solution, although not fully developed, ongoing research of Gupta and Kunnath [36], Chopra and Goel [37] provides relevant methodology. Since most of the affected structures in the Groningen region are such that fundamental mode of vibration leads the response, pushover analysis can prove to be a reliable method for estimation of inelastic demands which is expected to be provided by complex and computationally intensive non-linear time history analysis.

- For the case of non-linear assessment of concentrically braced frames, it was evident that load carrying capacity of compression brace need not be taken into account further to buckling as it may lead to unconservative estimation of capacity of the structure, although FEMA356 considers a residual capacity of 0.4 times the critical load, recommendations from EN1998-1 to consider the contribution of brace in tension leads to a conservative approach.

- The case study structure is not expected to be damaged based on the seismic intensity adopted in the Groningen region except for the possibility of a soft-storey mechanism at a higher seismic intensity of 0.53g corresponding to Type II response spectrum at a site with soil type C classification as per EN1998-1. Although this level of ground motion is unlikely to occur in the Groningen region, a Collapse Prevention limit state of assessment is likely to lead to an over designed structure.

- Full-strength non-dissipative moment connection was considered in the design of beam-column joint however, based on Equaljoints research project, prequalified equal strength joints (dissipative zones in the beam and connection) and partial strength joints (dissipative zones in the joint) would be included in the updated version of EN1998-1 satisfying different performance levels on the basis of strength, ductility, technological and cost considerations.

6.2 Recommendations

The present study provides an extensive review on the linear and non-linear seismic behaviour of steel structures in the form of a comprehensive understanding of the underlying principles on the which the assessment is based. Differences in analysis methodology based on NPR9998/EN1998-1 and FEMA356/ASCE41-13 were laid down in terms of material non-linearity.

- Unlike FEMA356, there is no specific guideline in EN1998 for acceptable drift limitations corresponding to performance limit states and non-linear modelling specifications (for example, residual moment capacity at a certain plastic rotation). Although, an elastic-perfectly plastic moment-rotation characteristic can be adopted for carrying out non-linear static pushover analysis, it is expected that it might lead to unconservative assessment of structural capacity in terms of ductility. In this regard, this should be explicitly outlined in the future revision of Eurocodes based on experimental investigations.

- A study on Pushover methods with adaptive load patterns, consideration of higher mode effects and modal response combination could be undertaken to compare the effectiveness of using load pattern considering fundamental mode shape alone.

- A time-history analysis with varying hysteretic rule taking into account strength & stiffness degradation under cyclic loading to be compared with the outcomes from nonlinear static analysis.

Further, this thesis serves as an understanding on the assessment of steel structures, additional studies to assess other kinds of structures could be undertaken forming on the basis of fundamental analysis methodologies adopted in this thesis.

- Assessment of damage to quay-walls and sheet piles, which have a major role in safe guarding harbours in the Netherlands, is recommended with additional study on the soil-structure interaction effects and alteration of structural behaviour to seismic loading.

Bibliography

[1] Hagoort, Jacques. "Empirical Model for Induced Earthquakes in the Groningen Gas Field"

[2] Statistical evidence of production driven seismicity at Groningen Field, TNO

[3] Danijela Sijacic, Frank Pijpers, Manuel Nepveu, Karin van Thienen-Visser, 2017. "Statistical evidence on the effect of production changes on induced seismicity"

[4] https://www.nen.nl/NEN-Shop/Eurocodes/Veilige-constructies-bij-aardbevingen.html

[5] NAM Groningen 2013, "Preliminary Structural Upgrading Strategy for Groningen". ARUP

[6] Elnashai,A., Di Sarno,L., 2008, " Fundamentals of Earthquake Engineering", Wiley.

[7] Staeuble, A.J. & Milius, G. (1970). Geology of Groningen gas field, Netherlands. Mem. - Am. Assoc. Pet. Geol.; (United States).

[8] NAM Groningen 2013, "Preliminary Structural Upgrading Strategy for Groningen". ARUP

[9] Study and Data Acquisition Plan Induced Seismicity in Groningen Update Post-Winningsplan 2016

[10] Toetsing van de bodemdalingsprognoses en seismische hazard ten gevolge van gaswinning van het Groningen veld. TNO report 2013 R11953, 23 December 2013. http://nlog.nl/resources/Aardbevingen%20Groningen/TNO_rapport_Groningen_15-01-2014_gelakt_pre-scan.pdf.

[11] https://earthquake.usgs.gov/learn

[12] De Luca, F., Kythreotis, S., Werner, M., & Verdon, J. (2017). Natural earthquakes as proxies for induced seismic hazard and risk: comparing peak and cyclic inelastic response. In World Conferences on Earthquake Engineering: online proceedings [1837]

[13] Chopra, A. K., 2012, "Dynamics of Structures: Theory and Applications to Earthquake Engineering", 4th edition, Prentice Hall, Englewood Cliffs, New Jersey.

[14] Tomaževič, Miha. (2009). Shear resistance of masonry walls and Eurocode 6: Shear versus tensile strength of masonry. Materials and Structures. 42. 889-907. 10.1617/s11527-008-9430-6.]

[15] NZSEE - New Zealand Society for Earthquake Engineering, 2015, "Assessment and Improvement of the Structural Performance of Buildings in Earthquakes"

[16] Tolles, E. L., F. A.Webster, A.Crosby, and E. E.Kimbro. 1996. Survey of damage to historic adobe buildings after the January 24 Northridge earthquake. Getty Conservation Institute Scientific Program Report, J. Paul Getty Trust Publication, Los Angeles, Calif.

[17] Tomazevic, M., 1999, "Earthquake-Resistant Design of Masonry Buildings", Slovenian National Building and Civil Engineering Institute, Imperial College Press.

[18] Ingham, J.M. and Griffith, M.C. (2011). The performance of unreinforced masonry buildings in the 2010/2011 Canterbury earthquake swarm, Report to the Royal Commission of Inquiry into Building Failure Caused by the Canterbury Earthquake. http://canterbury.royalcommission.govt.nz/documents-by-key/20110920.46.

[19] Bothara, J.K. and Hiçyılmaz, K. (2008). General observations of the building behaviour during the 8th October 2005 Pakistan earthquake, Bulletin of the New Zealand Society for Earthquake Engineering, Vol. 41, No. 4.

[20] FEMA 306 (1998). Evaluation of earthquake damaged concrete and masonry wall buildings, Federal Emergency Management Agency, FEMA Report 306, Washington, DC.

[21] Dizhur, D., Ingham, J.M., Moon, L., Griffith, M., Schultz, A., Senaldi, I., Magenes, G., Dickie, J., Lissel, S., Centeno, J., Ventura, C., Leiti, J. and Lourenco, P. (2011). Performance of masonry buildings and churches in the 22 February 2011 Christchurch earthquake, Bulletin of the New Zealand Society for Earthquake Engineering, 44, 4, Dec., 279-297.

[22] Dizhur, D., Campbell, J., Schultz, A. and Ingham, J.M. (2013). Observations from the 2010/2011 Canterbury earthquakes and subsequent experimental pull-out test program of wall-to-diaphragm adhesive anchor connections, Journal of the Structural Engineering Society of New Zealand, 26(1), April, 11-20.

[23] Campbell, Josiah & Dizhur, Dmytro & Hodgson, Michael & Fergusson, George & Ingham, Jason. (2012). Test results for extracted wall-diaphragm anchor plates from Christchurch unreinforced masonry buildings. Journal of the Structural Engineering Society of New Zealand. 25. 56-67.

[24] Priestley, M. J. N., 1985, “Seismic behavior of unreinforced masonry walls”, Bulletin of the New Zealand National Society for Earthquake Engineering, Vol. 18, No. 2, pp 191 – 205.

[25] MA ElGawady, P Lestuzzi, andMBadoux. „Retrofitting of masonry walls using shotcrete“. In: 2006 NZSEE Conference, Paper. Vol. 45. 2006.

[26] Priestley, M. J. N, Calvi, G. M, Kowalsky, M. J, 2007, “Displacement based seismic design of structures”, IUSS Press, Istituto Universitario Studi Superiori di Pavia.

[27] Elghazouli, A. Y. (2003) “Seismic Design Procedures for Concentrically Braced Frames”, Proceedings of the Institution of Civil Engineers, Structures and Buildings, 156, 381-394.

[28] Mohammad Agha, Houssam & Li, Yingmin & Asal Salih, Oday & Ssim Al-Jbori, A. (2018). NONLINEAR PERFORMANCE OF A TEN-STORY REINFORCED CONCRETE SPECIAL MOMENT RESISTING FRAME (SMRF).

[29] P.Fajfar,”A nonlinear analysis method for performance-based seismic design” Earthquake Spectra 2000,16(3):573-592

[30] N. M. Newmark and W. J. Hall, Earthquake Spectra and Design, Earthquake Engineering Research Institute, Berkeley, Calif., 1982, pp. 35 and 36

[31] FEMA 356 2000: Prestandard and commentary for the seismic rehabilitation of buildings.

[32] NIST GCR 17-917-45: Recommended Modelling Parameters and Acceptance Criteria for Nonlinear Analysis in Support of Seismic Evaluation, Retrofit and Design. NEHRP publication. https://doi.org/10.6028/NIST.GCR.17-917-45

[33] ATC-40. Seismic Evaluation and Retrofit of Concrete buildings, Applied Technology Council, Redwood City (1996)

[34] da Silva, A. T., C. Rebelo, L. S. da Silva, M. D'Aniello, R. Landolfo, and L. Lima. "Seismic performance of dual steel Concentrically Braced frames."

[35] Peter Fajfar: "General definition and basic relations", Moment resistant connections of steel frames in seismic areas. Design and reliability, Ed. F.M. Mazzolani, E&FN Spon, London, p. 565-578, 2000

[36] Gupta, B. and Kunnath, S.K. (2000). "Adaptive spectra-based pushover procedure for seismic evaluation of structures.", Earthquake Spectra, 16(2), 367-392

[37] Chopra, A.K. and Goel, R.K. (2002). "A modal pushover analysis procedure for estimating seismic demands for buildings." Earthquake Engineering and Structural Dynamics, 31,561-582.

[38] European pre-QUALified steel JOINTS (EQUAL JOINTS) Final report – Study. Directorate-General for Research and Innovation (European Commission). [available at EU Publications]

[39] Grecea, D., Stratan, A., Ciutina, A., & Dubina, D. (2004). Rotation capacity of MR beam-to-column joints under cyclic loading. Connections in Steel Structures V—Amsterdam, 141-154.

[40] EN 1998-1 2004: Design of structures for earthquake resistance - Part 1: General rules, seismic actions and rules for buildings.

[41] EN 1998-3 2005: Design of structures for earthquake resistance – Part 3: Assessment and retrofitting of buildings.

[42] NPR 9998 (en) 2017: Assessment of structural safety of buildings in case of erection, reconstruction and disapproval – Basic rules for seismic actions: induced earthquakes. NEN publication.

[43] NEN-EN 1993-1-1 2006: Design of steel structures – Part 1-1: General rules and rules for buildings.

[44] EN 1991-1-1: Actions on structures – Part 1-1: General actions – Densities, self-weight, imposed loads for buildings.

[45] SERIES – Seismic Engineering Research Infrastructure for European Synergies, Final report on BRACED – Brace Response and Assessment: Computation, Experiments and Design, July 2013

[46] Lecture Notes CIE5260 – Structural Response to Earthqukes, Seismic Analysis of Complex Structures. A. Tsouvalas, TU Delft.

[47] SAP2000 version 20, Computers & Structures, Inc. CSI Analysis Reference Manual.

Appendix I: MATLAB script for generation of Elastic Response Spectrum from input ground motion

```
%Script to generate Response Spectrum from Ground Motion%
%Newmark Numerical Integration%
clc;clear;close
load SCGM1.dat %.dat file with Column1 - time, Column2 - acceleration[g]
g=9.810;
Ag=g*SCGM1(:,2);
t=SCGM1(:,1);
dt=0.01; %enter recording time interval (s)%
zeta=5; %enter system damping in percentage%
endtime=4;
u=zeros(length(Ag),1);
v=zeros(length(Ag),1);
acc=zeros(length(Ag),1);
T(1)=0;
Ag(end+1)=0;
%Inital Calculations
for j=1:round(endtime/dt)
   omega(j)=2*pi/T(j);
   m=1;
   gamma=0.5;
   beta=1/6;
   c=2*m*omega(j)*zeta/100;
   k=(omega(j))^2*m;
   acc(1)=(-Ag(1)-c*v(1)-k*u(1))/m;
   a1=m*(1/(beta*dt^2))+c*(gamma/(beta*dt));
   a2=m*(1/(beta*dt))+c*(gamma/beta-1);
   a3=m*(1/(2*beta)-1)+c*dt*(gamma/(2*beta)-1);
   K=k+a1;
   P(1)=0;
   for i=1:length(u)-1
      P(i+1)=-Ag(i)+a1*u(i)+a2*v(i)+a3*acc(i);
      u(i+1)=P(i+1)/K;
      v(i+1)=(gamma/(beta*dt))*(u(i+1)-u(i))+(1-gamma/beta)*v(i)+...
         dt*(1-gamma/(2*beta))*acc(i);
      acc(i+1)=(1/(beta*dt^2))*(u(i+1)-u(i))-(1/(beta*dt))*v(i)-...
         (1/(2*beta)-1)*acc(i);
   end
   SD(j)=max(abs(u(:,1)));
   SV(j)=SD(j)*omega(j);
   SA(j)=SD(j)*(omega(j))^2/g;
   T(j+1)=T(j)+dt;
end
Ag(end)=[];
T(end)=[];
SD(2)=0;SV(1:2)=0;SA(1:2)=max(abs(Ag))/g;
```

```
figure('Name','Spectral Displacement','Numbertitle','off')
plot(T,SD,'g','LineWidth',1)
grid on
xlabel('TimePeriod (sec)','Fontsize',11);
ylabel('SD (m)','Fontsize',11);
title('Displacement Spectrum','Fontsize',13)

figure('Name','Pseudo-Spectral Acceleration','Numbertitle','off')
plot(T,SA,'b','LineWidth',1.5)
grid on
xlabel('TimePeriod (sec)','Fontsize',11);
ylabel('SA (g)','Fontsize',11);
title('Pseudo Acceleration Spectrum','Fontsize',13)

Ag=-Ag/g;
figure('Name','Input Time History','Numbertitle','off')
plot(t,Ag,'r','LineWidth',1)
grid on
xlabel('Time (sec)','Fontsize',11);
ylabel('Ag (g)','Fontsize',11);
title('Input Time History','Fontsize',13)
```

Appendix II: Calculation of Seismic Action effects (Lateral Force Analysis)

The seismic action effects for beams and columns of the lateral force resisting system are detailed in this appendix.

A. Calculation for Internal MRF

Calculation of Ω (Internal MRF)
Beam: IPE 400

Beam ID	$M_{pl,Rd,i}$ (kNm)	$M_{Ed,i}$ (kNm)	1/(1-θ)	Ω	Unity Check
16	463.985	-25.257	1.247	14.735	0.068
	463.985	-205.300	1.247	1.813	0.552
17	463.985	-47.239	1.248	7.867	0.127
	463.985	-190.280	1.248	1.953	0.512
18	463.985	-44.850	1.116	9.268	0.108
	463.985	-148.800	1.116	2.793	0.358
19	463.985	-62.651	1.247	5.940	0.168
	463.985	-190.920	1.247	1.949	0.513
20	463.985	-70.437	1.248	5.276	0.190
	463.985	-181.660	1.248	2.046	0.489
21	463.985	-86.607	1.116	4.799	0.208
	463.985	-134.740	1.116	3.085	0.324
22	463.985	-60.052	1.247	6.198	0.161
	463.985	-192.340	1.247	1.935	0.517
23	463.985	-71.452	1.248	5.201	0.192
	463.985	-180.280	1.248	2.061	0.485
24	463.985	-82.346	1.116	5.048	0.198
	463.985	-138.140	1.116	3.009	0.332
25	463.985	-63.552	1.247	5.856	0.171
	463.985	-181.960	1.247	2.045	0.489
26	463.985	-72.891	1.248	5.099	0.196
	463.985	-174.450	1.248	2.130	0.469
27	463.985	-91.579	1.116	4.539	0.220
	463.985	-110.590	1.116	3.759	0.266
			Ω_{min}	1.813	0.552

Sample Calculation
$M_{Ed} = M_{Ed,i} \cdot (1/1-\theta)$
$205.300 \cdot 1.247$
$= 256$ kNm
$\Omega = M_{pl,Rd,i} / M_{Ed}$
$= 463.985 / 256$
$= 1.813$
Unity Check
$U.C. = M_{Ed} / M_{pl,Rd,i}$
$= 256 / 463.985$
$= 0.552$

NOTE: The following analysis results have been extracted from SAP2000 postprocessor. Note that the gap at beam-column junction is just to show the results clearly. It has no implication that the results obtained are at an offset distance. These are the forces at beam-column junction.

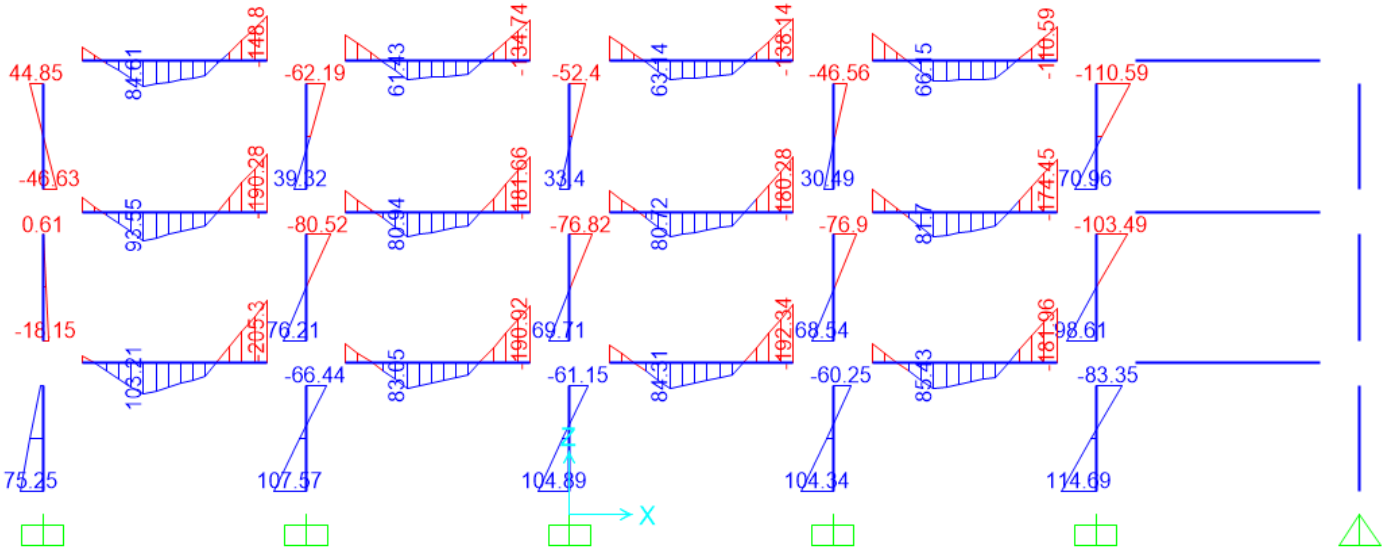

Unity Check for Shear Forces (Internal MRF)
Beam: IPE 400

Beam ID	$V_{pl,Rd,i}$ (kN)	$V_{Ed,G+\psi \cdot Q}$ (kN)	$V_{Ed,M}$ (kN)	1/(1-θ)	Unity Check
16	875.160	77.890	132.567	1.247	0.278
	875.160	85.950	132.567	1.247	0.287
17	875.160	79.240	132.567	1.248	0.280
	875.160	84.600	132.567	1.248	0.286
18	875.160	65.180	132.567	1.116	0.244
	875.160	76.960	132.567	1.116	0.257
19	875.160	82.390	132.567	1.247	0.283
	875.160	81.450	132.567	1.247	0.282
20	875.160	81.910	132.567	1.248	0.283
	875.160	81.930	132.567	1.248	0.283
21	875.160	71.740	132.567	1.116	0.251
	875.160	70.410	132.567	1.116	0.250
22	875.160	81.690	132.567	1.247	0.282
	875.160	82.160	132.567	1.247	0.283
23	875.160	82.160	132.567	1.248	0.283
	875.160	81.690	132.567	1.248	0.282
24	875.160	70.600	132.567	1.116	0.250
	875.160	71.540	132.567	1.116	0.251
25	875.160	86.190	132.567	1.247	0.287
	875.160	77.660	132.567	1.247	0.278
26	875.160	84.830	132.567	1.248	0.286
	875.160	79.020	132.567	1.248	0.279
27	875.160	77.160	132.567	1.116	0.257
	875.160	84.990	132.567	1.116	0.266
					0.287

Sample Calculation

$V_{Ed} = (V_{Ed,G+\psi Q} + V_{Ed,M} \cdot (1/1-\theta))$
$(85.95+132.567 \cdot 1.247)$
$= 251.270$ kN

$V_{Ed,M} = 2 \cdot M_{pl,Rd} / L$
$= 2 \cdot 463.985 / 7$
$= 132.567$ kN

Unity Check

$U.C. = V_{Ed} / V_{pl,Rd,i}$
$= 251.265 / 875.16$
$= 0.270$

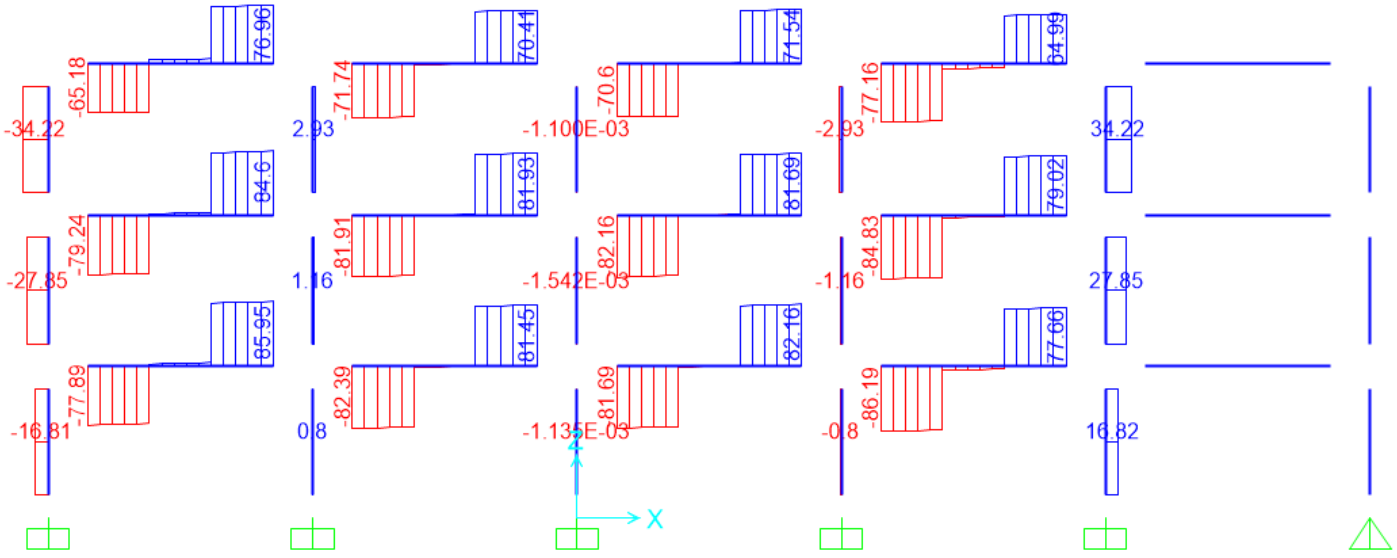

where
$V_{Ed,G}$ is design value of shear force due to non-seismic actions
$V_{Ed,M}$ is the design value of shear force due to application of plastic moments with opposite signs at the end sections of the beam. For a beam with dissipative zones at both ends,
$V_{Ed,M} = (M_{pl,Rd,A} + M_{pl,Rd,B}) / L$

Unity Check for Axial Forces (Internal MRF)
Beam: IPE 400

Beam ID	$N_{pl,Rd,i}$ (kN)	$N_{Ed,G+\psi \cdot Q+E}$ (kN)	1/(1-θ)	Unity Check
16	2999.750	12.970	1.247	0.005
	2999.750	12.970	1.247	0.005
17	2999.750	51.220	1.248	0.021
	2999.750	51.220	1.248	0.021
18	2999.750	111.470	1.116	0.041
	2999.750	111.470	1.116	0.041
19	2999.750	8.650	1.247	0.004
	2999.750	8.650	1.247	0.004
20	2999.750	37.420	1.248	0.016
	2999.750	37.420	1.248	0.016
21	2999.750	86.090	1.116	0.032
	2999.750	86.090	1.116	0.032
22	2999.750	3.770	1.247	0.002
	2999.750	3.770	1.247	0.002
23	2999.750	22.230	1.248	0.009
	2999.750	22.230	1.248	0.009
24	2999.750	64.640	1.116	0.024
	2999.750	64.640	1.116	0.024
25	2999.750	1.020	1.247	0.000
	2999.750	1.020	1.247	0.000
26	2999.750	5.140	1.248	0.002
	2999.750	5.140	1.248	0.002
27	2999.750	45.380	1.116	0.017
	2999.750	45.380	1.116	0.017
				0.041

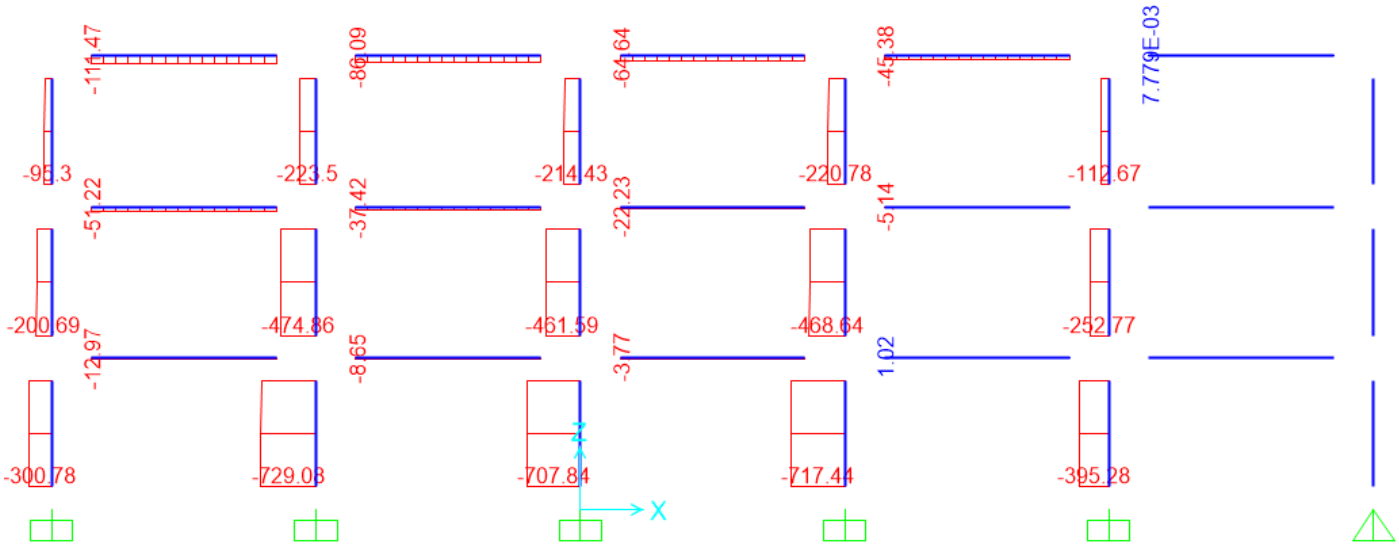

B. Calculation for External MRF

Calculation of Ω (External MRF)
Beam: IPE 400

Beam ID	$M_{pl,Rd,i}$ (kNm)	$M_{Ed,i}$ (kNm)	1/(1-θ)	Ω	Unity Check
16	463.985	44.176	1.245	8.436	0.119
	463.985	-156.561	1.245	2.380	0.420
17	463.985	22.070	1.250	16.824	0.059
	463.985	-139.930	1.250	2.654	0.377
18	463.985	0.898	1.118	462.124	0.002
	463.985	-96.928	1.118	4.280	0.234
19	463.985	14.803	1.245	25.175	0.040
	463.985	-144.862	1.245	2.572	0.389
20	463.985	3.617	1.250	102.662	0.010
	463.985	-132.665	1.250	2.799	0.357
21	463.985	-25.770	1.118	16.098	0.062
	463.985	-87.861	1.118	4.722	0.212
22	463.985	16.223	1.245	22.971	0.044
	463.985	-144.831	1.245	2.573	0.389
23	463.985	2.987	1.250	124.328	0.008
	463.985	-131.580	1.250	2.822	0.354
24	463.985	-23.374	1.118	17.749	0.056
	463.985	-89.195	1.118	4.651	0.215
25	463.985	17.918	1.245	20.798	0.048
	463.985	-148.702	1.245	2.506	0.399
26	463.985	4.544	1.250	81.714	0.012
	463.985	-134.506	1.250	2.761	0.362
27	463.985	-26.505	1.118	15.652	0.064
	463.985	-80.013	1.118	5.185	0.193
			Ω_{min}	2.380	0.420

Sample Calculation
$M_{Ed} = M_{Ed,i} \cdot (1/1-\theta)$
$= 156.561 \cdot 1.247$
$= 195.23$ kNm
$\Omega = M_{pl,Rd,i} / M_{Ed}$
$= 463.985 / 195.23$
$= 1.813$
Unity Check
$U.C. = M_{Ed} / M_{pl,Rd,i}$
$= 195.23 / 463.985$
$= 0.420$

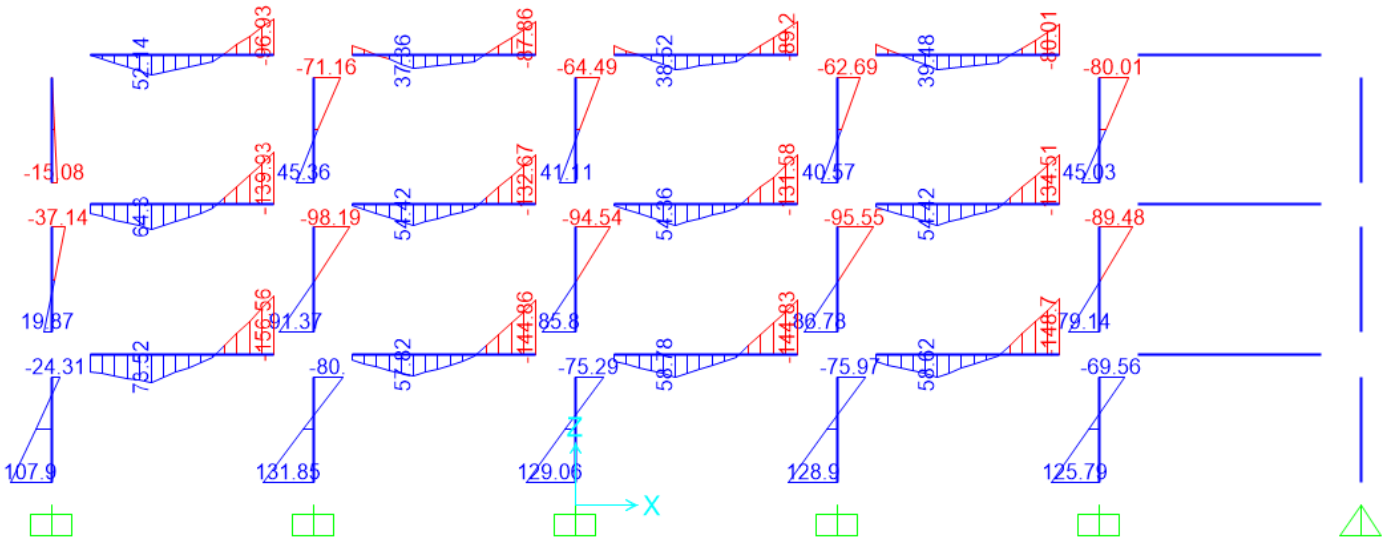

Unity Check for Shear Forces (External MRF)
Beam: IPE 400

Beam ID	$V_{pl,Rd,i}$ (kN)	$V_{Ed,G+\psi \cdot Q}$ (kN)	$V_{Ed,M}$ (kN)	1/(1-θ)	Unity Check
16	875.160	40.160	132.567	1.245	0.234
	875.160	44.290	132.567	1.245	0.239
17	875.160	40.850	132.567	1.250	0.236
	875.160	43.600	132.567	1.250	0.239
18	875.160	33.650	132.567	1.118	0.208
	875.160	39.690	132.567	1.118	0.215
19	875.160	42.460	132.567	1.245	0.237
	875.160	41.990	132.567	1.245	0.237
20	875.160	42.220	132.567	1.250	0.238
	875.160	42.230	132.567	1.250	0.238
21	875.160	37.010	132.567	1.118	0.212
	875.160	36.330	132.567	1.118	0.211
22	875.160	42.100	132.567	1.245	0.237
	875.160	42.350	132.567	1.245	0.237
23	875.160	42.350	132.567	1.250	0.238
	875.160	42.110	132.567	1.250	0.237
24	875.160	36.430	132.567	1.118	0.211
	875.160	36.920	132.567	1.118	0.212
25	875.160	44.410	132.567	1.245	0.239
	875.160	40.040	132.567	1.245	0.234
26	875.160	43.710	132.567	1.250	0.239
	875.160	40.740	132.567	1.250	0.236
27	875.160	39.790	132.567	1.118	0.215
	875.160	33.560	132.567	1.118	0.208
					0.239

Sample Calculation

$V_{Ed} = (V_{Ed,G+\psi Q} + V_{Ed,M} \cdot \cdot (1/1-\theta))$

$(44.29+132.567 \cdot 1.245)$

$= 209.33$ kN

$V_{Ed,M} = 2 \cdot M_{pl,Rd} / L$

$= 2 \cdot 463.985 / 7$

$= 132.567$ kN

Unity Check

$U.C. = V_{Ed} / V_{pl,Rd,i}$

$= 209.33 / 875.16$

$= 0.239$

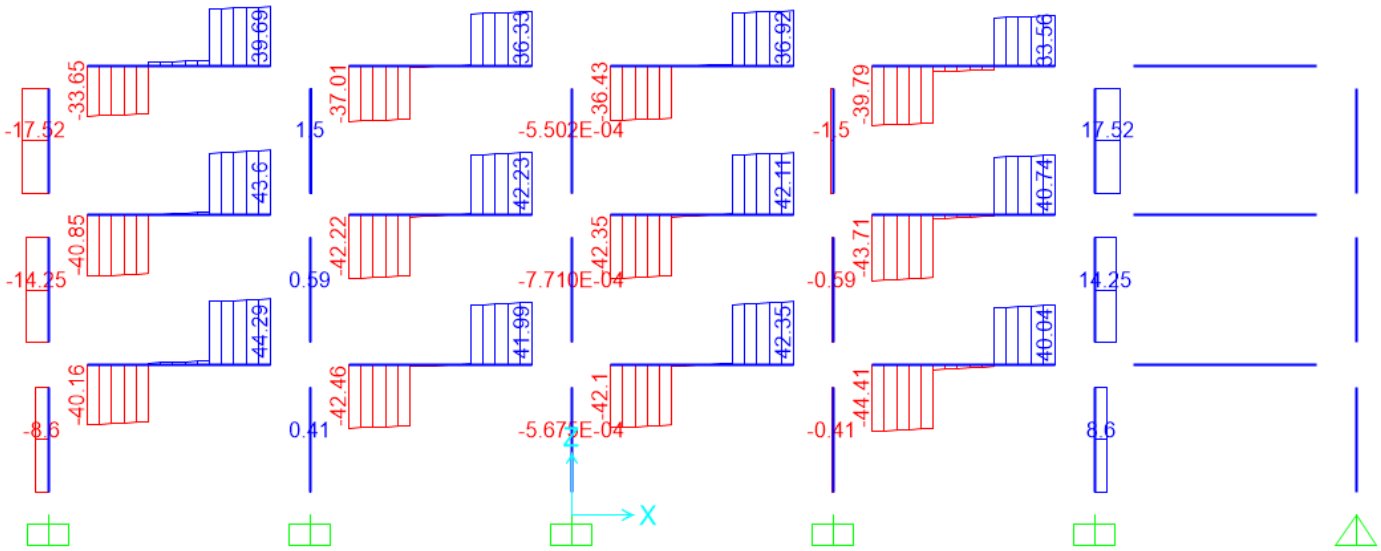

Unity Check for Axial Forces (External MRF)
Beam: IPE 400

Beam ID	$N_{pl,Rd,i}$ (kN)	$N_{Ed,G+\psi \cdot Q+E}$ (kN)	1/(1-θ)	Unity Check
16	2999.750	23.900	1.245	0.010
	2999.750	23.900	1.245	0.010
17	2999.750	67.600	1.250	0.028
	2999.750	67.600	1.250	0.028
18	2999.750	112.600	1.118	0.042
	2999.750	112.600	1.118	0.042
19	2999.750	18.320	1.245	0.008
	2999.750	18.320	1.245	0.008
20	2999.750	49.340	1.250	0.021
	2999.750	49.340	1.250	0.021
21	2999.750	83.470	1.118	0.031
	2999.750	83.470	1.118	0.031
22	2999.750	12.320	1.245	0.005
	2999.750	12.320	1.245	0.005
23	2999.750	30.660	1.250	0.013
	2999.750	30.660	1.250	0.013
24	2999.750	57.070	1.118	0.021
	2999.750	57.070	1.118	0.021
25	2999.750	6.680	1.245	0.003
	2999.750	6.680	1.245	0.003
26	2999.750	10.890	1.250	0.005
	2999.750	10.890	1.250	0.005
27	2999.750	31.250	1.118	0.012
	2999.750	31.250	1.118	0.012
				0.042

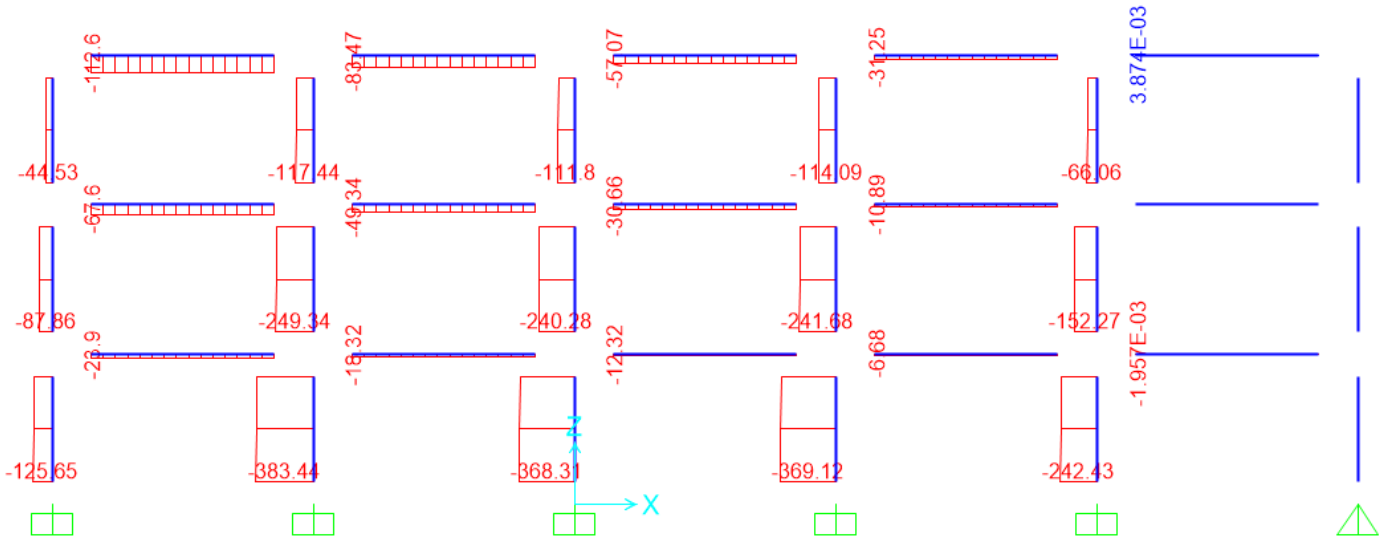

C. Calculation of design action effects for Internal MRF Columns

Design Bending Moments for Columns
Column: HEB 300

Column ID	$M_{pl,Rd,i}$ (kNm)	$M_{Ed,G+\psi \cdot Q}$ (kNm)	$M_{Ed,E}$ (kNm)	Ω	1/(1-θ)	M_{Ed} (kNm)
1	663.495	45.970	-38.860	1.813	1.247	-74.789
	663.495	-21.280	96.530	1.813	1.247	278.692
4	663.495	-2.460	-63.980	1.813	1.247	-201.281
	663.495	0.750	106.830	1.813	1.247	332.729
7	663.495	0.040	-61.190	1.813	1.247	-190.111
	663.495	0.032	104.860	1.813	1.247	325.889
10	663.495	2.540	-62.790	1.813	1.247	-192.583
	663.495	-0.680	105.020	1.813	1.247	325.675
13	663.495	-45.910	-37.440	1.813	1.247	-162.257
	663.495	21.350	93.330	1.813	1.247	311.377

Sample Calculation: $M_{Ed} = M_{Ed,G} + (1.1 \cdot \gamma_{ov} \cdot \Omega \cdot M_{Ed,E}) \cdot k_{\theta} = 0.75 + (1.1 \cdot 1.25 \cdot 1.813 \cdot 106.83) \cdot 1.247$
$= \mathbf{332.73}$ kNm

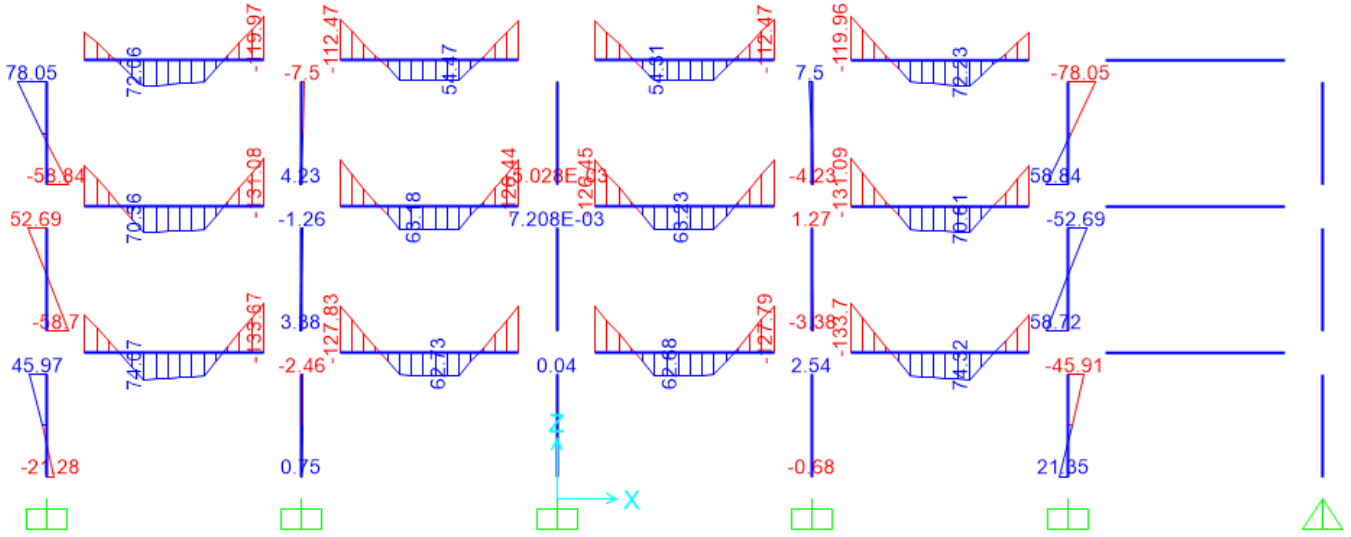

$M_{Ed,G+\psi \cdot Q}$ (kNm)

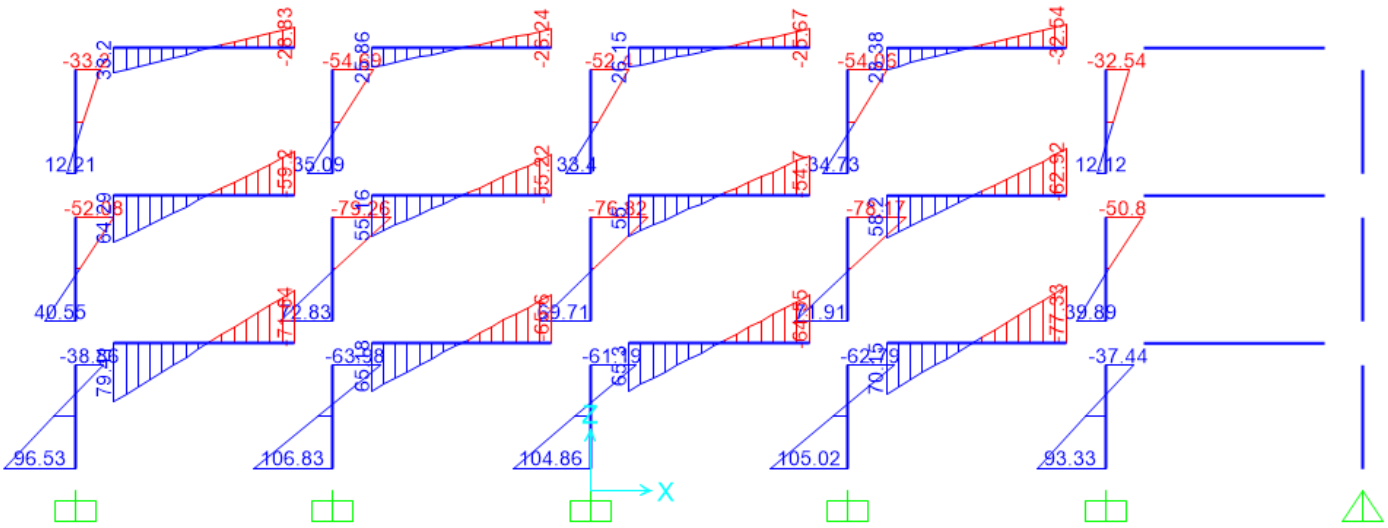

$M_{Ed,E}$ (kNm)

Design Shear Forces for Columns (Internal MRF)
Column: HEB 300

Column ID	$V_{pl,Rd,i}$ (kN)	$V_{Ed,G+\psi \cdot Q}$ (kN)	$V_{Ed,E}$ (kN)	Ω	1/(1-θ)	V_{Ed} (kN)
1	972.120	-16.810	33.850	1.813	1.247	88.380
	972.120	-16.810	33.850	1.813	1.247	88.380
4	972.120	0.800	42.700	1.813	1.247	133.492
	972.120	0.800	42.700	1.813	1.247	133.492
7	972.120	0.000	41.510	1.813	1.247	128.994
	972.120	0.000	41.510	1.813	1.247	128.994
10	972.120	-0.800	41.950	1.813	1.247	129.562
	972.120	-0.800	41.950	1.813	1.247	129.562
13	972.120	16.820	32.690	1.813	1.247	118.406
	972.120	16.820	32.690	1.813	1.247	118.406

Sample Calculation: $V_{Ed} = V_{Ed,G} + (1.1 \cdot \gamma_{ov} \cdot \Omega \cdot V_{Ed,E}) \cdot k_\theta = 0.800 + (1.1 \cdot 1.25 \cdot 1.813 \cdot 42.700) \cdot 1.247$
$= \mathbf{133.492}$ kN

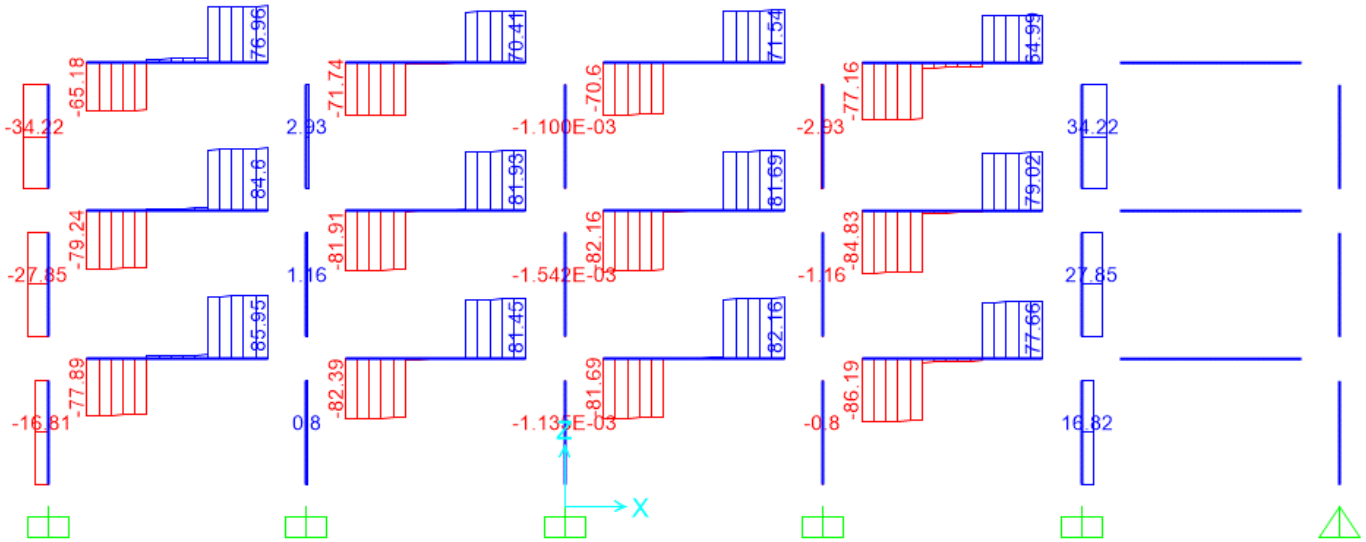

$V_{Ed,G+\psi \cdot Q}$ (kN)

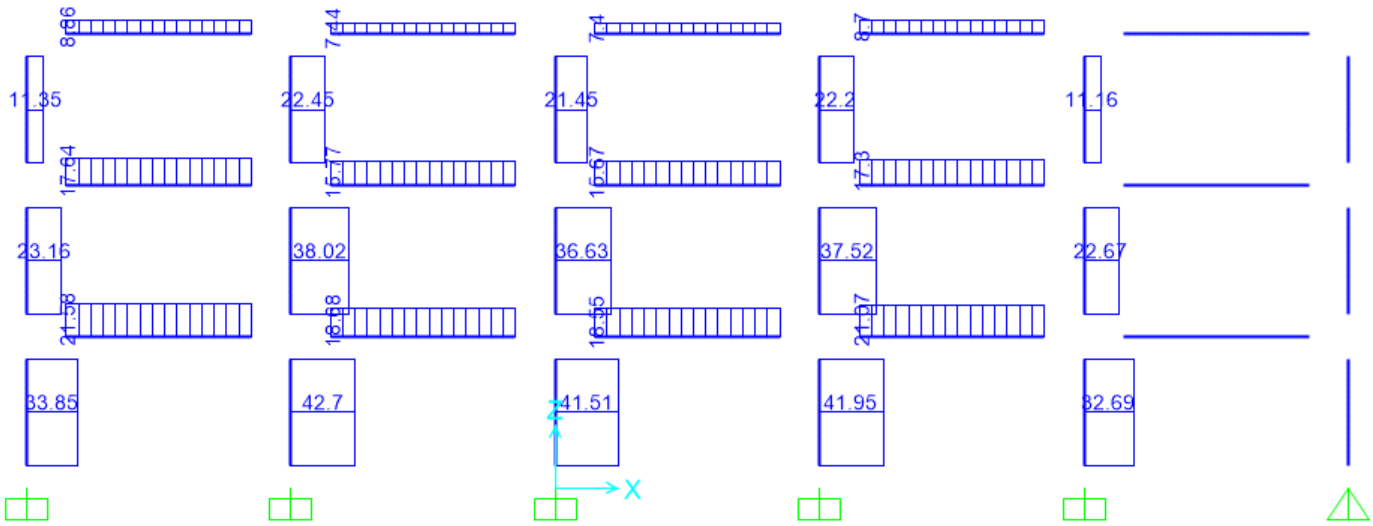

$V_{Ed,E}$ (kN)

Design Axial Forces for Columns (Internal MRF)
Column: HEB 300

Column ID	$N_{pl,Rd,i}$ (kN)	$N_{Ed,G+\psi \cdot Q}$ (kN)	$N_{Ed,E}$ (kN)	Ω	1/(1-θ)	N_{Ed} (kN)
1	5293.050	-344.272	48.080	1.813	1.247	-194.861
	5293.050	-348.360	48.080	1.813	1.247	-198.949
4	5293.050	-718.302	-6.190	1.813	1.247	-737.538
	5293.050	-722.890	-6.190	1.813	1.247	-742.126
7	5293.050	-702.978	-0.270	1.813	1.247	-703.817
	5293.050	-707.570	-0.270	1.813	1.247	-708.409
10	5293.050	-718.299	5.450	1.813	1.247	-701.363
	5293.050	-722.890	5.450	1.813	1.247	-705.954
13	5293.050	-343.620	-47.070	1.813	1.247	-489.892
	5293.050	-348.200	-47.070	1.813	1.247	-494.472

Sample Calculation: $N_{Ed} = N_{Ed,G} + (1.1 \cdot \gamma_{ov} \cdot \Omega \cdot N_{Ed,E}) \cdot k_\theta$ = 722.890 + (1.1·1.25·1.813·6.190)·1.247
= **742.126** kN

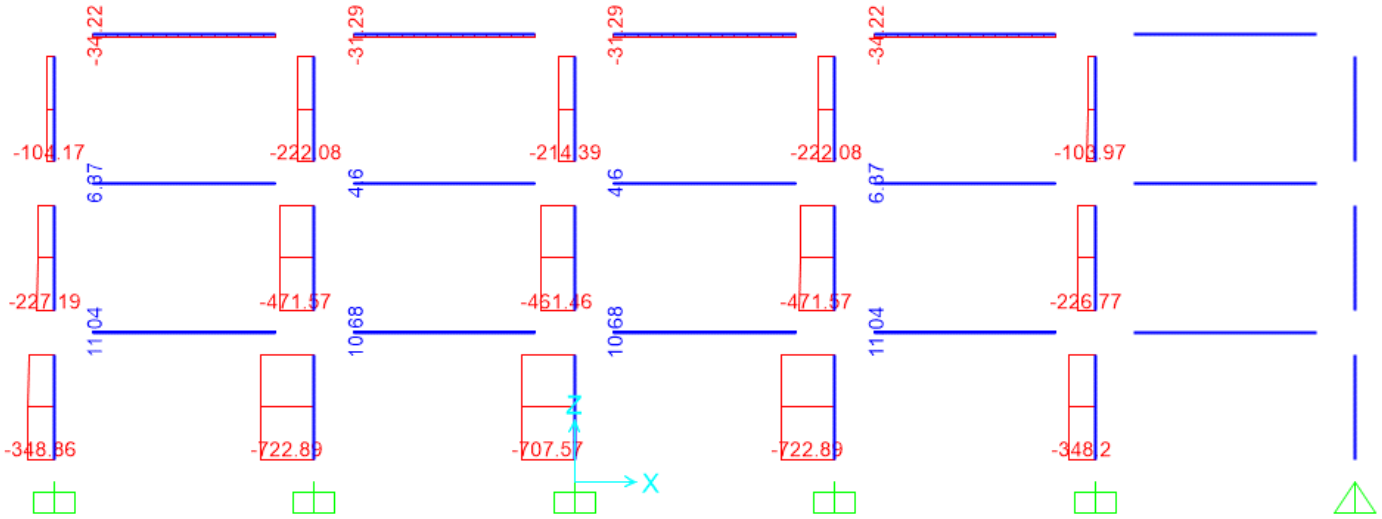

$N_{Ed,G+\psi \cdot Q}$ (kN)

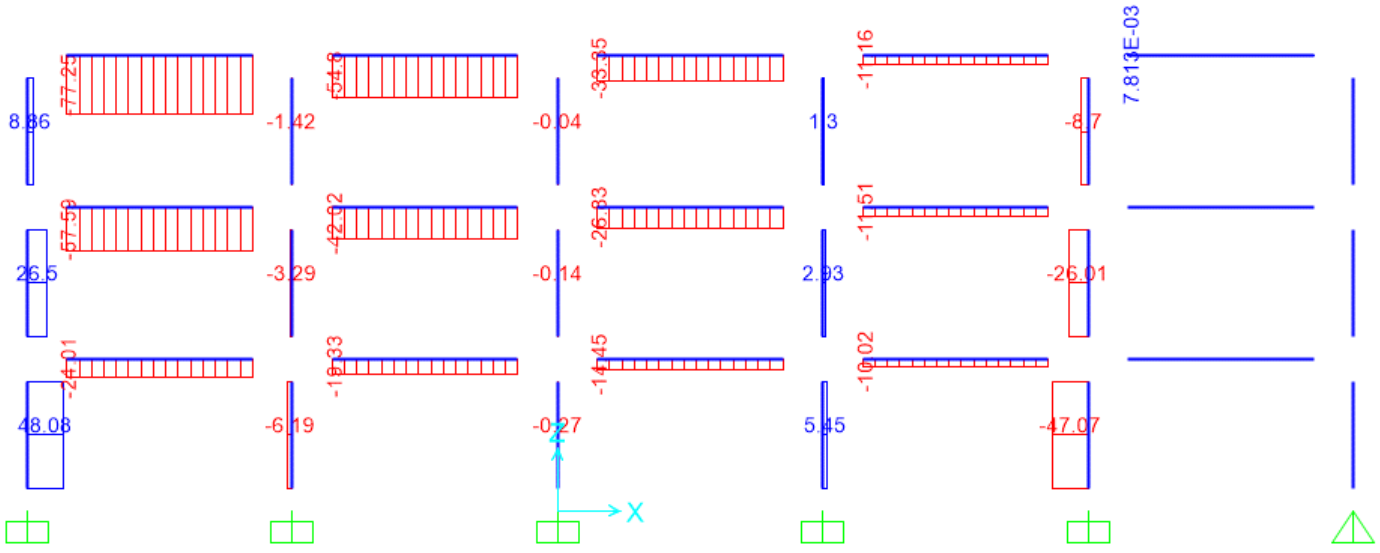

$N_{Ed,E}$ (kN)

D. Calculation of design action effects for External MRF Columns

Design Bending Moments for Columns
Column: HEB 300

Column ID	$M_{pl,Rd,i}$ (kNm)	$M_{Ed,G+\psi \cdot Q}$ (kNm)	$M_{Ed,E}$ (kNm)	Ω	1/(1-θ)	M_{Ed} (kNm)
1	663.495	23.530	-47.830	2.380	1.245	-171.375
	663.495	-10.890	118.790	2.380	1.245	473.175
4	663.495	-1.260	-78.740	2.380	1.245	-322.123
	663.495	0.380	131.470	2.380	1.245	536.115
7	663.495	0.020	-75.330	2.380	1.245	-306.947
	663.495	0.016	129.040	2.380	1.245	525.849
10	663.495	1.300	-77.270	2.380	1.245	-313.572
	663.495	-0.350	129.250	2.380	1.245	526.339
13	663.495	-23.490	-46.070	2.380	1.245	-211.224
	663.495	10.930	114.860	2.380	1.245	478.980

Sample Calculation: $M_{Ed} = M_{Ed,G} + (1.1 \cdot \gamma_{ov} \cdot \Omega \cdot M_{Ed,E}) \cdot k_{\theta} = 0.380 + (1.1 \cdot 1.25 \cdot 2.380 \cdot 131.470) \cdot 1.245$
$= \mathbf{536.115}$ kNm

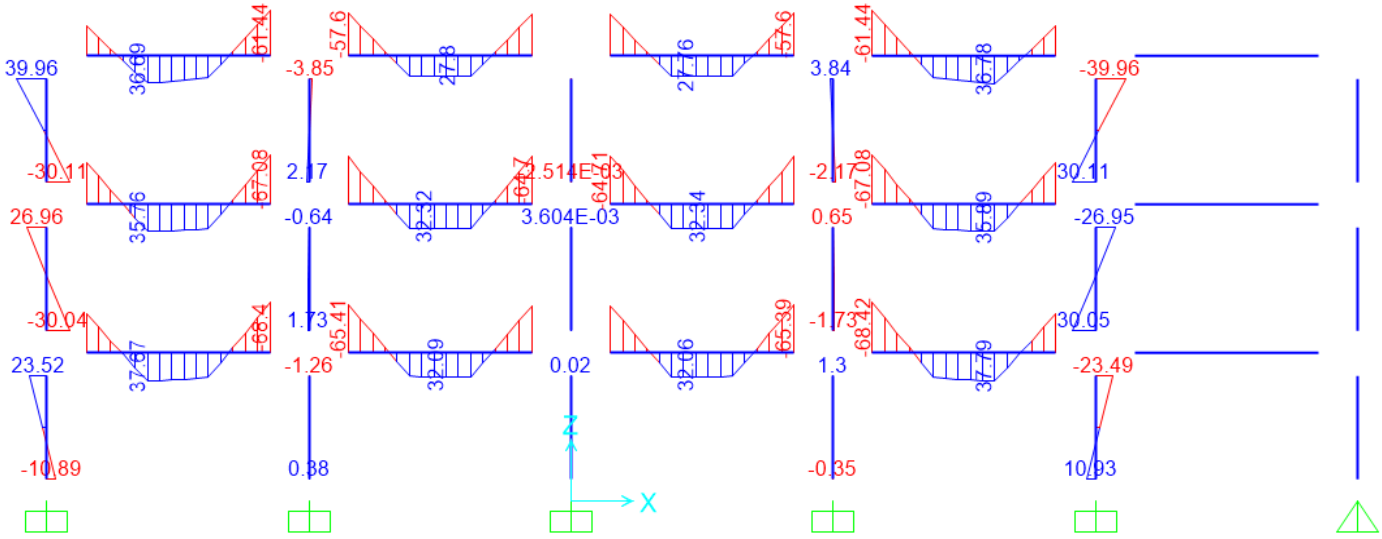

$M_{Ed,G+\psi \cdot Q}$ (kNm)

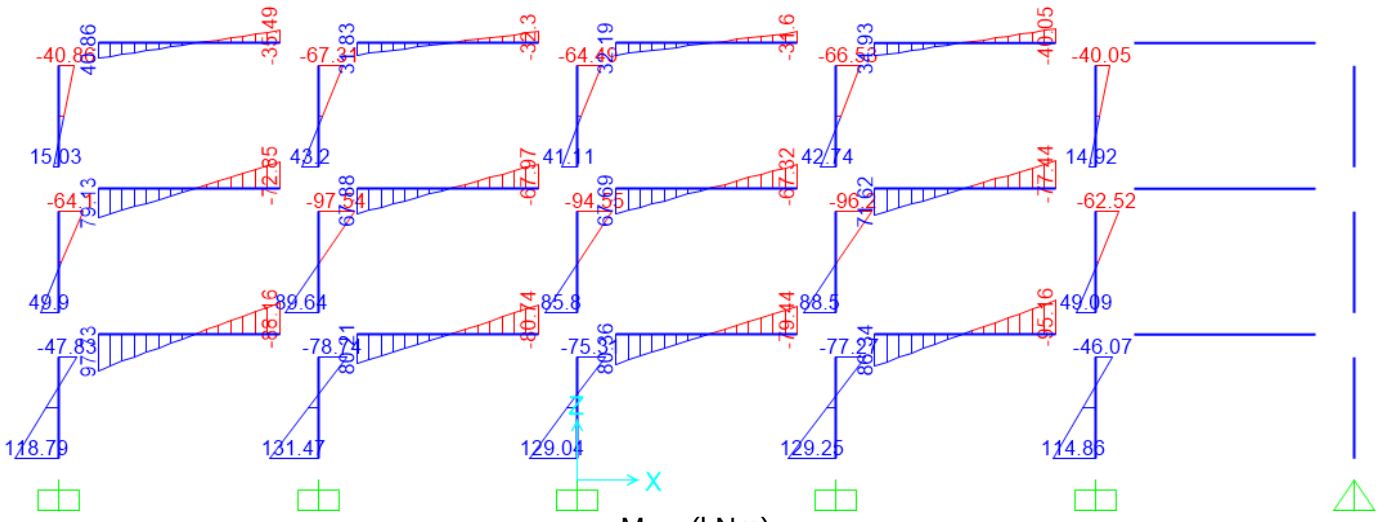

$M_{Ed,E}$ (kNm)

Design Shear Forces for Columns (External MRF)
Column: HEB 300

Column ID	$V_{pl,Rd,i}$ (kN)	$V_{Ed,G+\psi \cdot Q}$ (kN)	$V_{Ed,E}$ (kN)	Ω	1/(1-θ)	V_{Ed} (kN)
1	972.120	-8.600	41.660	2.380	1.245	161.163
	972.120	-8.600	41.660	2.380	1.245	161.163
4	972.120	0.410	52.550	2.380	1.245	214.549
	972.120	0.410	52.550	2.380	1.245	214.549
7	972.120	0.000	51.090	2.380	1.245	208.190
	972.120	0.000	51.090	2.380	1.245	208.190
10	972.120	-0.410	51.630	2.380	1.245	209.980
	972.120	0.410	51.630	2.380	1.245	210.800
13	972.120	8.600	40.230	2.380	1.245	172.536
	972.120	8.600	40.230	2.380	1.245	172.536

Sample Calculation: $V_{Ed} = V_{Ed,G} + (1.1 \cdot \gamma_{ov} \cdot \Omega \cdot V_{Ed,E}) \cdot k_{\theta} = 0.410 + (1.1 \cdot 1.25 \cdot 2.380 \cdot 52.550) \cdot 1.245$
$= \mathbf{214.549}$ kN

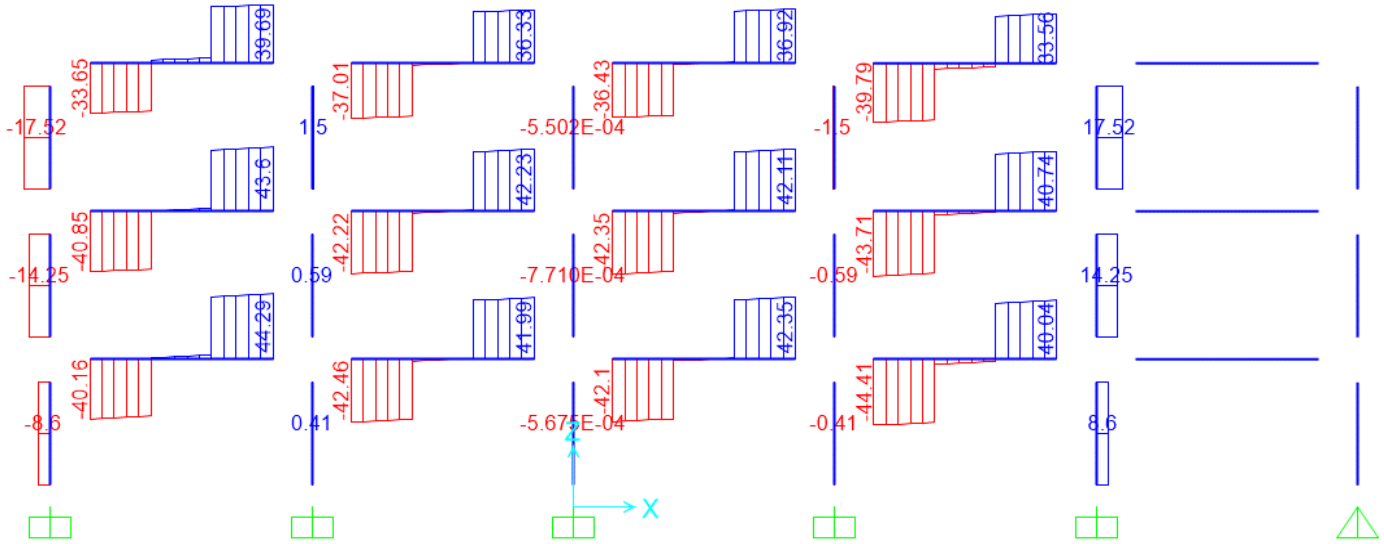

$V_{Ed,G+\psi \cdot Q}$ (kN)

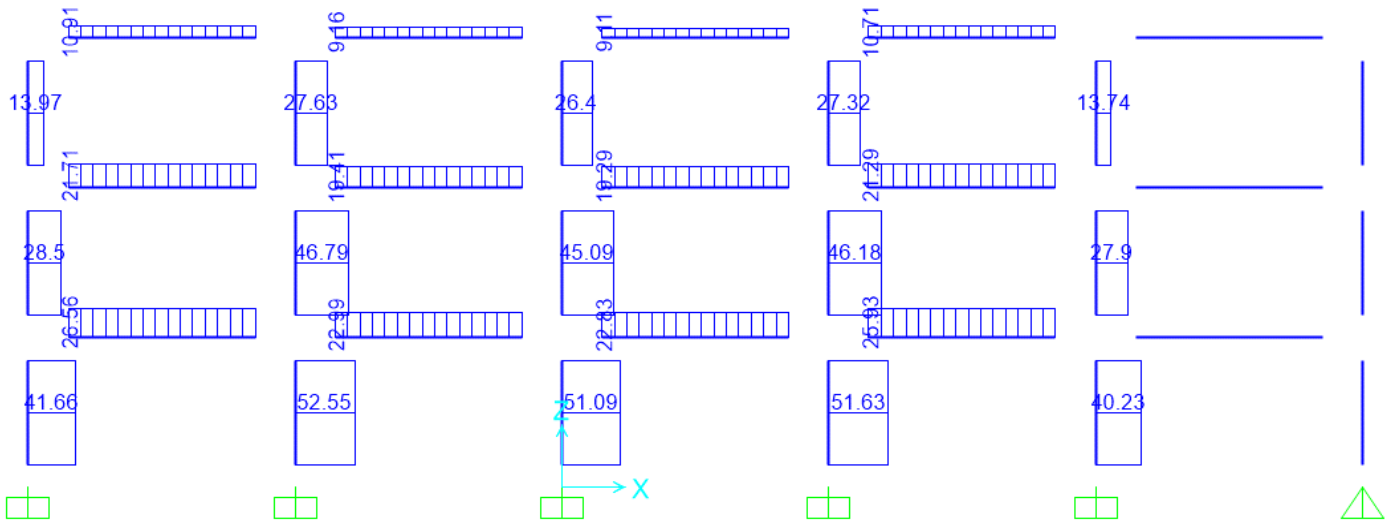

$V_{Ed,E}$ (kN)

Design Axial Forces for Columns (External MRF)
Column: HEB 300

Column ID	$N_{pl,Rd,i}$ (kN)	$N_{Ed,G+\psi \cdot Q}$ (kN)	$N_{Ed,E}$ (kN)	Ω	1/(1-θ)	N_{Ed} (kN)
1	5293.050	-180.233	59.170	2.380	1.245	60.883
	5293.050	-184.320	59.170	2.380	1.245	56.796
4	5293.050	-371.239	-7.610	2.380	1.245	-402.249
	5293.050	-375.820	-7.610	2.380	1.245	-406.830
7	5293.050	-363.390	-0.330	2.380	1.245	-364.735
	5293.050	-367.980	-0.330	2.380	1.245	-369.325
10	5293.050	-371.237	6.710	2.380	1.245	-343.894
	5293.050	-375.820	6.710	2.380	1.245	-348.477
13	5293.050	-179.906	-57.940	2.380	1.245	-416.009
	5293.050	-184.490	-57.940	2.380	1.245	-420.593

Sample Calculation: $N_{Ed} = N_{Ed,G} + (1.1 \cdot \gamma_{ov} \cdot \Omega \cdot N_{Ed,E}) \cdot k_{\theta} = 184.490 + (1.1 \cdot 1.25 \cdot 2.380 \cdot 57.940) \cdot 1.245$
$= \mathbf{420.593}$ kN

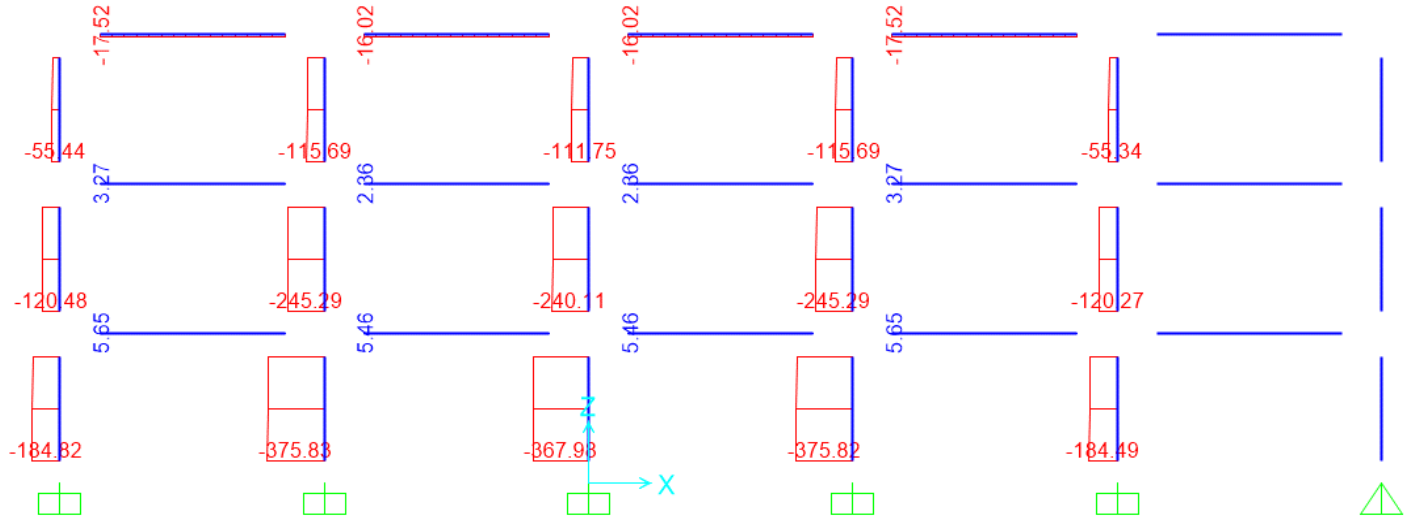

$N_{Ed,G+\psi \cdot Q}$ (kN)

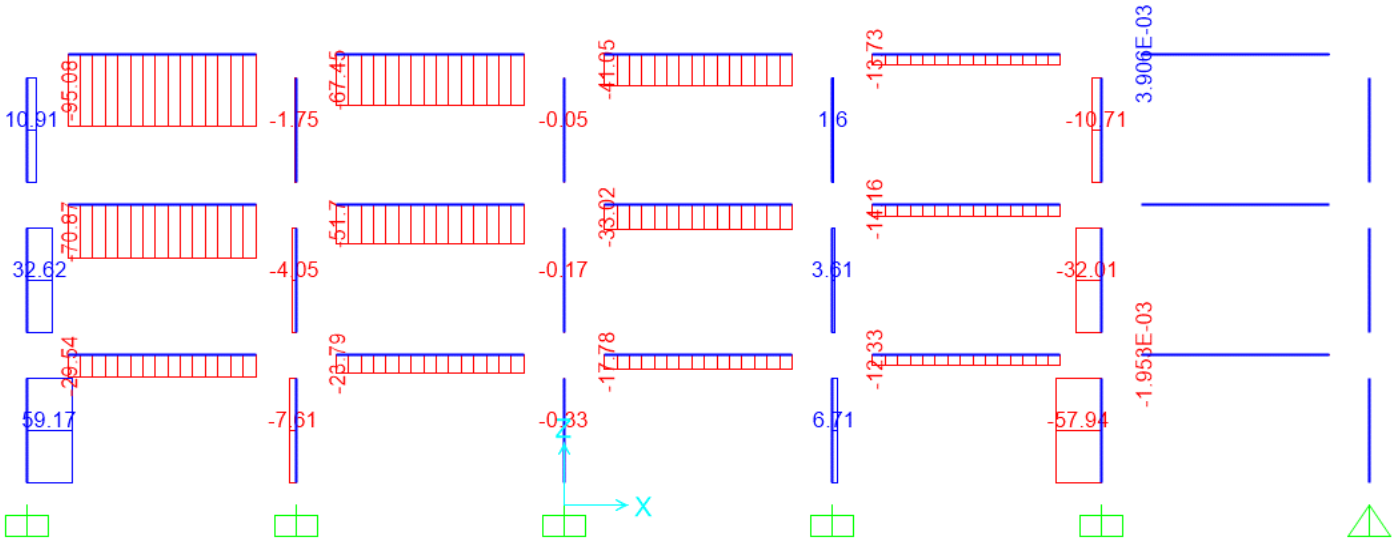

$N_{Ed,E}$ (kN)

Appendix III: Calculation of Seismic base shear results from SAP2000

The following calculation shows how the seismic base shear for response spectrum analysis was calculated using output results from the program.

Mode	T (s)	ω^2 $(rad/s)^2$	Modal Reaction (kN)		Modal Participation factor , Γ		Modal Acceleration (m/s^2)		Modal Amplitude	
			f_X	f_Y	U_X	U_Y	S_{aX}	S_{aY}	A_X	A_Y
1	1.308	23.06	-2.37E-03	-1.07E+03	-1.02E-04	-4.64E+01	0.2955	0.2955	-1.31E-06	-5.94E-01
2	0.614	104.79	-1.62E+00	6.34E+01	-1.54E-02	6.05E-01	0.6699	0.4123	-9.87E-05	2.38E-03
3	0.469	179.11	-8.37E+03	-1.50E-02	-4.67E+01	-8.40E-05	0.8758	0.5390	-2.28E-01	-2.53E-07
4	0.403	243.43	-2.40E-02	-4.12E+03	-9.80E-05	-1.69E+01	1.0211	0.6284	-4.11E-07	-4.37E-02
5	0.223	790.82	-1.20E-01	-6.61E+03	-1.52E-04	-8.35E+00	1.1053	0.6802	-2.12E-07	-7.18E-03
6	0.207	920.65	-6.11E+00	4.74E+02	-6.63E-03	5.15E-01	1.1053	0.6802	-7.96E-06	3.80E-04
7	0.163	1484.26	2.54E+04	1.22E-01	1.71E+01	-8.20E-05	1.1597	0.7967	1.34E-02	-4.40E-08

Modal Amplitude		Modal Reaction (kN)		Seismic Base Shear (kN)	
A_X	A_Y	f_X	f_Y	F_X	F_Y
-1.31E-06	-5.94E-01	-2.37E-03	-1.07E+03	3.09E-09	6.35E+02
-9.87E-05	2.38E-03	-1.62E+00	6.34E+01	1.60E-04	1.51E-01
-2.28E-01	-2.53E-07	-8.37E+03	-1.50E-02	1.91E+03	3.79E-09
-4.11E-07	-4.37E-02	-2.40E-02	-4.12E+03	9.87E-09	1.80E+02
-2.12E-07	-7.18E-03	-1.20E-01	-6.61E+03	2.55E-08	4.75E+01
-7.96E-06	3.80E-04	-6.11E+00	4.74E+02	4.86E-05	1.80E-01
1.34E-02	-4.40E-08	2.54E+04	1.22E-01	3.40E+02	-5.37E-09
			∑SRSS	**1940.69**	**622.20**

The modal amplitude computed above is $\Gamma \cdot S_a / \omega^2$ which is then multiplied with modal reactions to obtain the total seismic base shear corresponding to a certain mode. The modal base shear thus obtained per mode is combined using SRSS combination rule to obtain the total base shear in a particular direction.

Appendix IV: Calculation of Seismic Action effects (Response Spectrum Analysis)

The seismic action effects for beams and columns of the lateral force resisting system are detailed in this appendix.

A. Calculation for Internal MRF

Calculation of Ω (Internal MRF)
Beam: IPE 400

Beam ID	$M_{pl,Rd,i}$ (kNm)	$M_{Ed,G+\psi \cdot Q}$ (kNm)	$M_{Ed,E}$ (kNm)	$M_{Ed,i}$ (kNm)	1/(1-θ)	Ω	Unity Check
280	463.985	-104.254	55.000	-49.254	1.268	7.429	0.135
	463.985	-134.117	-49.824	-183.941	1.268	1.989	0.503
281	463.985	-112.683	44.852	-67.831	1.247	5.485	0.182
	463.985	-130.447	-41.501	-171.948	1.247	2.164	0.462
282	463.985	-79.664	25.646	-54.018	1.123	7.651	0.131
	463.985	-119.105	-22.277	-141.383	1.123	2.923	0.342
283	463.985	-127.856	45.680	-82.176	1.268	4.453	0.225
	463.985	-12.428	-46.122	-58.550	1.268	6.250	0.160
284	463.985	-126.095	38.973	-87.122	1.247	4.270	0.234
	463.985	-126.321	-39.124	-165.445	1.247	2.249	0.445
285	463.985	-112.980	20.001	-92.979	1.123	4.445	0.225
	463.985	-108.374	-20.377	-128.751	1.123	3.210	0.312
286	463.985	-125.469	46.122	-79.347	1.268	4.612	0.217
	463.985	-127.814	45.680	-82.135	1.268	4.455	0.224
287	463.985	-126.349	39.124	-87.226	1.247	4.265	0.234
	463.985	-126.067	-38.973	-165.040	1.247	2.254	0.444
288	463.985	-108.383	20.377	-88.005	1.123	4.696	0.213
	463.985	-112.970	-20.001	-132.972	1.123	3.108	0.322
289	463.985	-134.159	49.824	-84.335	1.268	4.339	0.230
	463.985	-104.207	-55.000	-159.207	1.268	2.298	0.435
290	463.985	-130.471	41.501	-88.970	1.247	4.182	0.239
	463.985	-112.656	-44.852	-157.508	1.247	2.362	0.423
291	463.985	-119.109	22.277	-96.832	1.123	4.268	0.234
	463.985	-79.658	-25.646	-105.304	1.123	3.925	0.255
					Ω_{min}	1.989	0.503

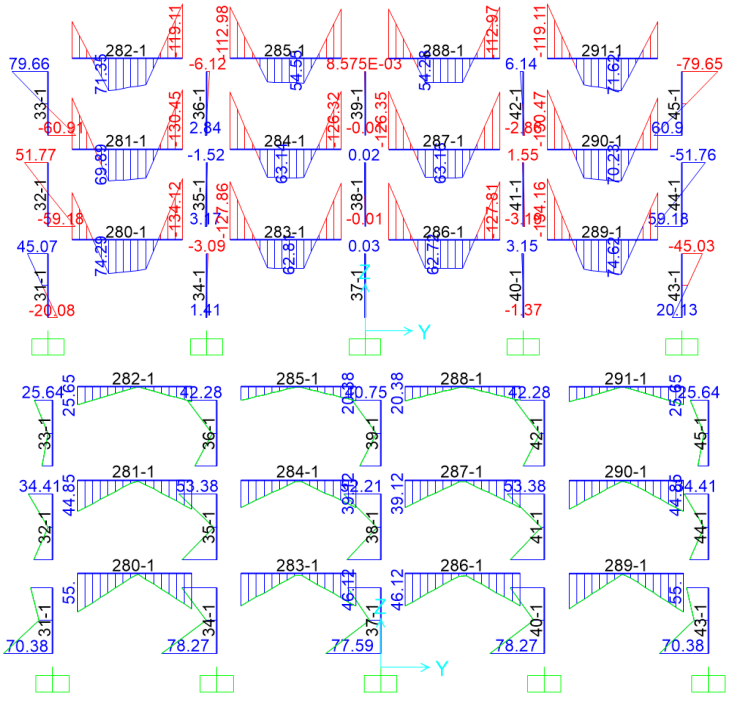

Sample Calculation

$M_{Ed} = M_{Ed,i} \cdot (1/1-\theta)$
$= 183.941 \cdot 1.268$
$= 233.24$ kNm

$\Omega = M_{pl,Rd,i} / M_{Ed}$
$= 463.985 / 233.24$
$= 1.989$

Unity Check

$U.C. = M_{Ed} / M_{pl,Rd,i}$
$= 233.24 / 463.985$
$= 0.502$

Unity Check for Shear Forces (Internal MRF)
Beam: IPE 400

Beam ID	$V_{pl,Rd,i}$ (kN)	$V_{Ed,G+\psi \cdot Q}$ (kN)	$V_{Ed,M}$ (kN)	1/(1-θ)	Unity Check
280	875.160	77.800	132.567	1.268	0.281
	875.160	86.150	132.567	1.268	0.291
281	875.160	79.530	132.567	1.247	0.280
	875.160	84.420	132.567	1.247	0.285
282	875.160	65.570	132.567	1.123	0.245
	875.160	76.680	132.567	1.123	0.258
283	875.160	82.420	132.567	1.268	0.286
	875.160	81.540	132.567	1.268	0.285
284	875.160	82.040	132.567	1.247	0.283
	875.160	81.920	132.567	1.247	0.283
285	875.160	71.860	132.567	1.123	0.252
	875.160	70.390	132.567	1.123	0.250
286	875.160	81.740	132.567	1.268	0.285
	875.160	82.220	132.567	1.268	0.286
287	875.160	82.110	132.567	1.247	0.283
	875.160	81.840	132.567	1.247	0.282
288	875.160	70.550	132.567	1.123	0.251
	875.160	71.700	132.567	1.123	0.252
289	875.160	86.350	132.567	1.268	0.291
	875.160	77.600	132.567	1.268	0.281
290	875.160	84.620	132.567	1.247	0.286
	875.160	79.340	132.567	1.247	0.280
291	875.160	76.840	132.567	1.123	0.258
	875.160	65.410	132.567	1.123	0.245
					0.291

Sample Calculation

$V_{Ed} = (V_{Ed,G+\psi Q} + V_{Ed,M} \cdot (1/1-\theta))$

$(86.15+132.567 \cdot 1.268)$

$= 254.25$ kN

$V_{Ed,M} = 2 \cdot M_{pl,Rd} / L$

$= 2 \cdot 463.985 / 7$

$= 132.567$ kN

Unity Check

$U.C. = V_{Ed} / V_{pl,Rd,i}$

$= 254.25 / 875.16$

$= 0.29$

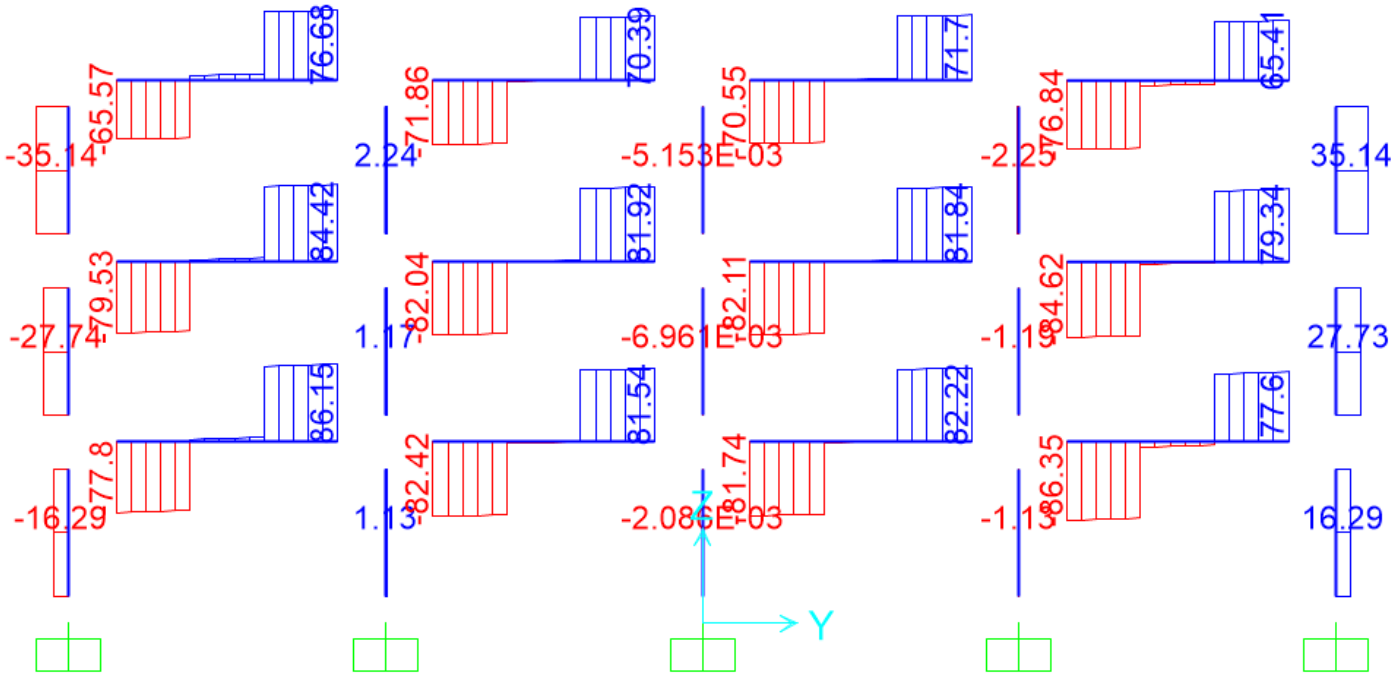

B. Calculation for External MRF

Calculation of Ω (External MRF)
Beam: IPE 400

Beam ID	$M_{pl,Rd,i}$ (kNm)	$M_{Ed,G+\psi \cdot Q}$ (kNm)	$M_{Ed,E}$ (kNm)	$M_{Ed,i}$ (kNm)	1/(1-θ)	Ω	Unity Check
256	463.985	-56.272	56.495	0.223	1.268	1644.577	0.001
	463.985	-73.244	-51.195	-124.439	1.268	2.941	0.340
257	463.985	-60.262	46.075	-14.186	1.247	26.226	0.038
	463.985	-71.652	-42.665	-114.317	1.247	3.255	0.307
258	463.985	-40.444	26.437	-14.007	1.123	29.508	0.034
	463.985	-61.445	-23.033	-84.478	1.123	4.893	0.204
259	463.985	-69.490	46.784	-22.706	1.268	16.115	0.062
	463.985	-68.120	-47.250	-115.370	1.268	3.172	0.315
260	463.985	-68.630	39.797	-28.834	1.247	12.903	0.077
	463.985	-68.560	-39.964	-108.524	1.247	3.428	0.292
261	463.985	-57.924	20.397	-37.526	1.123	11.014	0.091
	463.985	-55.414	-20.807	-76.220	1.123	5.423	0.184
262	463.985	-68.118	47.250	-20.868	1.268	17.535	0.057
	463.985	-69.493	-46.784	-116.277	1.268	3.147	0.318
263	463.985	-68.544	39.964	-28.580	1.247	13.018	0.077
	463.985	-68.647	-39.796	-108.444	1.247	3.431	0.291
264	463.985	-55.397	20.806	-34.590	1.123	11.949	0.084
	463.985	-57.935	-20.397	-78.332	1.123	5.276	0.190
265	463.985	-73.241	51.196	-22.045	1.268	16.599	0.060
	463.985	-56.275	-56.495	-112.770	1.268	3.245	0.308
266	463.985	-71.628	42.666	-28.962	1.247	12.846	0.078
	463.985	-60.287	-46.076	-106.364	1.247	3.498	0.286
267	463.985	-61.422	23.034	-38.388	1.123	10.767	0.093
	463.985	-40.470	-26.438	-66.908	1.123	6.177	0.162
					Ω_{min}	2.941	0.340

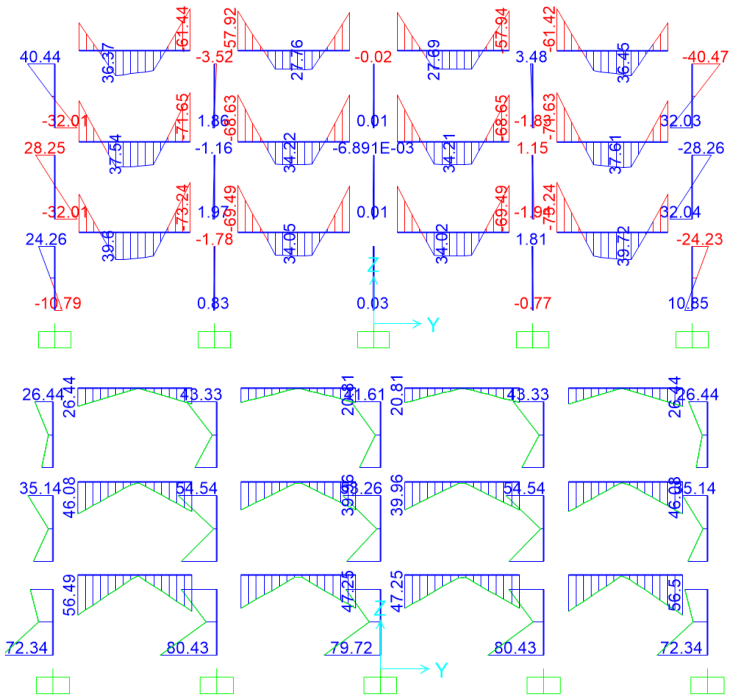

Sample Calculation

$M_{Ed} = M_{Ed,i} \cdot (1/1-\theta)$
$= 124.439 \cdot 1.268$
$= 157.80$ kNm

$\Omega = M_{pl,Rd,i} / M_{Ed}$
$= 463.985 / 157.80$
$= 2.941$

Unity Check

$U.C. = M_{Ed} / M_{pl,Rd,i}$
$= 157.80 / 463.985$
$= 0.340$

Unity Check for Shear Forces (External MRF)
Beam: IPE 400

Beam ID	$V_{pl,Rd,i}$ (kN)	$V_{Ed,G+\psi \cdot Q}$ (kN)	$V_{Ed,M}$ (kN)	1/(1-θ)	Unity Check
256	875.160	43.300	132.567	1.268	0.242
	875.160	48.040	132.567	1.268	0.247
257	875.160	44.100	132.567	1.247	0.239
	875.160	47.240	132.567	1.247	0.243
258	875.160	33.720	132.567	1.123	0.209
	875.160	39.630	132.567	1.123	0.215
259	875.160	45.920	132.567	1.268	0.245
	875.160	45.420	132.567	1.268	0.244
260	875.160	45.730	132.567	1.247	0.241
	875.160	45.600	132.567	1.247	0.241
261	875.160	37.080	132.567	1.123	0.212
	875.160	36.270	132.567	1.123	0.211
262	875.160	45.530	132.567	1.268	0.244
	875.160	45.810	132.567	1.268	0.244
263	875.160	45.710	132.567	1.247	0.241
	875.160	45.630	132.567	1.247	0.241
264	875.160	36.360	132.567	1.123	0.212
	875.160	36.990	132.567	1.123	0.212
265	875.160	48.150	132.567	1.268	0.247
	875.160	43.190	132.567	1.268	0.241
266	875.160	47.350	132.567	1.247	0.243
	875.160	43.990	132.567	1.247	0.239
267	875.160	39.720	132.567	1.123	0.215
	875.160	33.630	132.567	1.123	0.208
					0.247

Sample Calculation

$V_{Ed} = (V_{Ed,G+\psi Q} + V_{Ed,M} \cdot (1/1-\theta))$
$(48.040+132.567 \cdot 1.268)$
$= 216.135$ kN

$V_{Ed,M} = 2 \cdot M_{pl,Rd} / L$
$= 2 \cdot 463.985 / 7$
$= 132.567$ kN

Unity Check

$U.C. = V_{Ed} / V_{pl,Rd,i}$
$= 216.135 / 875.16$
$= 0.247$

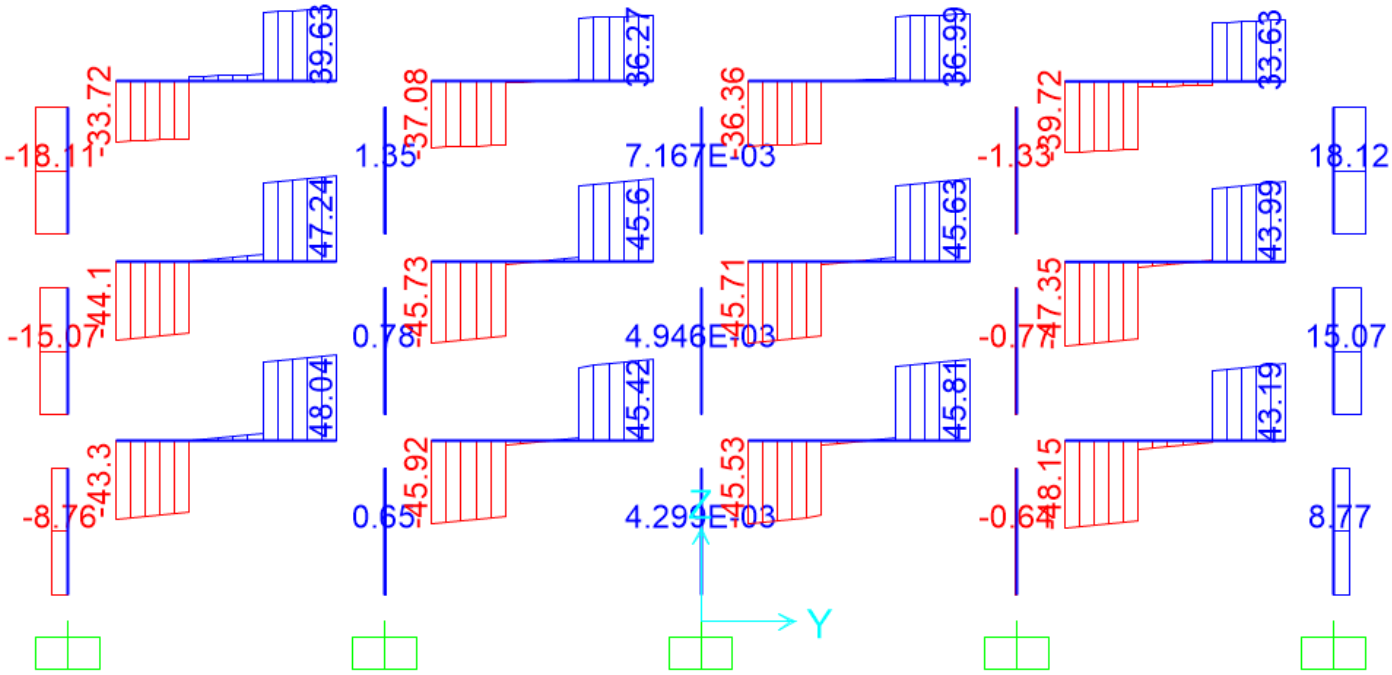

C. Calculation of design action effects for Internal MRF Columns

Design Bending Moments for Columns
Column: HEB 300

Column ID	$M_{pl,Rd,i}$ (kNm)	$M_{Ed,G+\psi \cdot Q}$ (kNm)	$M_{Ed,E}$ (kNm)	Ω	1/(1-θ)	M_{Ed} (kNm)
31	663.495	45.070	31.532	1.989	1.268	154.437
	663.495	-20.080	70.380	1.989	1.268	224.026
34	663.495	-3.090	-48.818	1.989	1.268	-172.412
	663.495	1.410	78.270	1.989	1.268	272.882
37	663.495	0.030	-48.665	1.989	1.268	-168.760
	663.495	0.020	77.590	1.989	1.268	269.133
40	663.495	3.150	-48.818	1.989	1.268	-166.172
	663.495	-1.370	78.200	1.989	1.268	269.859
43	663.495	-45.030	-31.532	1.989	1.268	-154.397
	663.495	20.130	70.380	1.989	1.268	264.236

Sample Calculation: $M_{Ed} = M_{Ed,G} + (1.1 \cdot \gamma_{ov} \cdot \Omega \cdot M_{Ed,E}) \cdot k_{\theta} = 1.410 + (1.1 \cdot 1.25 \cdot 1.989 \cdot 78.27) \cdot 1.268$
$= \mathbf{272.882}$ kNm

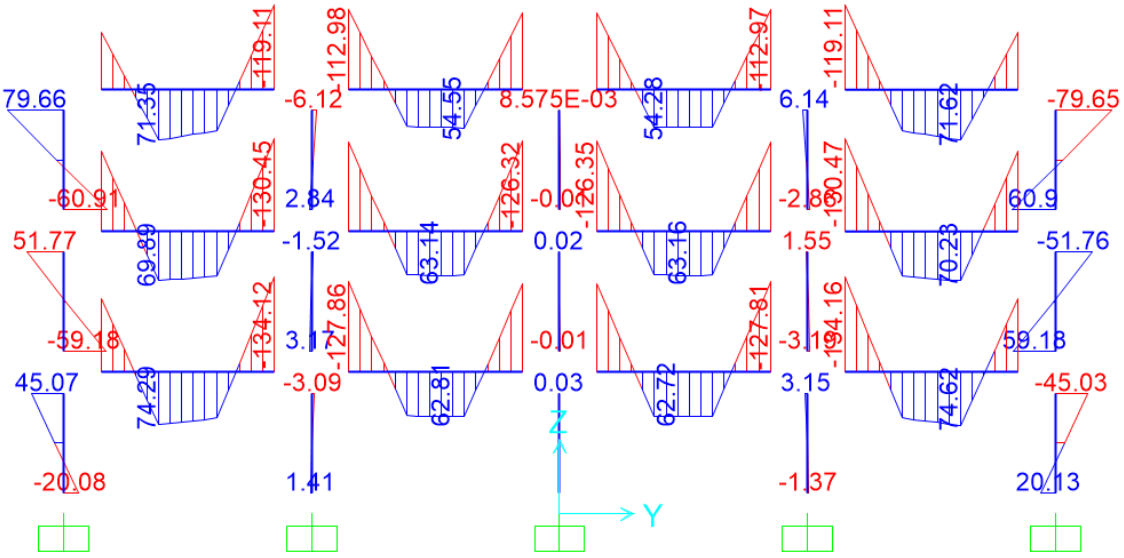

$M_{Ed,G+\psi \cdot Q}$ (kNm)

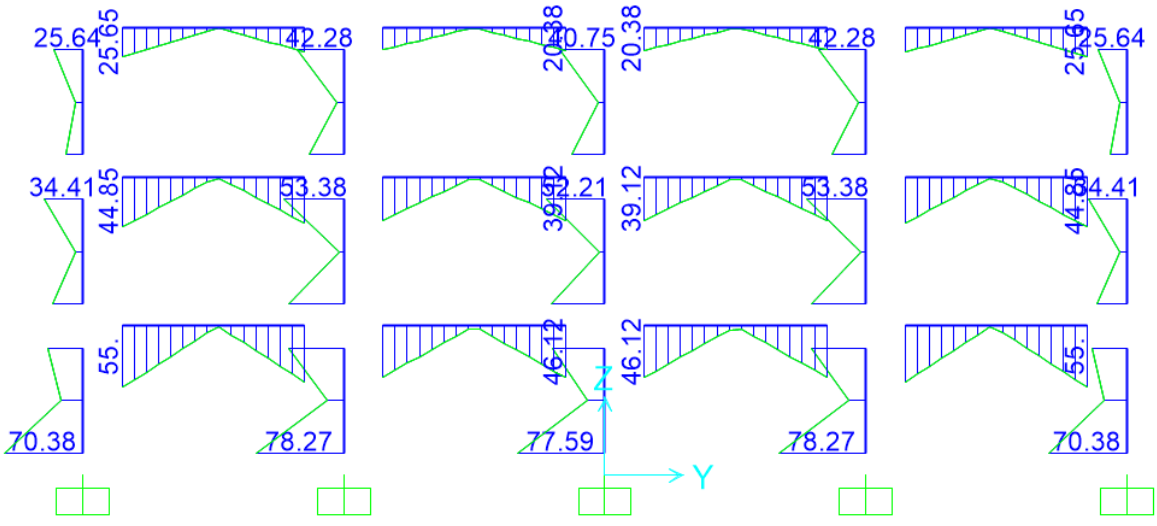

$M_{Ed,E}$ (kNm)

Design Shear Forces for Columns (Internal MRF)
Column: HEB 300

Column ID	$V_{pl,Rd,i}$ (kN)	$V_{Ed,G+\psi \cdot Q}$ (kN)	$V_{Ed,E}$ (kN)	Ω	1/(1-θ)	V_{Ed} (kN)
31	972.120	-16.290	25.380	1.989	1.268	71.738
	972.120	-16.290	25.380	1.989	1.268	71.738
34	972.120	1.130	31.740	1.989	1.268	111.217
	972.120	1.130	31.740	1.989	1.268	111.217
37	972.120	0.000	31.200	1.989	1.268	108.214
	972.120	0.000	31.200	1.989	1.268	108.214
40	972.120	-1.130	31.740	1.989	1.268	108.957
	972.120	-1.130	31.740	1.989	1.268	108.957
43	972.120	16.290	25.380	1.989	1.268	104.318
	972.120	16.290	25.380	1.989	1.268	104.318

Sample Calculation: $V_{Ed} = V_{Ed,G} + (1.1 \cdot \gamma_{ov} \cdot \Omega \cdot V_{Ed,E}) \cdot k_{\theta} = 1.130 + (1.1 \cdot 1.25 \cdot 1.989 \cdot 31.740) \cdot 1.268$
$= \mathbf{111.217}$ kN

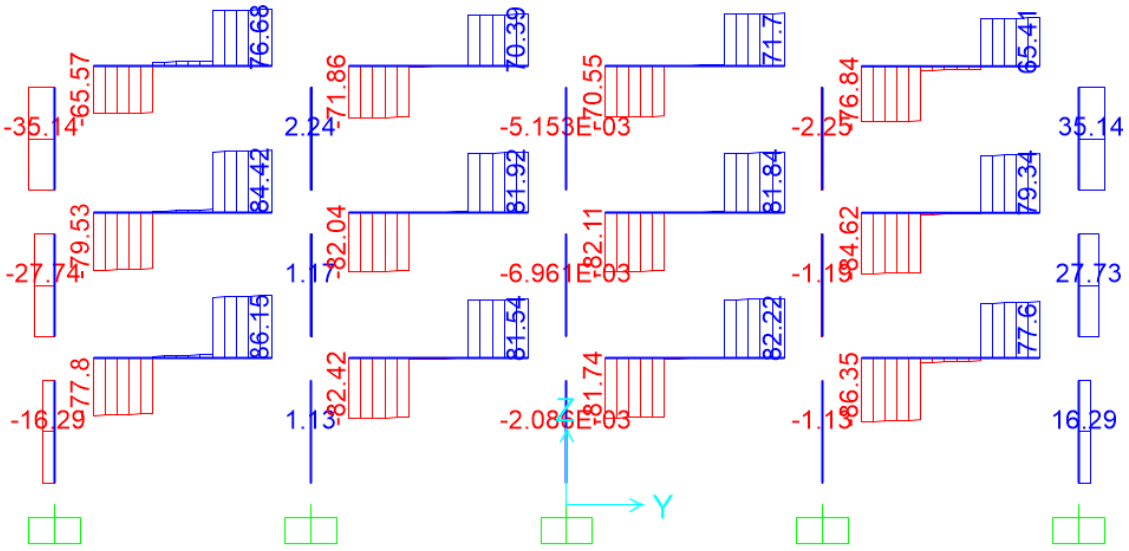

$V_{Ed,G+\psi \cdot Q}$ (kN)

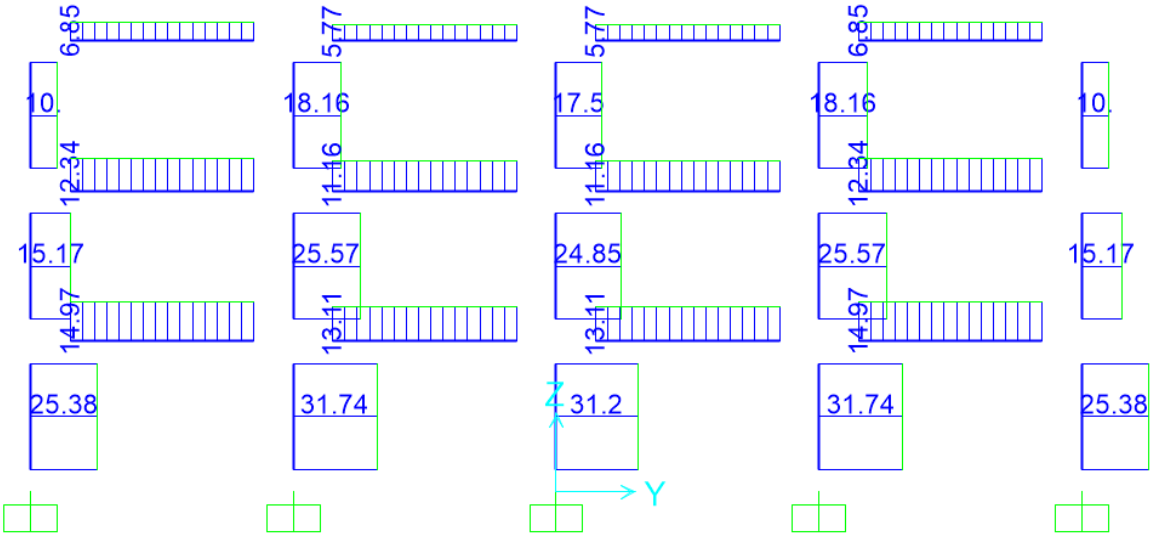

$V_{Ed,E}$ (kN)

Design Axial Forces for Columns (Internal MRF)
Column: HEB 300

Column ID	$N_{pl,Rd,i}$ (kN)	$N_{Ed,G+\psi \cdot Q}$ (kN)	$N_{Ed,E}$ (kN)	Ω	1/(1-θ)	N_{Ed} (kN)
31	5293.050	-371.290	33.620	1.989	1.268	-254.68
	5293.050	-375.880	33.620	1.989	1.268	-259.27
34	5293.050	-725.540	4.010	1.989	1.268	-711.63
	5293.050	-730.120	4.010	1.989	1.268	-716.21
37	5293.050	-710.200	0.000	1.989	1.268	-710.20
	5293.050	-714.790	0.000	1.989	1.268	-714.79
40	5293.050	-725.540	-4.010	1.989	1.268	-739.45
	5293.050	-730.120	-4.010	1.989	1.268	-744.03
43	5293.050	-370.740	-33.620	1.989	1.268	-487.35
	5293.050	-375.320	-33.620	1.989	1.268	-491.93

Sample Calculation: $N_{Ed} = N_{Ed,G} + (1.1 \cdot \gamma_{ov} \cdot \Omega \cdot N_{Ed,E}) \cdot k_{\theta} = 730.120 + (1.1 \cdot 1.25 \cdot 1.989 \cdot 4.010) \cdot 1.268$
$= \mathbf{744.03}$ kN

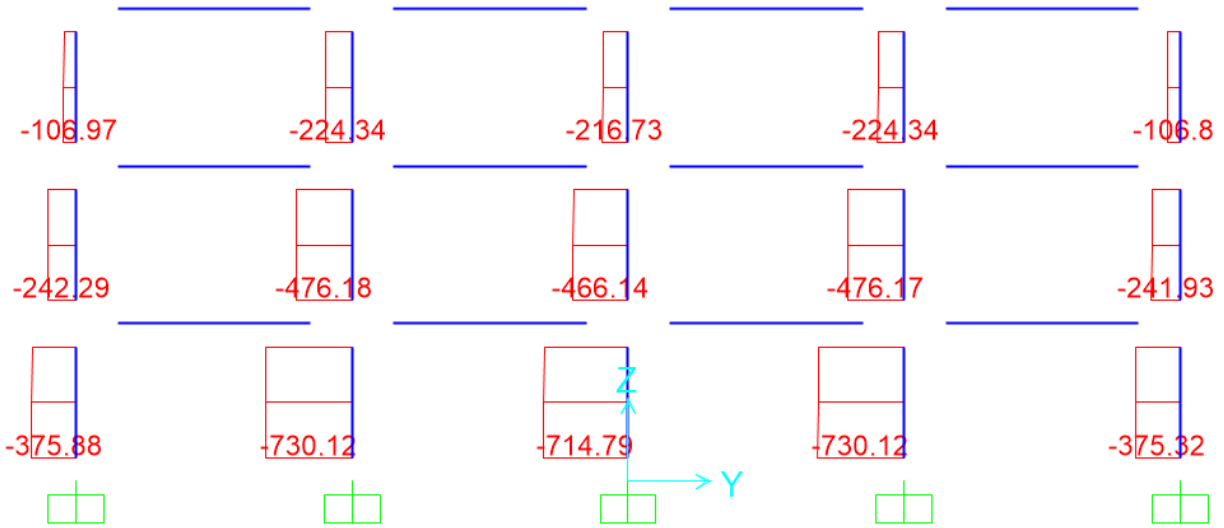

$N_{Ed,G+\psi \cdot Q}$ (kN)

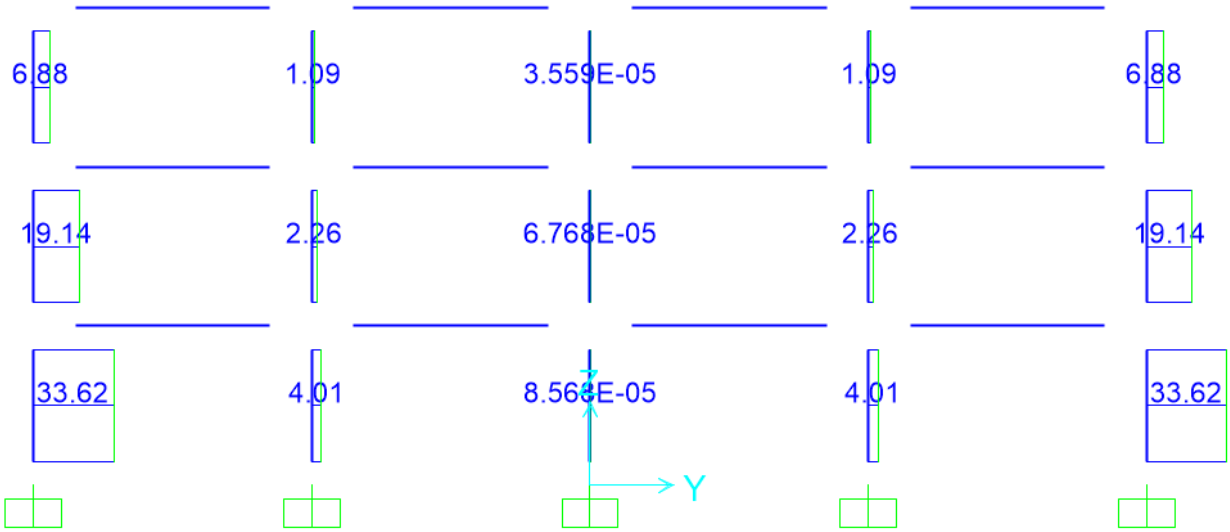

$N_{Ed,E}$ (kN)

D. Calculation of design action effects for External MRF Columns

Design Bending Moments for Columns
Column: HEB 300

Column ID	$M_{pl,Rd,i}$ (kNm)	$M_{Ed,G+\psi \cdot Q}$ (kNm)	$M_{Ed,E}$ (kNm)	Ω	1/(1-θ)	M_{Ed} (kNm)
1	663.495	24.260	-32.531	2.941	1.268	-142.521
	663.495	-10.790	72.340	2.941	1.268	360.085
4	663.495	-1.780	-50.257	2.941	1.268	-259.441
	663.495	0.830	80.430	2.941	1.268	413.183
7	663.495	0.020	-48.665	2.941	1.268	-249.478
	663.495	0.030	79.716	2.941	1.268	408.720
10	663.495	1.810	-50.257	2.941	1.268	-255.852
	663.495	-0.770	80.432	2.941	1.268	411.592
13	663.495	-24.230	-32.531	2.941	1.268	-191.012
	663.495	10.850	72.340	2.941	1.268	381.726

Sample Calculation: $M_{Ed} = M_{Ed,G} + (1.1 \cdot \gamma_{ov} \cdot \Omega \cdot M_{Ed,E}) \cdot k_{\theta} = 0.83 + (1.1 \cdot 1.25 \cdot 2.941 \cdot 80.43) \cdot 1.268$
$= \mathbf{413.183}$ kNm

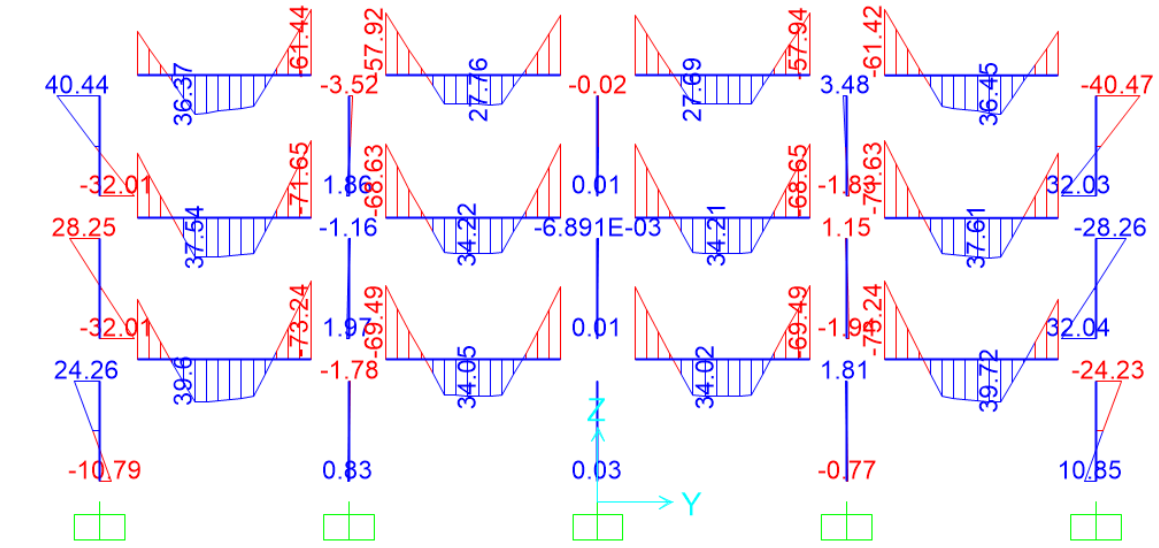

$M_{Ed,G+\psi \cdot Q}$ (kNm)

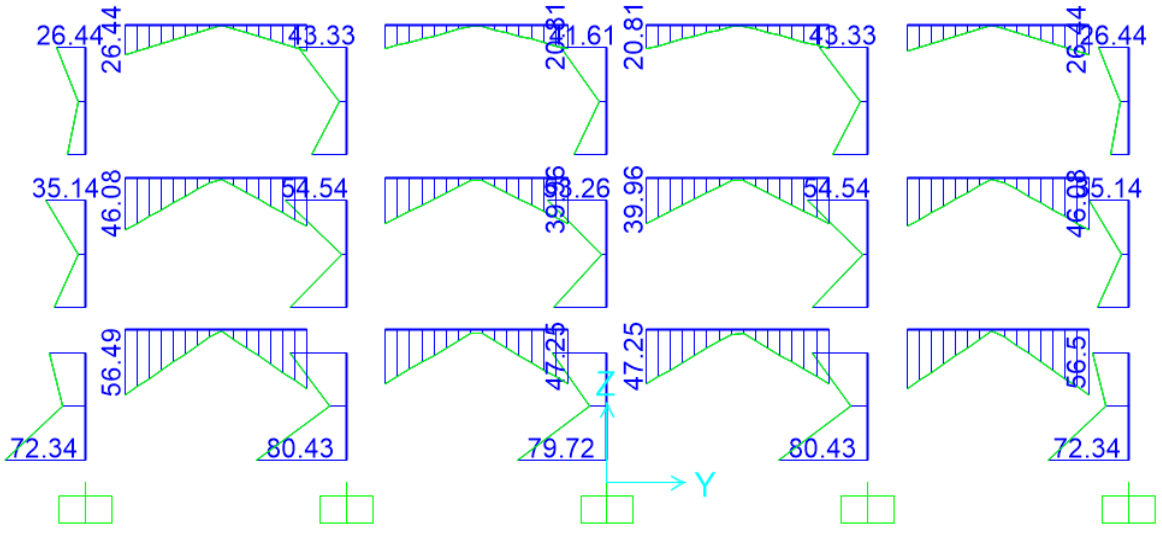

$M_{Ed,E}$ (kNm)

Design Shear Forces for Columns (External MRF)
Column: HEB 300

Column ID	$V_{pl,Rd,i}$ (kN)	$V_{Ed,G+\psi \cdot Q}$ (kN)	$V_{Ed,E}$ (kN)	Ω	1/(1-θ)	V_{Ed} (kN)
1	972.120	-8.760	26.130	2.941	1.268	125.205
	972.120	-8.760	26.130	2.941	1.268	125.205
4	972.120	0.650	32.640	2.941	1.268	167.990
	972.120	0.650	32.640	2.941	1.268	167.990
7	972.120	0.000	32.060	2.941	1.268	164.367
	972.120	0.000	32.060	2.941	1.268	164.367
10	972.120	-0.640	32.640	2.941	1.268	166.700
	972.120	-0.640	32.650	2.941	1.268	166.752
13	972.120	8.770	26.130	2.941	1.268	142.735
	972.120	8.770	26.130	2.941	1.268	142.735

Sample Calculation: $V_{Ed} = V_{Ed,G} + (1.1 \cdot \gamma_{ov} \cdot \Omega \cdot V_{Ed,E}) \cdot k_{\theta} = 0.65 + (1.1 \cdot 1.25 \cdot 2.941 \cdot 32.640) \cdot 1.268$
$= \mathbf{167.990}$ kN

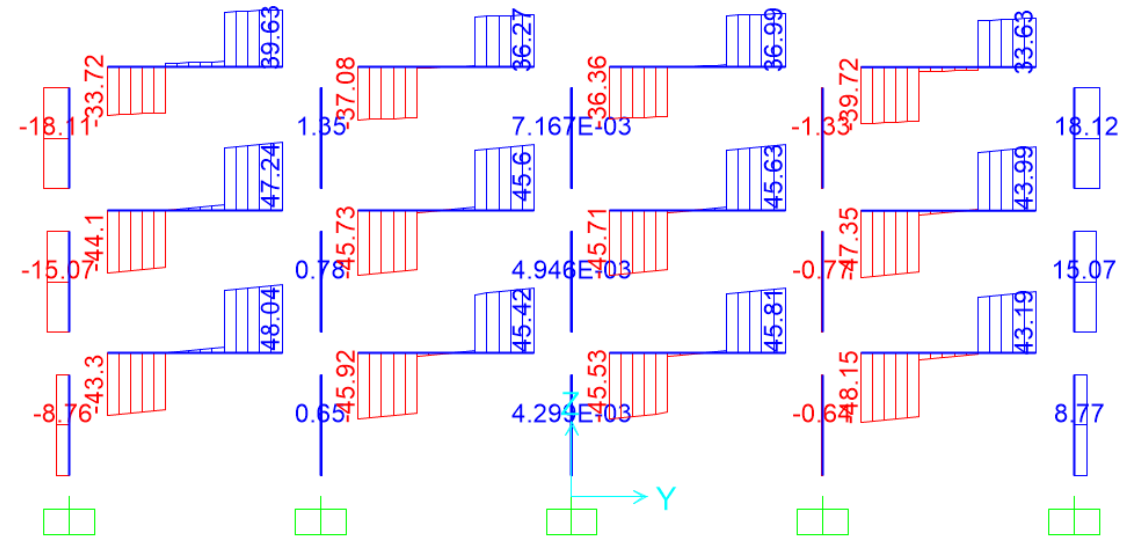

$V_{Ed,G+\psi \cdot Q}$ (kN)

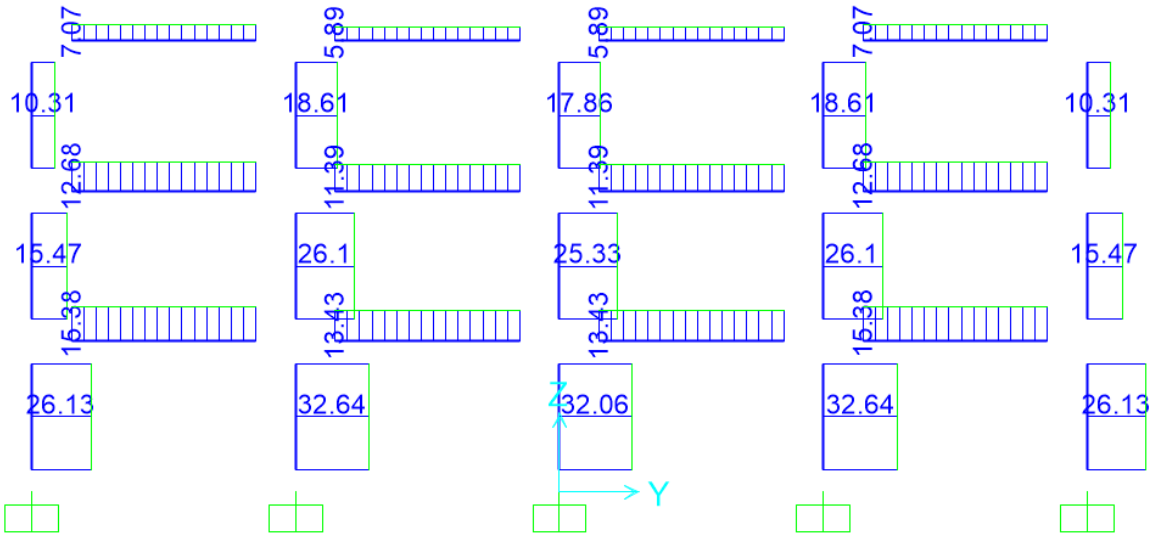

$V_{Ed,E}$ (kN)

Design Axial Forces for Columns (External MRF)
Column: HEB 300

Column ID	$N_{pl,Rd,i}$ (kN)	$N_{Ed,G+\psi \cdot Q}$ (kN)	$N_{Ed,E}$ (kN)	Ω	1/(1-θ)	N_{Ed} (kN)
1	5293.050	-265.181	313.490	2.941	1.268	1342.04
	5293.050	-269.770	313.490	2.941	1.268	1337.45
4	5293.050	-389.210	4.790	2.941	1.268	-364.65
	5293.050	-393.800	4.790	2.941	1.268	-369.24
7	5293.050	-380.460	0.540	2.941	1.268	-377.69
	5293.050	-385.040	0.540	2.941	1.268	-382.27
10	5293.050	-389.210	-4.790	2.941	1.268	-413.77
	5293.050	-393.790	-4.790	2.941	1.268	-418.35
13	5293.050	-264.800	-313.600	2.941	1.268	-1872.58
	5293.050	-269.380	-313.600	2.941	1.268	-1877.16

Sample Calculation: $N_{Ed} = N_{Ed,G} + (1.1 \cdot \gamma_{ov} \cdot \Omega \cdot N_{Ed,E}) \cdot k_{\theta} = 269.38 + (1.1 \cdot 1.25 \cdot 2.941 \cdot 313.600) \cdot 1.268$
$= \mathbf{1877.16}$ kN

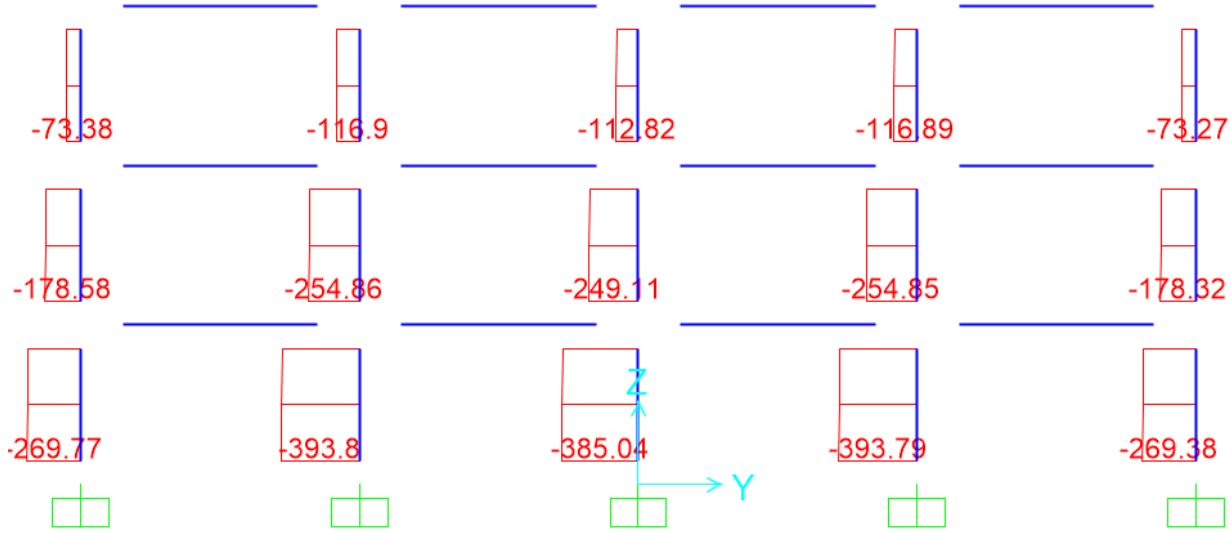

$N_{Ed,G+\psi \cdot Q}$ (kN)

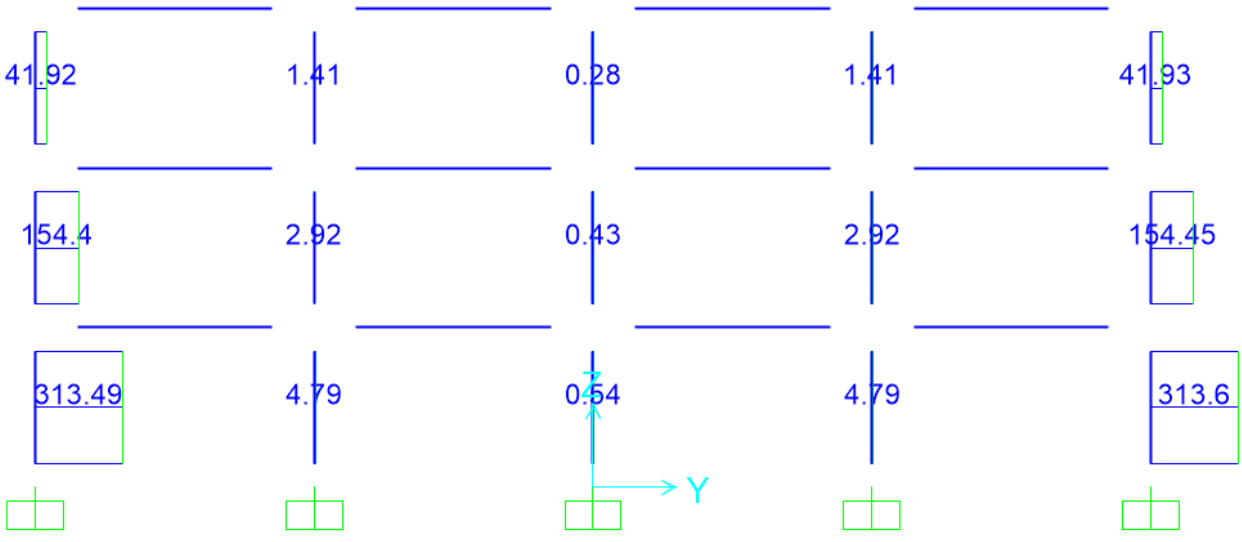

$N_{Ed,E}$ (kN)

Summary of Interaction checks for Column

Internal Moment Resisting Frame
Column: HEB300

Column ID	M_{Ed} (kNm)	N_{Ed} (kN)	C_{my}	k_{yy}	k_{zy}	Interaction 1 Eq. 6.61 EN1993-1-1	Interaction 2 Eq. 6.62 EN1993-1-1
1	154.437	-254.68	0.876	0.885	0.531	0.352	0.246
	224.026	-259.27					
4	-172.412	-711.63	0.400	0.412	0.247	0.316	0.287
	272.882	-716.21					
7	-168.76	-710.2	0.400	0.412	0.247	0.313	0.285
	269.133	-714.79					
10	-166.172	-739.45	0.400	0.412	0.247	0.320	0.293
	269.859	-744.03					
13	-154.397	-487.35	0.400	0.408	0.245	0.263	0.225
	264.236	-491.93					

External Moment Resisting Frames
Column: HEB300

Column ID	M_{Ed} (kNm)	N_{Ed} (kN)	C_{my}	k_{yy}	k_{zy}	Interaction 1 Eq. 6.61 EN1993-1-1	Interaction 2 Eq. 6.62 EN1993-1-1
1	-142.521	1342.04	0.442	0.466	0.531	0.280	0.526
	360.085	1337.45					
4	-259.441	-364.65	0.400	0.406	0.247	0.244	0.328
	413.183	-369.24					
7	-249.478	-377.69	0.400	0.406	0.247	0.244	0.328
	408.72	-382.27					
10	-255.852	-413.77	0.400	0.407	0.247	0.244	0.338
	411.592	-418.35					
13	-191.012	-1872.58	0.400	0.431	0.245	0.259	0.631
	381.726	-1877.16					

Appendix V: Calculation of Seismic Action effects (Braced Frames)

The seismic action effects for braces, beams and columns of the lateral force resisting system in longitudinal direction are detailed in this appendix.

A. Calculation for CBF (Lateral Force Method)

Calculation of Ω
Brace 1: CHS193.7x6.3
Brace 2: CHS168.3x6.3
Brace 3: CHS168.3x4

A compression limit of zero was assigned to the braces in compression and by running the lateral load case as non-linear, all the lateral force is being transferred as tension. This is equivalent to running the model without modelling compression brace. However, it is necessary to model the compression brace in order to have correct modal characteristics. The results are shown below. Notice that in the figure below, the braces carry negligible compression forces.

Brace ID	$N_{pl,Rd,i}$ (kN)	$N_{Ed,E}$ (kN)	1/(1-θ)	Ω	Unity Check
10	1020.250	657.530	1.000	1.552	0.644
12	882.750	535.640	1.000	1.648	0.607
14	566.500	303.760	1.000	1.865	0.536
			Ω_{min}	1.552	

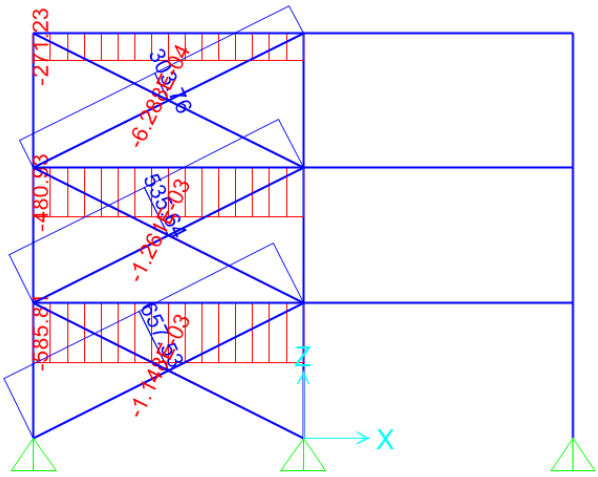

Axial forces on columns and beams considering capacity design.

Member	Brace ID	$N_{pl,Rd,i}$ (kN)	$N_{Ed,E}$ (kN)	1/(1-θ)	Ω	$N_{Ed,m}$ (kN)
Column	1	-63.110	316.710	1.000	1.552	612.592
Column	4	-63.110	-728.130	1.000	1.552	-1616.579
Beam	7	3.700	-585.810	1.000	1.552	-1246.129

The column axial effects need to be combined with axial forces due to lateral loading being acted upon on the moment frames of the structure.

Appendix VI: Lateral loads and Linearization parameters for Pushover Analysis

The loading protocol for carrying pushover analysis as discussed in the relevant section was i) 1st mode pattern and ii) uniform load proportional to the story mass. The calculated loads are summarized below.

A. Modal Pattern

Story	Modal Load Pattern					
	Moment Resisting Frames			Concentrically Braced Frames		
	φ_i	m_i	$m_i \cdot \varphi_i$	φ_i	m_i	$m_i \cdot \varphi_i$
3	1	158174.30	158174.30	1	138257.30	138257.30
2	0.736	172107.10	126670.80	0.657	139987.90	92023.08
1	0.321	172107.10	55246.40	0.305	140016.20	42764.65

where φ_i is mode shape vector normalized to top story of the structure and m_i is the story mass

B. Uniform Load Pattern

The uniform load pattern is based on the distribution of mass along the height of the building to the total mass multiplied by the seismic base shear force.

Story	Modal Load Pattern					
	Moment Resisting Frames			Concentrically Braced Frames		
	m_i	$m_i / \sum m_i$	$V_b \cdot m_i / \sum m_i$	m_i	$m_i / \sum m_i$	$V_b \cdot m_i / \sum m_i$
3	158174.30	0.315	60.67	138257.30	0.331	194.10
2	172107.10	0.343	66.00	139987.90	0.335	196.53
1	172107.10	0.343	66.00	140016.20	0.335	196.57
$\sum$	502388.50			418261.42		

Calculation of adopted parameters for conversion of MDoF system to equivalent SDoF system

C. Moment Resisting Frames

Story	Moment Resisting Frames					
	φ_i	m_i	$m_i \cdot \varphi_i$	$m_i \cdot \varphi_i^2$	$m^* = \sum m_i \varphi_i$	$\Gamma = \frac{\sum m_i \varphi_i}{\sum m_i \varphi_i^2}$
3	1	158174.30	158174.30	158174.30		
2	0.736	172107.10	126670.80	93229.72		
1	0.321	172107.10	55246.40	17734.09		
$\sum$			340091.50	269138.10	340091.50	1.264

Equivalent SDoF displacement and base shear

$d^* = d / \Gamma$

$V^* = V / \Gamma$

$S_d = d^*$

$S_a = V^* / m^*$

where S_d and S_a are the parameters for Capacity Spectrum used to plot along with elastic spectra in ADRS format to compute target displacement.

d^*	V^*	S_d	S_a
(m)	(N)	(m)	(m/s^2)
0	0	0	0
0.19	1483890	0.19	4.245
0.42	1483890	0.42	4.245

D. Concentrically Braced Frames

Story	Moment Resisting Frames					
	φ_i	m_i	$m_i \cdot \varphi_i$	$m_i \cdot \varphi_i^2$	$m^* = \sum m_i \varphi_i$	$\Gamma = \frac{\sum m_i \varphi_i}{\sum m_i \varphi_i^2}$
3	1	138257.30	138257.30	138257.30		
2	0.657	139987.90	92023.08	60492.69		
1	0.305	140016.20	42764.65	13061.45		
∑			273044.98	211811.40	273044.98	1.281

d*	V*	S_d	S_a
(m)	(N)	(m)	(m/s^2)
0	0	0	0
0.048	1054600	0.048	3.862
0.186	1054600	0.186	3.862